CAPITAL UNIVERSITY OF SCIENCE AND
TECHNOLOGY, ISLAMABAD

Eco-driving Control of Electric Vehicle with Realistic Constraints

by

Hafiz Muhammad Yasir Naeem

A thesis submitted in partial fulfillment for the
degree of Doctor of Philosophy

in the

Faculty of Engineering
Department of Electrical Engineering

2023

Eco-driving Control of Electric Vehicle with Realistic Constraints

By

Hafiz Muhammad Yasir Naeem

(DEE171001)

Dr. Kamran Iqbal, Professor

University of Arkansas at Little Rock, USA

(Foreign Evaluator 1)

Dr. Shen Yin, Professor

Norwegian University of Science and Technology, Norway

(Foreign Evaluator 2)

Dr. Aamer Iqbal Bhatti

(Thesis Supervisor)

Dr. Noor Muhammad Khan

(Head, Department of Electrical Engineering)

Dr. Imtiaz Ahmad Taj

(Dean, Faculty of Engineering)

DEPARTMENT OF ELECTRICAL ENGINEERING

CAPITAL UNIVERSITY OF SCIENCE AND TECHNOLOGY

ISLAMABAD

2023

This thesis is dedicated to the memory of my beloved father

CAPITAL UNIVERSITY OF SCIENCE & TECHNOLOGY
ISLAMABAD
Expressway, Kahuta Road, Zone-V, Islamabad
Phone:+92-51-111-555-666 Fax: +92-51-4486705
Email: info@cust.edu.pk Website: https://www.cust.edu.pk

CERTIFICATE OF APPROVAL

This is to certify that the research work presented in the thesis, entitled "**Eco-driving Control of Electric Vehicle with Realistic Constraints**" was conducted under the supervision of **Dr. Aamer Iqbal Bhatti**. No part of this thesis has been submitted anywhere else for any other degree. This thesis is submitted to the **Department of Electrical Engineering, Capital University of Science and Technology** in partial fulfillment of the requirements for the degree of Doctor in Philosophy in the field of **Electrical Engineering**. The open defence of the thesis was conducted on **January 27, 2023**.

Student Name : Hafiz Muhammad Yasir Naeem
(DEE171001)

The Examining Committee unanimously agrees to award PhD degree in the mentioned field.

Examination Committee :

(a) External Examiner 1: Dr. Muhammad Abid
Professor
PIEAS, Islamabad

(b) External Examiner 2: Dr. Laiq Khan
Professor
COMSATS University, Islamabad

(c) Internal Examiner : Dr. Fazal ur Rehman
Professor
CUST, Islamabad

Supervisor Name : Dr. Aamer Iqbal Bhatti
Professor
CUST, Islamabad

Name of HoD : Dr. Noor Muhammad Khan
Professor
CUST, Islamabad

Name of Dean : Dr. Imtiaz Ahmed Taj
Professor
CUST, Islamabad

AUTHOR'S DECLARATION

I, **Hafiz Muhammad Yasir Naeem (Registration No. DEE171001)**, hereby state that my PhD thesis entitled, '**Eco-driving Control of Electric Vehicle with Realistic Constraints**' is my own work and has not been submitted previously by me for taking any degree from Capital University of Science and Technology, Islamabad or anywhere else in the country/ world.

At any time, if my statement is found to be incorrect even after my graduation, the University has the right to withdraw my PhD Degree.

(Hafiz Muhammad Yasir Naeem)

Dated: 27 January, 2023

Registration No : DEE171001

PLAGIARISM UNDERTAKING

I solemnly declare that research work presented in the thesis titled "**Eco-driving Control of Electric Vehicle with Realistic Constraints**" is solely my research work with no significant contribution from any other person. Small contribution/ help wherever taken has been duly acknowledged and that complete thesis has been written by me.

I understand the zero-tolerance policy of the HEC and Capital University of Science and Technology towards plagiarism. Therefore, I as an author of the above titled thesis declare that no portion of my thesis has been plagiarized and any material used as reference is properly referred/ cited.

I undertake that if I am found guilty of any formal plagiarism in the above titled thesis even after award of PhD Degree, the University reserves the right to withdraw/ revoke my PhD degree and that HEC and the University have the right to publish my name on the HEC/ University Website on which names of students are placed who submitted plagiarized thesis.

(Hafiz Muhammad Yasir Naeem)

Dated: 27 January, 2023

Registration No : DEE171001

List of Publications

It is certified that following publication(s) have been made out of the research work that has been carried out for this thesis:–

Journal Publication

1. **Naeem, Hafiz Muhammad Yasir**, Aamer Iqbal Bhatti, Yasir Awais Butt, and Qadeer Ahmed. "Eco-driving control of electric vehicle with battery dynamic Model and multiple traffic signals." Proceedings of the Institution of Mechanical Engineers, Part D: Journal of Automobile Engineering 236, no. 6 (2022): 1133-1143.

Conference Publication(s)

1. **Naeem, Hafiz Muhammad Yasir**, Yasir Awais Butt, Qadeer Ahmed, and Aamer Iqbal Bhatti. "Eco-driving Control of Electric Vehicle with Traffic Signals and Battery Dynamic Model." In 2022 13th Asian Control Conference (ASCC), pp. 2320-2326. IEEE, 2022.

2. **Naeem, Hafiz Muhammad Yasir**, Aamer Iqbal Bhatti, Yasir Awais Butt, and Qadeer Ahmed. "Velocity profile optimization of an electric vehicle (ev) with battery constraint using pontryagin's minimum principle (pmp)." In 2019 IEEE Conference on Control Technology and Applications (CCTA), pp. 750-755. IEEE, 2019.

3. **Naeem, Hafiz Muhammad Yasir**, Aamer Iqbal Bhatti, Yasir Awais Butt, and Qadeer Ahmed. "Velocity profile optimization of an electric vehicle with battery dynamic model." In 2019 12th Asian Control Conference (ASCC), pp. 609-614. IEEE, 2019.

(Hafiz Muhammad Yasir Naeem)
Registration No: DEE171001

Acknowledgement

All Praises to ALLAH Almighty, the Most Gracious and the Most Merciful.

I am highly grateful to my supervisor Dr. Aamer Iqbal Bhatti, whose continuous guidance and support has always been a source of inspiration during my post-graduation studies. I am especially thankful to my co-supervisor Dr. Yasir Awais Butt for his invaluable and untiring support and technical guidance in PhD research work. I also wish to thank Dr. Qadeer Ahmed, who has been a mentor throughout my PhD research work for his assistance and constructive feedback.
I would like to thank Dr. Fazal ur Rehman, Dr. Raza Samar, Dr. Imtiaz Taj, Dr. Umer Amir Khan and Dr. Noor Muhammad Khan for their guidance and inspirational teaching during PhD course work. I am also grateful to Dr. Ghulam Murtaza for giving me technical understanding and assistance on SUMO. I am also thankful to my colleague Mr. Qaswar Abbas at NUST for his continuous support in taking up my official responsibilities to focus on my PhD research.
I am thankful to all members of Control and Signal Processing Research Group (CASPR), Dr. Raheel Anjum, Dr. Athar Hanif, Dr. Ahmed Yar, Dr. Ali Arshad, Dr. Rizwan Azam, Dr. Abdul Rehman Yasin and Dr. Bilal Javed for their assistance on various technical topics and support during my research work. I am also thankful to my colleagues, Mr. Usman, Mr. Farhan, Mr. Abrar Hashmi, Mr. Zohaib, Mr. Azmat, Mr. Faheem Manzoor, Mr. Faheem Gulzar, Mr. Ahmed Mehmood, Mr. Shujaat and Ms. Sidra for their guidance and encouragement.
Above all, I am highly grateful to my mother, who taught me the patience, devotion and commitment with affection. I am thankful to my wife, and our kids Ammaar and Bareera for understanding and accompanying me in difficult times. I am also indebted to my sisters who have always provided me motivation and relentless support to pursue higher studies.

(Hafiz Muhammad Yasir Naeem)

Abstract

Eco-driving is a strategy that provides a significant advantage by advising a velocity profile to the driver that consumes optimal energy. Extra energy consumption through imprudent driving reduces overall range of EVs per charging cycle. Moreover, frequent charging accelerates the degradation process of battery thus reduces it's life cycle. Furthermore, careless and unbounded charging and discharging adds another factor to effect the battery's health. This work focuses on the eco-driving based solution for EV to provide a velocity trajectory that not only improves the range of EV through minimizing energy consumption but also indirectly improves the life of battery. Pontryagin's Minimum Principle (PMP) is used to provide the optimal results in both unconstrained and constrained traffic environments. Longitudinal dynamics of EV and battery dynamic model is used to improve the range of EV and to see the instant effect of optimized velocity on battery's energy consumption and life. Problem is further extended to Powertrain Limitation based Speed Guidance Model (PLSGM) that provides the exact tracking of advised speed with the consideration of powertrain and actuator limitations. Zero order ideal and First order Thevenin models of battery are used for separate scenarios. Charging and discharging of a battery is bounded through constraints on its dynamics i.e., State of Charge (SoC). Further energy consumption is optimized through crossing the traffic signals during their green duration with minimum use of brakes. Traffic signals are considered as interior point constraints, hence solved using Multi Point Boundary Value Problem (MPBVP) that converts the multi-phase problem into single phase using continuity condition i.e., continuity of co-states through the use of multiple shooting technique. Speed limits are applied to add the safety factor to the problem.

Traffic is the key feature of driving environment and are considered as both single and multiple leading vehicles on the route. Urban traffic is solved as either single or multiple leading vehicle constraints to ensure the safe gap between EV with eco-driving assistance and leading vehicles. Seven different scenarios with different routes, battery models, boundary conditions, battery sizes and constraints are considered i.e., from simple unconstrained case to complex driving environment

with traffic signals, urban traffic, speed bounds, charging/discharging limits on the selected $5.3km$ route of Islamabad, Pakistan from Jinnah Avenue as starting destination to Faisal Mosque as final destination. Simulation of Urban Mobility (SUMO) is used for the evaluation of traffic signals and traffic forecasting. Achieved results for different scenarios prove the usefulness of applied strategy as energy minimum solution that has improved ranging from $5 - 20\%$ for different scenarios, along with range. Furthermore, energy consumption comparison is also performed between results achieved using MPBVP and TPBVP and results show fair advantage with MPBVP. Moreover, overall affect of using the achieved optimal velocity profile indirectly improves the life of battery through minimizing number of charging cycles. Battery life saving analysis is performed through the comparison of charging rates and terminal DoD between EV using eco-driving and leading vehicles without eco-driving assistance.

Contents

List of Figures

List of Tables

Abbreviations

AC	Alternating Current
BEV	Battery Electric Vehicle
$\boldsymbol{CO}$	Carbon Monoxide
DC	Direct Current
DoD	Depth of Discharge
DP	Dynamic Programming
ECMS	Equivalent Consumption Minimization Strategy
EM	Electric Motor
EMF	Electro-Motive Force
EMPC	Explicit Model Predictive Control
EMS	Energy Management Strategy
EV	Electric Vehicle
FCEV	Fuel Cell Electric Vehicle
GM	General Motor
GPS	Global Positioning System
HEV	Hybrid Electric Vehicle
ICE	Internal Combustion Engine
IEA	International Energy Agency
MBPVP	Multi Point Boundary Value Problem
$\boldsymbol{NMVOC_x}$	Non-Methane Volatile Organic Compounds
$\boldsymbol{NO_x}$	Nitrogen Oxides
OCP	Optimal Control Problem
PCC	Predictive Cruise Control
PHEV	Plugin Hybrid Electric Vehicle

PLSGM	Powertrain Limitation based Speed Guidance Model
PM	Particular Matters
PMP	Pontryagins Minimum Principle
PMSM	Permanent Magnet Synchronous Motor
RC	Resistor Capacitor
SAS	Speed Advisory System
$\boldsymbol{SO_x}$	Sulphur Oxides
$\boldsymbol{SoC}$	State of Charge
SUMO	Simulation of Urban Mobility
TPBVP	Two Point Boundary Value Problem

Symbols

M	Mass of vehicle	kg
$F_{inertia}$	Inertial force	N
F_{trac}	Force of traction	N
F_{roll}	Force to overcome rolling resistance	N
F_{aero}	Force to overcome aerodynamic drag force	N
F_{grade}	Force to overcome gradient of road	N
g	Gravitational acceleration	$\frac{m}{sec^2}$
θ	Road slope	$^\circ$, Degrees
v	Velocity	$\frac{m}{s}$
ρ	Air density	$\frac{kg}{m^3}$
A_f	EV frontal area	m^2
C_d	Drag co-efficient	Unit less
C_r	Rolling resistance co-efficient	Unit less
τ	Torque	Nm
τ^+	Accelerating torque	Nm
τ^-	Braking torque	Nm
η	Powertrain efficiency	Unit less
E	Energy	J
SoC	State of Charge	Unit less
DoD	Depth of discharge	Unit less
v_t	Terminal voltage	V
v_{oc}	Open circuit voltage	V
$I(t)$	Load current	Amp
r_0	Internal resistance	Ω

P_{batt}	Battery power	W
Q_{norm}	Nominal capacity	AH
η_{col}	Columbic efficiency	Unit less
R_a	Diffusion resistance	Ω
C_a	Diffusuion capacitance	F
R_i	Charging/discharging resistance	Ω
v_r	voltage through charging resistance	V
v_{oc}	Open circuit voltage	V
v_a	Voltage through diffusion resistance	V
P_{mech}	Mechanical power	W
η_m	Motor efficiency	Unit less
$R_{self-discharge}$	Self discharging resistance	Ω
R_{charge}	Resistance during charging	Ω
$R_{discharge}$	Resistance during discharging	Ω
$x(t_0)$	Initial position	m
$v(t_0)$	Initial velocity	$\frac{m}{s}$
$x(t_f)$	Final position	m
$v(t_f)$	Final velocity	$\frac{m}{s}$
J	Cost functional	Same as energy
$h(t_f)$	Terminal cost	Same as energy
L	Running cost	Same as energy
t_0	Initial time	sec
t_f	Final time	sec
H	Hamiltonian	Same as energy
λ	co-state	Unit less
u^*	Optimal control	Same as torque
α	Convergence rate	Unit less
Λ	Estimated co-state	Related to state
$\lambda(t_i^+)$	Co-state just after junction point	Unit less
$\lambda(t_i^-)$	Co-state just before junction point	Unit less
t_i^+	Time just after junction point	sec
t_i^+	Time just before junction point	sec

t_i	Time of junction	sec
$P(x)$	Penalty function	Same as energy
K	Penalty cost	Same as energy
F_{pwt}	Force applied by powertrain	N
x_{min}	Minimum state value allowed	m
x_{max}	Maximum state value allowed	m
W	Maximum braking force	N
D	Final destination	m
SoC_{min}	Minimum SoC allowed	Unit less
SoC_{max}	Maximum SoC allowed	Unit less
λ	Actual co-state	Related to state
β_1	Penalty of position	Same as energy
β_2	Penalty of velocity	Same as energy
μ_1	Penalty of velocity	Same as energy
μ_2	Penalty of SoC	Same as energy
$x(t_i)$	Position of junction	m
$v(t_i)$	Velocity of junction	$\frac{m}{s}$
τ_M	Maximum motor torque	Nm
τ_m	Minimum motor torque	Nm
τ	Torque through PMP	Nm
x	Position	m
R_t	Wheel radius	m
$\tau_{reqfeedback}$	Torque request feedback	Nm
$\tau_{reqfeedforward}$	Torque request feedforward	Nm
τ_{setpt}	Torque set point	Nm
v_{setpt}	Velocity set point	$\frac{m}{s}$
v_{actual}	Actual velocity followed by driver	$\frac{m}{s}$
ω	Angular velocity	$\frac{rad}{s}$
F_{brk}	Braking force	N
δJ	Variation in cost functional	Same as energy
δx	Variation in state	Same as state

Chapter 1

Introduction

From the last few decades, an exponential rise is seen in number of personal vehicles on roads. Relaxed payment plans provided by the banks even in underdeveloped countries can also be one of the major causes of this increase in personal vehicles. Refer to Fig. 1.1 showing the trend of increase in sale of personal vehicles worldwide from 2010 to 2022 [1]. It can be observed in Fig. 1.1 that rise in sale of personal vehicles is much larger in the last 4 years, which put more stress on the roads and available infrastructure.

This rise has highlighted certain questions, which need to be answered not only

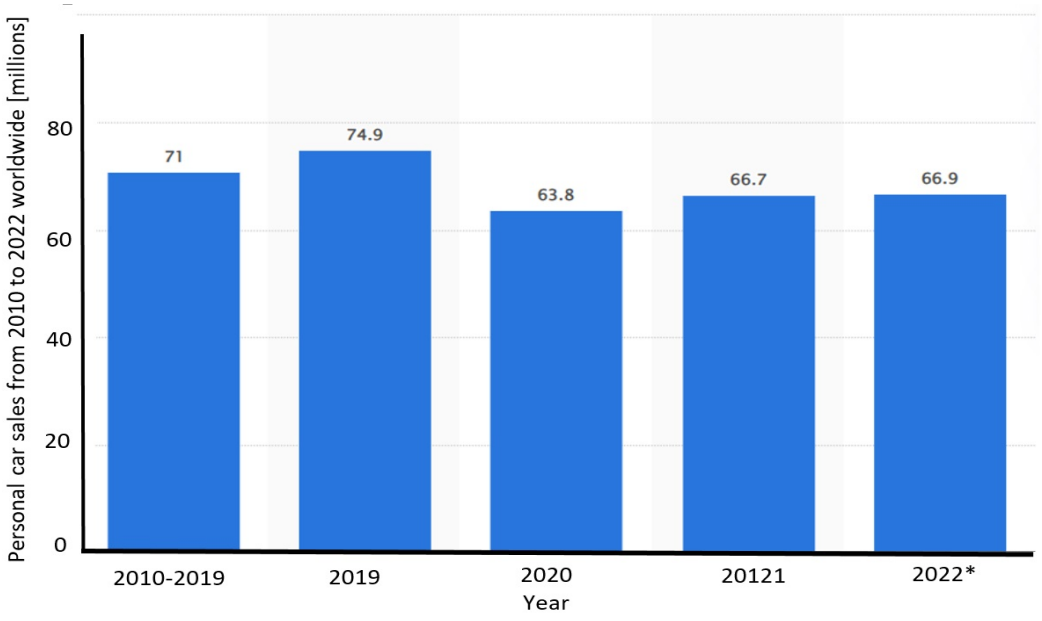

FIGURE 1.1: Trend of increase in sale of personal vehicles world wide [1]

by automotive manufacturers but also by policymakers. Especially in underdeveloped countries, where road capacities have not increased as required by the current traffic demand due to certain limitations. Traffic congestion during peak hours, high fuel consumption, long idle time at the signals, and increase in number of accidents are the major consequences being faced every day by the drivers. Lack of coordination between automobile manufacturers and road development and maintenance authorities is also one of the main causes as the development and efficiency of modern vehicles depend on traffic and road conditions as well.
There is no doubt that the transportation sector has served the humanity in an extraordinary way, but it has raised certain environmental and economic concerns. Environmental concerns include emission of toxic materials into the atmosphere that has detrimental effects on human health and the eco-system. Main pollutants of air pollution are Carbon Monoxide (CO), Non-Methane Volatile Organic Compounds ($NMVOCs$), Particular Matters (PM), Sulphur Oxides (SO_x), Nitrogen Oxides (NO_x) and etc. Another major concern with this increase in number of vehicles is an accelerated depletion in oil reservoirs because high percentage of vehicles on the roads are still based on gasoline engines which completely depend on fossil fuels.

1.1 Motivation and Background

Since the development of first gasoline-based engine back in 1886, tremendous technological advancement is seen with every passing year. Major drawbacks with gasoline engines are complete fossil fuel dependency and pollution emissions. These concerns led the researchers and manufacturers to come up with some alternative idea. As a result, concept of HEVs (Hybrid Electric Vehicles) was proposed. The superiority of HEV over conventional vehicle is the combination of both Internal Combustion Engine (ICE) and Electric Motor (EM). Introduction of EM along with ICE has minimized oil dependency and emission rate of gases but has not completely eliminated, as the engine is still present.
To overcome both these issues, Electric Vehicles (EVs) were introduced as EVs

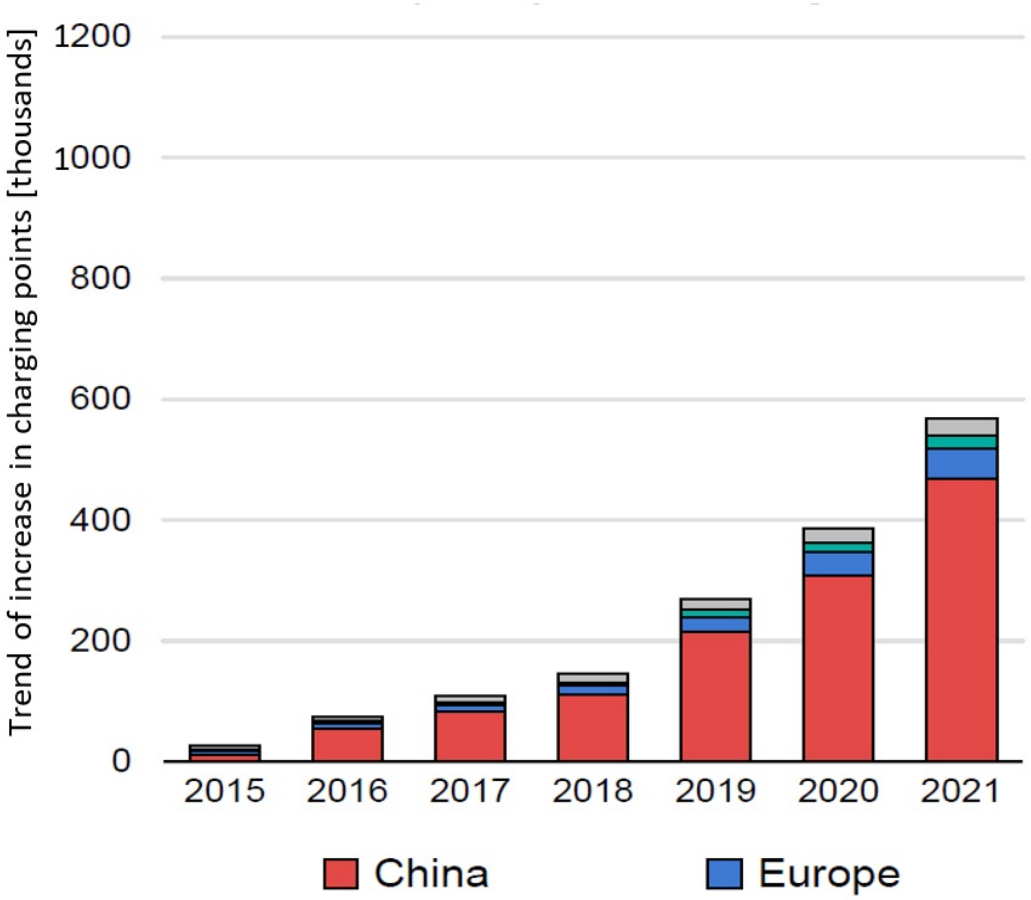

FIGURE 1.2: Trend of increase in number of charging points in China and Europe
[1]

use cleaner and greener source of energy and have no oil dependency. However, EVs face limited capacity and life cycle of battery and are directly related to its range. Battery capacity increases with an increase in its bulk weight, which has certain limitations. This requires selection of optimal size of components, known as component optimization. On the other hand, life cycle of battery can be improved through careful use e.g., fast and unbounded charging. Early degradation or replacement of battery increases the overall cost of the operation. Furthermore, range of EV can also be enhanced by installing more charging stations on the route, as Fig. 1.2 shows an increasing trend in number of charging stations in China and Europe from 2015 to 2021 [1]. Another way to increase the range of EVs is the meticulous use of available energy by drivers e.g., selection of optimal route, trip time, use traffic and signal information, optimal speed, etc. All these factors may combine together can save energy consumption during a trip.

1.2 Thesis Objectives

The objective of this thesis revolves around applying an optimization algorithm to an EV. This is achieved by finding optimal velocity to optimize energy consumption. Energy management as a research field refers to optimizing the energy consumption of a vehicle with respect to some cost parameters, when EV moves from one point to the other. Applying optimal velocity during a trip is known as velocity profile optimization or alternatively eco-driving. Eco-driving will be more frequently used in this thesis. Real time traffic environment faces different kinds of constraints, which degrade the performance of eco-driving. Furthermore, If early replacement of battery is needed due to careless use, total cost of operation also rises, as it is a very expensive component of EV. Driving environment strongly decides, which driving behaviour is best suitable from energy consumption point of view.
In view of the above discussion, major thesis objectives are:

1. Eco-driving formulation as necessary conditions of optimality to enhance the range of EV.
2. Improve battery's life through charging/discharging limits.
3. Study the impact of optimized velocity profile on battery's life using terminal Depth of Discharge and charging rate analysis.
4. Study the robustness of eco-driving as energy optimization strategy in real world traffic environment.

1.3 Proposed Strategy

As discussed in previous sections that main contribution of this research is to find velocity profile for EV for the sake of not only energy saving but battery's life optimization. We have adopted model based approach that considers the dynamics

of EV, battery and other components as the model based approaches allow use of analytical approaches for optimization and more time efficient than heuristic approaches [2–4].

Longitudinal dynamic model is considered to apply an appropriate speed control strategy. Battery dynamics is also considered in the management of instantaneous power supply and range extension of EV. Battery capacity is an important and decisive factor and its remaining value must be checked before planning a trip. This thesis also covers the development of different dynamic models of battery. Traffic environment faces many constraints, some of which are traffic signals, speed limits and traffic itself. Moreover, for the safe operation and slow degradation of battery, constraints related to charging and discharging are considered. In order to exactly follow the advised optimal velocity profile, vehicle backward simulator is used and to consider te powertrain limitations, forward simulator is used. Whereas, to include powertrain limitations with exact tracking of advised optimal velocity, Powertrain Limitation based Speed Guidance Model (PLSGM) that uses both simulators, is included [5].

Indirect optimization technique finds the optimal solution by satisfying optimal and boundary conditions i.e., by solving the differential equations, is considered in this thesis. One of the indirect trajectory optimization techniques i.e., Pontryagin's Minimum Principle (PMP) is chosen as an optimization tool, as it is computationally less extensive algorithm and has the ability to handle both equality and inequality constraints [6]. PMP finds the optimal trajectory using open loop optimal control and satisfying set of necessary conditions. Moreover, PMP can also handle both boundary and intermediate constraints through TPBVP and MPBVP simultaneously to achieve the optimal results.

1.4 Research Contributions

Main contribution of the research work presented in this thesis is the development of eco-driving control strategy for EVs that consumes less energy with putting positive impact on battery, which ultimately becomes useful in extending the range of EV. This framework is proposed for both linear and non-linear dynamic backward

model of EV with the inclusion of battery model. Problem contains inequality, terminal and interior point constraints. Proposed technique has transformed the multi phase problem to single phase problem, when interior point constraints are active.

Research work in this dissertation has following major contributions:

1. Concatenation of both EV and battery dynamic model to achieve energy efficient velocity profile.
2. Development of PMP framework in the presence of road, EV, battery and road constraints.
3. Use of SUMO (Simulation of Urban Mobility) environment for traffic and signals forecasting to provide real traffic environment on the route of Islamabad, Pakistan.
4. Transformation of TPBVP (Two Point Boundary Value Problem) to MPBVP (Multipoint Boundary Value Problem) to solve multi-phase problem.
5. Problem extension to PLSGM to follow exactly the optimal velocity profiles with the consideration of powertrain limitations.

1.5 Overview of the Thesis

In this section, thesis chapter wise overview is discussed and explained as in Fig. 1.3. In chapter 1, general issues related to present transport system are discussed. Motivation and background behind this research is also discussed in details. Furthermore, benefits and development that can contribute to the latest transport system with focus on improvement in energy efficiency is also notified. Furthermore, research contribution using the proposed strategy is also highlighted. In chapter 2 literature related to optimization framework for EVs and HEVs are discussed. Literature survey contains discussion on past efforts related to eco-driving control for both HEVs and EVs and modeling of battery dynamics.

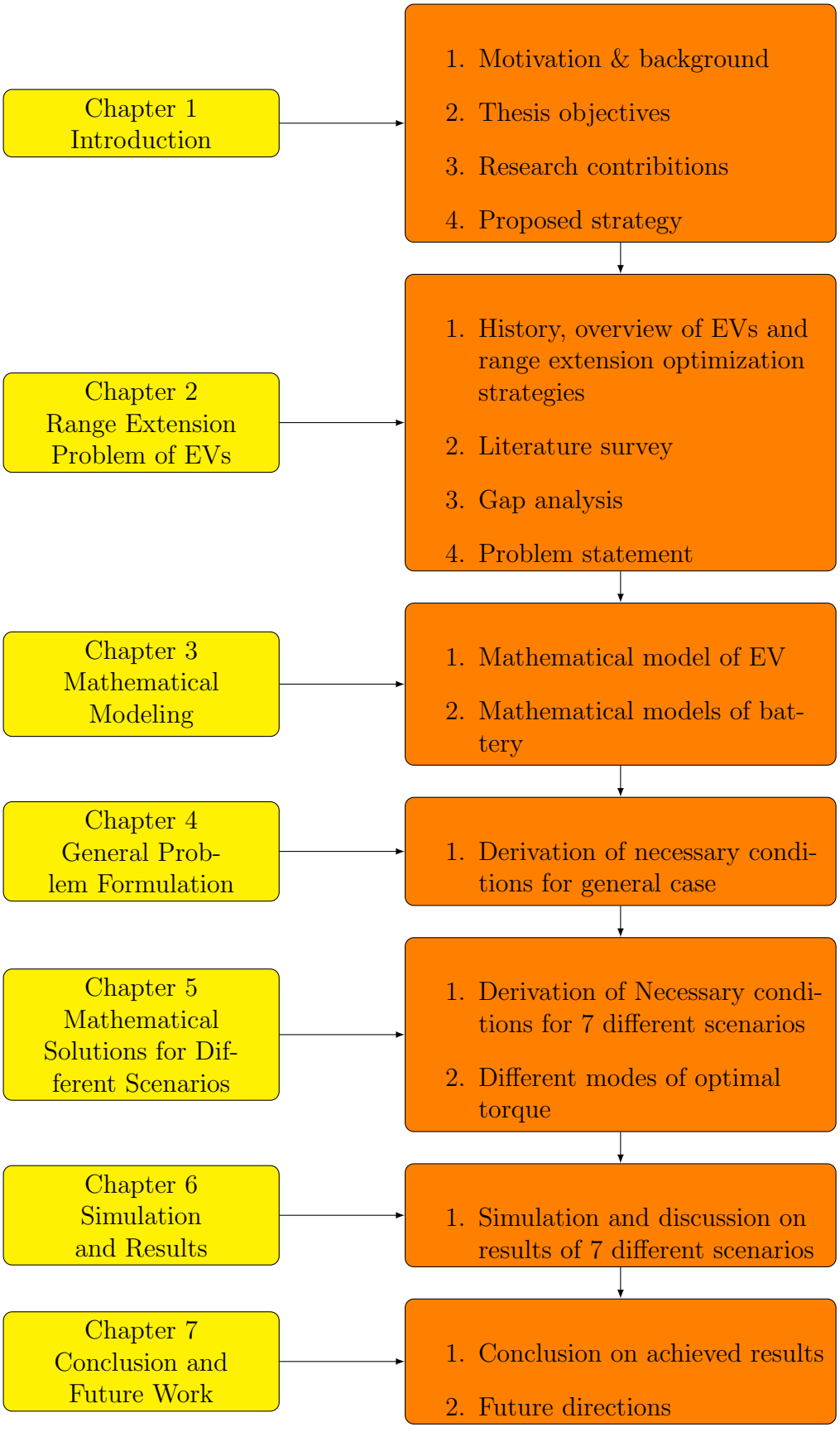

FIGURE 1.3: Overview of Thesis

Chapter 3 discusses mathematical modeling of EV and battery. Second order backward vehicle model is discussed. For a simple case, linear model is considered and then for a complex case, nonlinear model is considered. Two different mathematical models of battery are discussed in this thesis. Zero order ideal model and first order Thevenin models are used in this problem with some modeling assumptions.

In chapter 4, general optimization framework of PMP with terminal, inequality and interior point constraints, is discussed. As the problem contains both terminal and intermediate constraints. Examples of terminal and interior point constraints are initial and final positions of a trip and location of traffic signal respectively. For a simple scenario i.e., without interior point constraints, TPBVP (Two Point Boundary Value Problem) is used as an iterative technique to satisfy necessary and sufficient conditions of optimality. For more complex scenarios i.e., with traffic signals as interior point constraints, MPBVP (Multipoint Boundary Value Problem) is used to satisfy necessary and sufficient conditions of optimality and also continuity condition. Moreover, PMP with both iterative techniques, is used for the solution of eco-driving control problem for considered cases. Both cases contain two sub problems i.e., non-urban and urban traffic.

In chapter 5, necessary conditions are derived for the considered scenarios of this thesis that include unconstrained case, case with the inclusion of zero order ideal battery model with free final velocity, inclusion of zero order ideal battery model with fix final velocity, solution with interior point constraints, solution with interior point constraints and speed limits, inclusion of SoC dependent open circuit voltage and internal resistance and inclusion of traffic constraint with both single and multiple leading vehicles on the route.

In chapter 6, simulation and results are discussed and compared for different driving environments. Finally in chapter 7, future recommendations are discussed in details.

Chapter 2

Range Extension Problem of Electric Vehicle - An Overview

2.1 Introduction

With the detailed description about the summary and objectives of the thesis in chapter 1, chapter 2 will focus towards the overview of EVs and its types. Furthermore, past efforts in bringing advancement in the field of automotive will also be reviewed along with gap analysis and proposed strategy. Finally short and precise problem statement is given for the easy understanding of proposed approach to the reader.

2.2 Overview of EVs (Electric Vehicles)

2.2.1 The Beginning

The first practical EV was produced in 1880s, however they were made popular in late 19th and early 20th century, when electricity became the preferable method for vehicle propulsion system. The General Motor (GM) EV1 was the first commercial and modern designed EV produced by GM from 1996 to 1999 [7]. However,

with more advancement in gasoline engines, vehicles based on ICE (Internal Combustion Engine) started dominating the market. ICE works on the principle of gas law in which ICE acts as a heat engine to produce mechanical energy in the form of rotational motion of the crankshaft from chemical energy of fossil fuels. This burning of fossil fuel releases noxious gases, whose major pollutants are discussed in chapter 1. As a result, idea of replacing conventional vehicles with EVs again started dominating the market from the last decade. Another factor which made possible of EVs domination in the market is the development of cheaper and reliable energy storage devices i.e., battery technologies. Recent development in the field of energy storage devices focuses on reducing battery size and charging time with prolonged discharging time. Government in number of countries have increased the incentives for automobile industries to manufacture more EVs. Global Electric Car stock has increased in the last decade, as shared in report published by IEA (International Energy Agency) in 2022 [1].

2.2.2 Classification of EVs

Depending upon the working principle and design configuration, EVs are broadly classified into three main types, as defined below and shown in Fig. 2.2:-

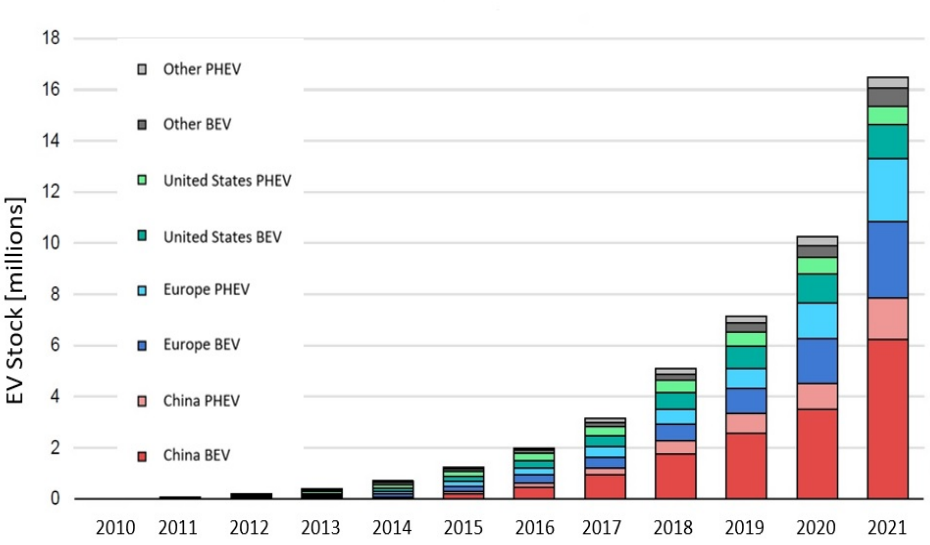

FIGURE 2.1: Trend of increase in EVs stock [1]

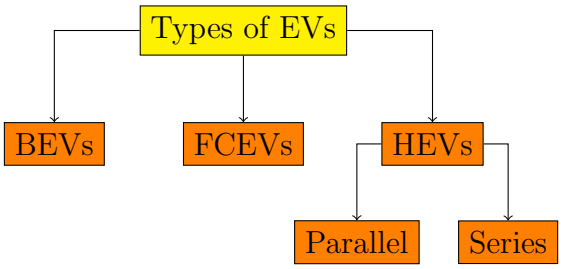

FIGURE 2.2: Types of EVs

1. Hybrid Vehicles
   (a) Hybrid Electric Vehicles (HEVs) / Parallel HEVs
   (b) Series HEVs / Plugin Hybrid Electric Vehicles (PHEVs)
2. Fuel Cell Electric Vehicles (FCEVs)
3. Battery Electric Vehicles (BEVs)

2.2.2.1 Hybrid Vehicles

As the name suggests, HEVs have both ICEs and Electric Motors (EMs). ICE gets energy through the burning of gasoline fuel, while EM gets energy from energy storage system i.e., battery. HEVs are further classified into two main categories; parallel and series. In a parallel HEV, both the EM and the ICE provide power to the vehicle and are connected to the transmission. When fuel flows to the engine or when the EM is turned on, the power that is generated, is used to propel the car. A controller decides when EM is to provide power to the vehicle and when to switch to the ICE. Standard HEVs are parallel in configuration. Battery pack in parallel HEV is only charged through regenerative mechanism. Examples of parallels HEVs available in the market are Honda Civic Hybrid, Toyota Prius, Toyota Camry etc. Fig. 2.3. shows Parallel HEV with its basic architecture and main components.

Series HEV has different architecture, in which EM is solely responsible for providing power to the vehicle. EM is powered by the battery pack or by the generator, which is powered by the gasoline engine. The gasoline engine in a series hybrid is not connected directly to the wheels of the vehicles and hence does

not directly provide power to the car. Battery pack in HEV is charged through regenerative braking mechanism or an electric outlet. A controller in series HEV determines how much power is needed to move the vehicle and whether to pull it from the battery or the generator. Series HEVs are also known as Plugin Hybrid Electric Vehicles (PHEVs). Few examples of available models in the market are Porsche Cayenne S E-Hybrid, Chevy Volt, Chrysler Pacifica, Ford C-Max Energi, Ford Fusion Energi, Mercedes C350e, Mercedes S550e, Mercedes GLE550e etc. Fig. 2.4. shows PHEV with its basic architecture and main components.

2.2.2.2 Fuel Cell Electric Vehicles (FCEVs)

FCEVs are the other types of EVs, and are also referred to as "ZERO EMISSION" EVs. FCEVs are powered by compressed hydrogen gas and directly transform the chemical energy into electrical energy. Few available models in the market are Toyota Mirai, Hyundai Tucson FCEV, Riversimple Rasa, Honda Clarity Fuel Cell, Hyundai Nexo etc. Fig. 2.5. shows Fuel Cell HEV with its basic architecture and main components.

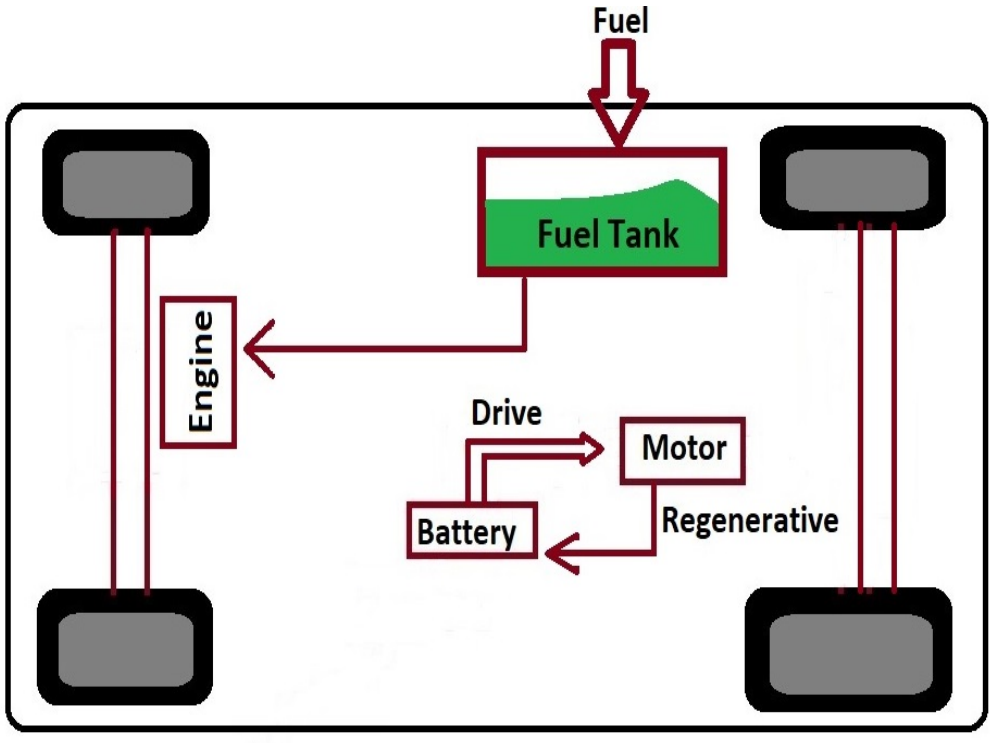

FIGURE 2.3: Basic components and configuration of Parallel HEVs

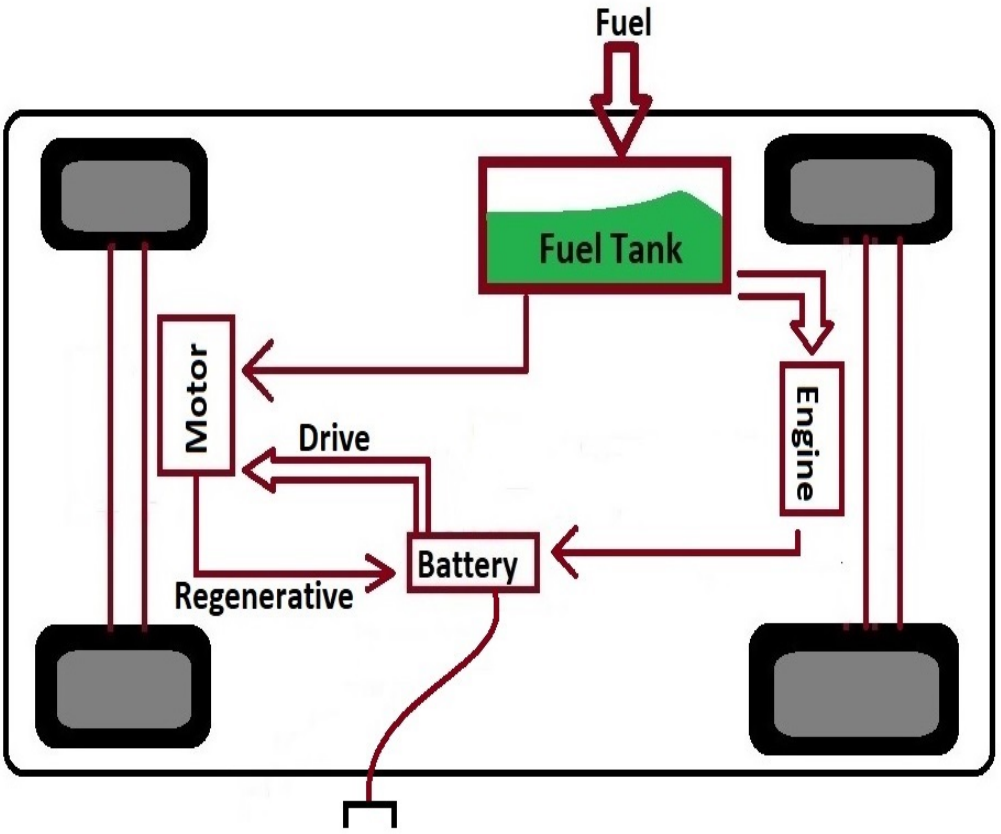

FIGURE 2.4: Basic components and configuration of Plugin HEVs

2.2.2.3 Battery Electric Vehicles (BEVs) / Electric Vehicles (EVs)

EVs use EMs as propulsion system instead of ICEs. Battery is used as a sole source of electric power to the system. Few of the available models in the markets are Volkswagen e-Golf, Tesla Model 3, BMW i3, Chevy Bolt, Chevy Spark, Nissan LEAF, Ford Focus Electric, etc. Basic configuration of EV is shown in Fig. 2.6. Main components of EV are mentioned below:

1. Battery pack
2. Rectifier
3. Controller
4. EM
5. Transmission

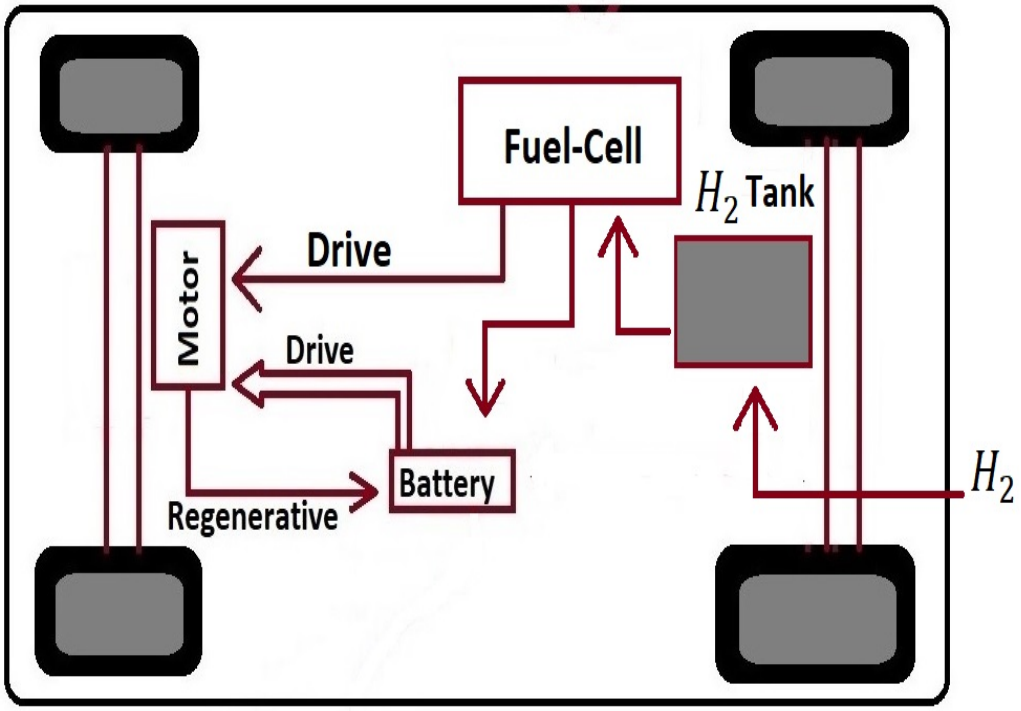

FIGURE 2.5: Basic components and configuration of Fuel Cell HEVs

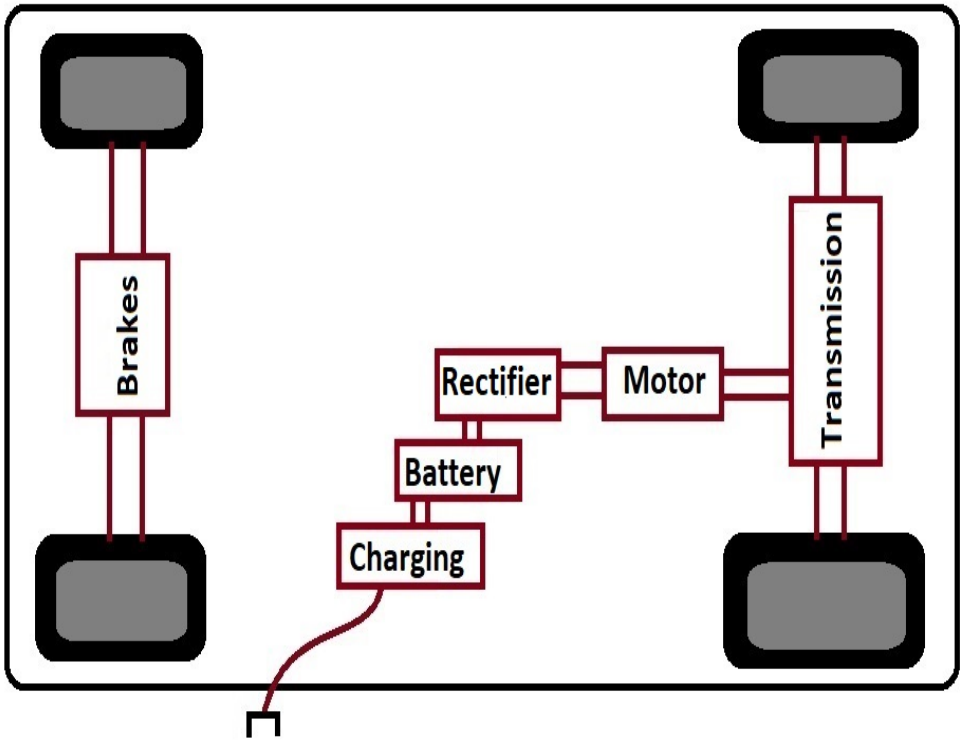

FIGURE 2.6: Basic components and configuration of EVs

6. Converter

7. Charging port

2.2.2.4 Battery pack

Battery pack in an EV acts as a source of DC power source. If power is required by an EV, it gets a signal from the controller, where DC electrical energy will transfer to the rectifier to be used to drive the vehicle. There are various types of batteries used in EVs, with the most widely used are Lithium-Ion batteries, Lead Acid batteries and Nickel-Metal Hydride batteries.

2.2.2.5 Rectifier

Rectifier is present in the EV system for power conversion. Electric outlet gets the direct power from the socket to charge the battery. Power comes from the socket, is the Alternating Current (AC), while power required to charge the battery is DC hence, this power conversion from AC to DC is done through a rectifier.

2.2.2.6 Controller

The controller acts as the brain of an EV and controls the rate of charging and discharging of a battery. Controller gets the input from car pedal and it transfers the signal to the battery through a rectifier to supply the required power. It manages the flow of electrical energy to control the speed of EM and torque it produces.

2.2.2.7 Electric Motor (EM)

Main function of EM is to convert the electrical energy from the battery to mechanical energy to turn the wheels. Few of the types of EM used in EVs are Direct Current (DC) motor, Alternating Current (AC) motor, Permanent Magnet Synchronous Motor (PMSM), etc.

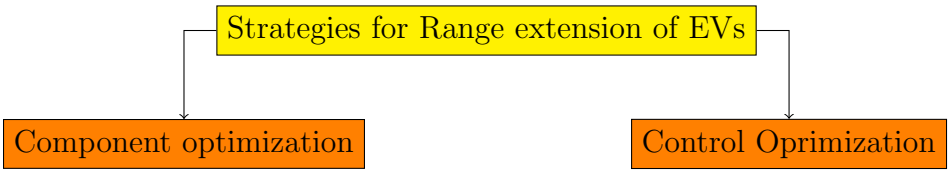

FIGURE 2.7: Basic optimization strategies for the enhancement of range of EVs

2.2.2.8 Converter

The main function of the converter is to convert AC supply to DC supply. It is used in EVs to domestic AC supply to DC to charge the battery.

2.2.2.9 Charging Port

Charging port connects the power socket to an external power supply to charge the battery.

2.3 Range Extension of Electric Vehicles through Optimization Strategy

With the latest trend in automotive industry, domination of EVs is on the rise. As seen in Fig. 2.6, battery acts as the only power providing block to the whole traction system. Range of EV is limited as the battery capacity is also limited. To get efficient results with minimum use of resources is the main customer requirement. To enhance the range of EVs, careful use of available capacity is required, which in terms of modern control theory is known as optimization strategy. Optimization strategy is classified into two main categories, as mentioned in Fig. 2.7.

2.3.1 Component Optimization

Range of EV has a direct relation with battery's capacity. Range of EV can be improved with an increase in capacity of battery. Unfortunately, battery capacity can be enhanced within certain limits as more increase in capacity requires an

increase in size and weight of a battery. On the other hand, size of a battery cannot be increased beyond a certain limit as it causes an increase in bulk weight of vehicle and hence, more power is required to move a car of huge weight. This discussion shows neither a very large nor a very small size of battery gives best results in enhancing range of EVs hence, some optimal size is required. On the other hand, one size of battery or EM may give best results for one vehicle but worst for others e.g., EM size versus mass of a vehicle [8–10]. This selection of optimal size of battery or any other component can be done through an optimization technique, known as component optimization.

2.3.2 Control Optimization

Driving style has a direct link to energy consumption during a trip. Moving with either smooth input or abrupt changes in pedal position cause huge difference in energy consumption. This selection of optimal control input is called as control optimization [11].

2.3.2.1 Velocity Control as an Energy Minimization Strategy

Velocity has a strong relation with energy consumption. Moving a vehicle either at very high or very low speed is not an excellent option from an energy consumption point of view. Driving with high speed consumes maximum energy with minimum trip time whereas, low speed driving takes more time but consumes minimum energy. Velocity profile optimization works on finding the best velocity that consumes minimum energy. This selection of optimal velocity profile is known as velocity profile optimization or eco-driving [12].

2.4 Literature Survey

In this section, very detailed literature survey is discussed. As the main focus of this thesis is to work on eco-driving control of EVs in real traffic scenarios.

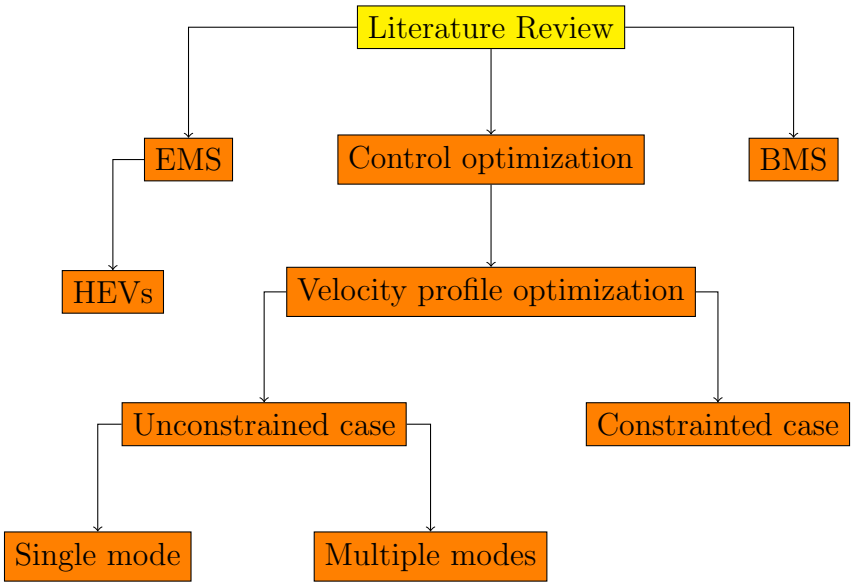

FIGURE 2.8: Literature Survey

Eco-driving is a strategy that does not depend on types of vehicles, hence related works on every kind of vehicle is discussed here. Literature is divided as Energy Management Strategy (EMS) foe HEVs and control optimization for EVs with respect to different traffic environment. Traffic environment contains unconstrained scenario, scenarios with different constraints such as signals, speed limits, urban traffic, etc.

2.4.1 Energy Management Strategy (EMS) for HEVS

Energy Management Strategy (EMS) i.e., splitting of power between EM and engine in HEVs during vehicle operation has been proposed in several works. In the past, EMS has proved to be a very useful strategy in minimizing energy consumption in HEVs [13]. Rule based EMS for PHEVs was proposed in [14]. In this approach, selection of battery mode or engine mode depends upon the power requirement. If power required exceeds the maximum power limit of EM, then engine provides the remaining power, else EM will provide the required traction demand. Charging of the battery is either provided by regenerative mechanism or by the engine. In another problem, Adaptive rule based EMS was proposed for parallel HEVs [15]. The effectiveness of this adaptive rule based EMS over conventional EMS is the ability to dynamically adjusts the boundary between the

motor region and the engine region according to the requirement of the duty cycle. This boundary is adjusted intelligently such that an optimal behavior is achieved by avoiding low efficiency regions. In this article, feedback controller based on Dynamic Programming (DP) and Equivalent Consumption Minimization Strategy (ECMS) was analyzed to find system behaviour that is closed to optimal solution. Path-dependent control of HEV was applied to improve fuel economy by optimizing charging and discharging of battery on known route [16]. Route was decomposed into series of segments with some known parameters. DP was used to achieve the global optimal results. The idea of predictive planning of velocity control of vehicle for reducing fuel consumption was proposed in [17]. DP was used with estimated traffic flow surface was used as the upper bound on the velocity with the target of improving fuel economy.

In all these research problems, DP was used as OCP, which provides global optimal results [18]. The main issue with DP is its high computational cost. Review on the EMS for HEVs are compared in terms of adaptability, computation time and results accuracy [19].

2.4.2 Velocity Profile Optimization Strategy

2.4.2.1 Unconstrained Cases

Velocity profile optimization is a very advanced methodology, used for the minimization of energy consumption during a trip. This technique is not vehicle dependent and is being applied to every kind of vehicle with large variations in energy consumption models and small in dynamical models. Several works on velocity profile optimization for HEVs are available in the literature from simple to complex problems. A framework was proposed to solve energy minimization problem through finding the optimal velocity profile. Optimization problem was solved using cloud computing environment with the assumption that a route is known in advance. Spatial domain DP was used to achieve the global optimal results to send back to the driver for velocity advisory [20]. Velocity profile optimization for HEVs was proposed in [21]. In this approach, DP was used to achieve the optimal

velocity. In another problem, which was proposed by the same authors, velocity profile optimization problem for HEV was solved [22]. In this problem, one aspect of the problem i.e., varying road grade was incorporated into an optimization framework. However, route was divided into small intervals and road grade was considered constant for each interval. In this problem, again DP was used as an OCP to achieve the optimal results. PMP based optimal solution was proposed for energy consumption minimization problem for HEV [23]. Road grade, speed limits and gear shifting constraints were incorporated.

Velocity profile optimization has been applied to EVs as well. Eco-driving strategy for EV was proposed using inversion based approach [24]. Single mode of optimal control using only accelerating torque was considered in this problem with DC as a mechanical source to the propulsion system. The problem was extended by the same authors in [25]. In this problem instead of DC, AC motor was used as a source of mechanical power to the propulsion system. Problem was taken one step ahead by considering multiple modes of operation. Similar problem of eco-driving control of EV was extended with Permanent Magnet Synchronous Motor (PMSM) as a mechanical source [26]. In this problem PMP was used as an OCP with constraints on vehicle speed. Two Point Boundary Value Problem (TPBVP) was used to satisfy boundary constraints and necessary and sufficient conditions of optimality. Energy sensing ecological control of EV was proposed in [27]. Shortest time and maximum cruise distance problem were established separately. Relation between vehicle longitudinal dynamics and energy consumption was analyzed. Eco-driving control strategy for electric vehicle, which is based on powertrain, was proposed in [28]. Battery thermal effect was taken into consideration however, DP was used to solve the problem without road constraints.

2.4.2.2 Presence of Traffic Signals on the Route

Traffic signals are the key features of urban traffic environment. Traffic signals are normally installed on the roads to control huge traffic network through Stop&Go but they pose an adverse impact on energy consumption by standing idle for the signals to turn green. Several works on reducing this idle time have been found

in the literature. An analytical solution to energy minimization problem for HEV was proposed using PMP [29]. In the first step, unconstrained case was solved i.e., without a traffic signal and then constrained case was solved with a fixed single traffic signal. Problem was divided into two phases. First phase started from initial point of a trip and ended up at a signal location. Whereas, second phase is a region from a signal location to a concluding point of a trip. Fuel consumption for constrained case was added up as terminal cost to the fuel consumption of the unconstrained case. Analytical and numerical solution to HEV with three traffic signals were proposed [30]. PMP was used with equality (point wise) constraints. Problem was formulated as multi-phase, where first phase started at the starting point and ended up at a first signal and so on. Signal reaching time was assumed to be constant. Connected vehicles equipped with Speed Advisory system (SAS) was proposed to reduce fuel consumption by reducing idling time at the signals during their red light [31]. Vehicle switches between engine mode on and off using bang-bang control that caused discomfort to the vehicle occupants.

Review on energy saving potential of connected and automated vehicles using optimal control theory and latest communication protocols were addressed [32]. Authors proposed the use of short range radar with known traffic signal information for the prediction and to schedule a velocity trajectory with implementation of algorithm in cruise control system [33, 34]. Single vehicle based scenario was considered in this problem using Predictive Cruise Control (PCC). Authors proposed a pruning algorithm to cross traffic signals during their green light [35]. Multistage optimal control of EV on signalized intersection was proposed [36]. Velocity profile optimization strategy with time constraint was applied without the consideration of traffic.

2.4.2.3 Urban Traffic Scenario

Traffic is an essential feature and posses an adverse impact not only on the energy consumption but time consumption of the trip. An Explicit Model Predictive Control (EMPC) was developed to realize real time control for the purpose to reduce energy consumption with minimum distance between preceding vehicles

[37]. However, linearized vehicle model without battery dynamics and absence of traffic signals on the route made the scope very limited. Authors presented an analytical and numerical solution using velocity profile strategy for EVs [38]. Authors showcased the benefit of full and partial road preview with traffic signals, speed limits and car following constraints separately.

2.4.3 Inclusion of Battery Dynamics in Eco-driving Problems

Battery plays a very critical role in EMS of HEVs and in range extension of EVs, as discussed in above sections. Different models of battery are discussed for problems related to HEVs. However, it is observed in the literature that integration and consideration of both EV and battery dynamics is not available in the literature. The simplest model is the zero order ideal model [5]. It is a circuit based approach with State of Charge (SoC) i.e., battery remaining capacity as the system dynamics. To get more detailed analysis and to add more complexities to the system, first order Thevenin model is discussed [39]. In this approach also, SOC is the only considered system dynamic. Basic difference between Thevenin model and ideal model is the inclusion of RC block to the system. Open circuit voltage and internal resistance are normally SoC dependent, however, range of operation of battery is the decisive factor in this dependency.

2.5 Research Analysis

Existing literature has been extensively reviewed to study optimal control strategy for all types of vehicles. Efforts are mentioned in sequence; starting from an unconstrained case of HEVs and EVs to complex scenarios i.e., with increasing number of constraints. However main focus was on EMS for HEVs and velocity profile optimization approach for HEVs, EVs and conventional vehicles. The first part of the literature focused on simple rule based and adaptive EMS approaches for HEVs. EMS showed very efficient results, however, strategy and scope are limited

to HEVs. In the next part of the literature survey, velocity profile optimization for both HEVs and EVs is discussed. It has been observed that efforts to minimize energy consumption using velocity profile optimization for HEVs have been fruitful. Problem formulation was done in multiple steps, starting from a very simple unconstrained case to complex scenarios i.e., with the number of constraints and close to real traffic environment. It has been observed in the literature that many constraints i.e., traffic signals and urban traffic were handled separately.

Velocity profile optimization solution for EVs are developed in multiple steps. In the first step, simple unconstrained case with single mode of operation and DC motor is discussed. Problem was modernized with different complex mathematical models and more than one mode of operations. Simple DC motor was replaced with more complex motor models i.e., AC motor and PMSM etc. In the next part of the literature, works related to the handling of traffic signals in the optimization problem were discussed for both HEVs and EVs. Several works have been discussed to avoid or minimize the idle time at the signals. Similar approach using PMP is also included in the literature, however, necessary and sufficient conditions of the optimality were not properly followed because of multi-phase nature of the problem. Most of the problems did not include urban traffic and on the other hand, if traffic is considered, then signals are avoided to limit the complexity of the problem.

To the best of our knowledge, eco-driving with the consideration of its impact on battery is not available in the literature. It goes without saying that battery is the most critical component and the only source of power in the electric vehicle and hence its role in range extension of EVs cannot be further emphasized. Battery capacity affects the range on one trip and measured in terms of State of Charge or Depth of Discharge. Moreover, battery life which is measured in terms of charging and discharging cycles, is an indirect long term benefit. Early replacement of battery due to careless behaviour during either charging or discharging increases the overall operational cost of the vehicle over its lifetime of 5 or 10 years.

The overall Gap, which is drawn from the discussed literature, is this thesis covers not only eco-driving control strategy for EV, but also the issues that EV can face due to the careless use of battery. Furthermore, when the impact of important

factors on battery's health are ignored e.g., maximum charging/discharging limits, charging rates and number of charging/discharging cycles, its degradation process accelerates. Furthermore, the combination and number of constraints covered, have not found in the literature at this level of generality.

2.6 Problem Statement

To solve an eco-driving problem of an EV with battery constraints such as charging/discharging limits, road constraints such as speed limits, preceding vehicles and traffic signals along with motor torque limits through Powertrain Limitation based Speed Guidance Model (PLSGM).

2.7 Chapter Summary

After the discussion on thesis objectives, proposed strategy and research contribution in chapter 1, in this chapter past efforts in the extension of range of EVs are discussed in details. At the start of the chapter, beginning and evolution of EV technology is discussed. Furthermore, overview of EV with basic types and architecture are discussed with basic components of EVs and their working principles. Range extension problem of EV through different optimization strategies i.e., component and control optimization are explained with pictorial representations. Past efforts through detailed literature survey are explained through velocity control as energy minimization strategy. Literature survey is well divided further into EMS for HEVs and velocity profile optimization for EVs for both unconstrained and different constrained scenarios. Chapter is concluded with a problem statement based on research analysis and gap.

Chapter 3

Mathematical Modeling

3.1 Introduction

Velocity profile optimization is one of the energy minimization strategies being applied to control or minimize the energy consumption of vehicle during a trip. Modeling for velocity profile optimization may have two approaches: create plant to apply and test energy minimization strategy, or create embedded models to solve analytically or numerically. Plant models are more accurate and computationally heavier than embedded models. The main objective in both approaches is to reproduce the energy flow from vehicle to powertrain, which is further used to accurately estimate the fuel consumption based on both the driver inputs and the road load. Other quantities e.g., battery aging, pollutant emissions etc may be of interest and depends upon applications.

There are so much losses in the powertrain at every step that the mechanical power produced at the wheels is very less as compared to electrical power produced by the battery. Furthermore, conversion from one form of energy to the other form of energy adds more losses to the system by further reducing the output power e.g., electrical to mechanical conversion through EM. Moreover, when power transfers from one device to other, there occurs friction losses in the system. Energy losses is modeled using efficiency map, in which efficiency is obtained based on operating conditions of the system e.g., EM efficiency as a function of input torque and

output angular speed, as explained in Fig. 3.10. EV energy consumption can be calculated using both backward and forward vehicle modeling approaches [5, 40–42]. The backward modeling method is a quasi-static approach that works on the assumption that a prescribed velocity is exactly followed by EV. In this approach, drive cycle is divided into small time intervals, during which speed, acceleration and torque remain constant. Moreover, internal powertrain dynamics are neglected and average values of all variables are taken during the selected sampling time. Each component of powertrain is modeled using efficiency map, fuel consumption map or power loss map. On the other hand, forward modeling approach works on first-principle description of each components of powertrain. Dynamic equations describing the evolution of its state and the degree of modeling detail depend on the time scale and the nature of the phenomena that the model should predict. In backward modeling approach, force follows velocity and then tractive force is calculated. In this approach, it is assumed that vehicle is following a prescribed velocity. On the other hand, in forward modeling approach, desired drive cycle is compared with actual speed and braking or throttle command is generated using a driver model.

3.2 Vehicle Energy Analysis

In this thesis, vehicle energy analysis, in which EV is considered as a point mass with interaction to external factors, is studied to measure power and energy to move on particular velocity. The approach is useful to understand the longitudinal dynamics and energy characteristics of EV.

3.2.1 Kinematic Model

Dynamic equation of motion with equilibrium forces on EV with point mass of M moving with velocity v in longitudinal direction, as shown in Fig. 3.1, can be expressed as [43]:

TABLE 3.1: Description of symbols used in EV modeling

Symbol	**Unit**	**Description**
F_{trac}	N	Tractive force
M	kg	Mass of vehicle
g	$\frac{m}{s^2}$	Gravitational acceleration
F_{roll}	N	Rolling resistance force
θ	$^\circ$, Degrees	Road gradient
F_{grade}	N	Force to cover gradient
$F_{inertia}$	N	Force of inerta
F_{aero}	N	Aerodynamic force
v	$\frac{m}{s}$	Velocity of EV
F_{pwt}	N	Force applied by powertrain
F_{brake}	N	Braking force
ρ	$\frac{kg}{m^3}$	Air density
A_f	m^2	EV frontal area
C_d	Unit less	Drag co-efficient
C_r	Unit less	Rolling resistance co-efficient
τ	Nm	Motor torque
η	Unit less	Transmission efficiency
γ	Unit less	Transmission ratio
R_t	m	Wheel radius
x	m	Position of EV
τ_{setpt}	Nm	Desired torque
$\tau_{reqfeedfwd}$	Nm	Torque request feed forward
$\tau_{reqfeedback}$	Nm	Torque request feedback
$v_{feedback}$	$\frac{m}{s}$	Velocity feedback
v_{setpt}	$\frac{m}{s}$	Desired velocity
$v_{actualspeed}$	$\frac{m}{s}$	Actual velocity

$$M\dot{v} = F_{inertia} = F_{trac} - F_{roll} - F_{aero} - F_{grade} \tag{3.1}$$

where M is the mass of EV, v is the longitudinal velocity, $F_{inertia}$ is the inertial force, $F_{trac} = F_{pwt} - F_{brake}$ is the tractive force. Tractive force is positive when vehicle is moving in forward direction and gets negative when it is moving in opposite direction. F_{roll} is the rolling resistance, F_{aero} is the aerodynamic drag force and F_{grade} is the gradient force.

Definition 3.2.1. Aerodynamic drag force is the resistive force which is acting upon

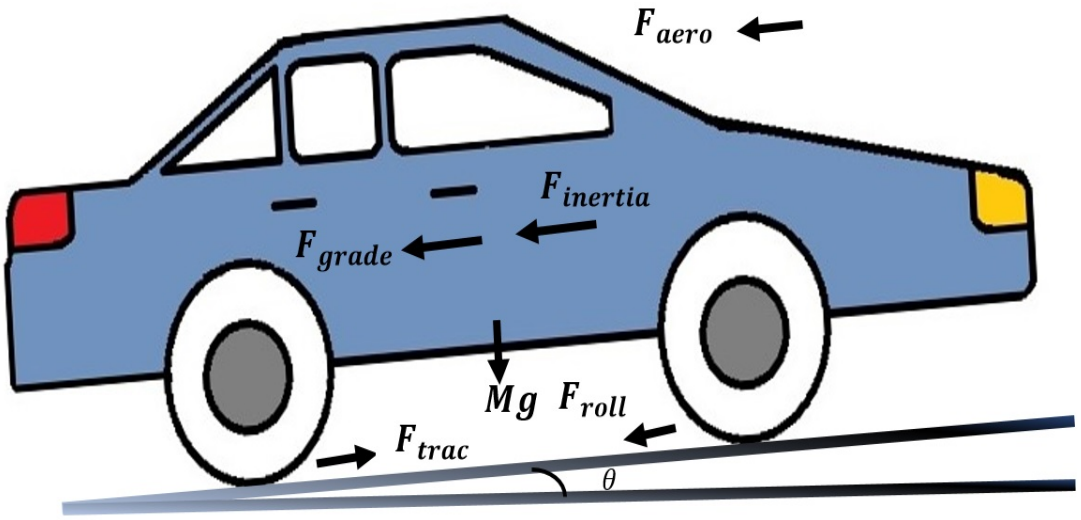

FIGURE 3.1: Forces acting on vehicle

the vehicle gushing through the air in opposite direction to the motion of vehicle. The aerodynamic drag force is expressed as:

$$F_{aero} = \frac{\rho A_f C_d v^2}{2} \tag{3.2}$$

where ρ is the air density, A_f is the EV frontal area, C_d is the drag co-efficient.

Definition 3.2.2. Rolling resistance forces are offered by the tires during the motion on any hard surface. Resistance of these forces increases with the increase in hardness or roughness of the material. Reaction forces act on the centre of wheels to oppose these forces and to keep the wheel rolling and moving. The rolling resistance force is expressed as [44]:

$$F_{roll} = C_r mg\cos(\theta) \tag{3.3}$$

where C_r is the rolling resistance co-efficient, g is the gravitation force and θ is the angle of road gradient with respect to tires.

Definition 3.2.3. Gradient force is the force that is produced by the weight of the vehicle during a slope on the road in either direction. Gradient force expressed as:

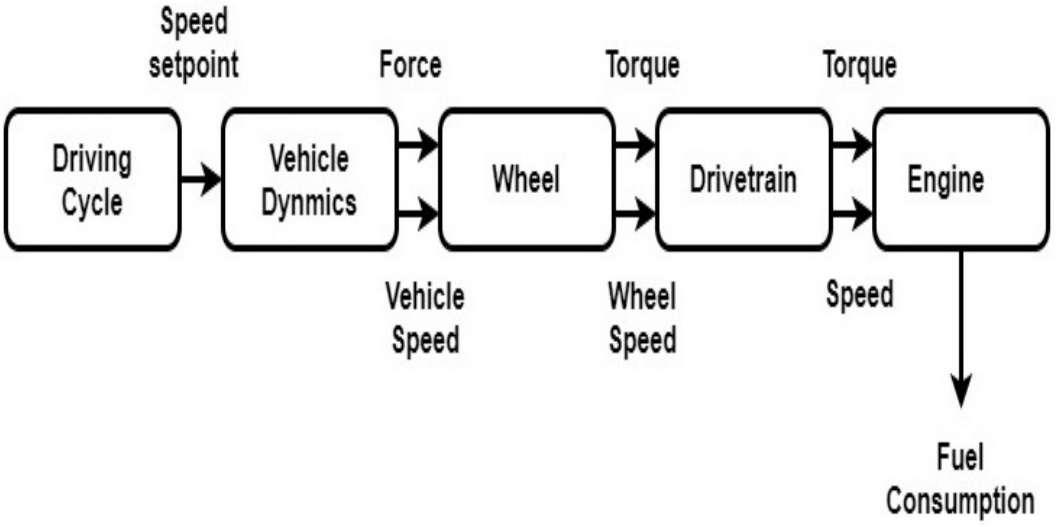

FIGURE 3.2: Backward vehicle simulator

$$F_{grade} = Mg\sin(\theta) \tag{3.4}$$

As mentioned above, backward and forward are the two modeling approaches considered for vehicle energy analysis, as mentioned below with their mathematical relations and block diagrams.

3.2.2 Backward Modeling Approach

In backward modeling approach, force follows velocity and then tractive force is calculated based on the velocity with which vehicle is following, as shown in Fig. 3.2. Eqn. (3.1) can be rearranged to obtain backward simulator equation as follows:

$$F_{trac} = F_{pwt} - F_{brake} = F_{inertia} + F_{roll} + F_{aero} + F_{grade} \tag{3.5}$$

Energy required to move the vehicle is calculated based on the expression as:

$$E = F_{trac}v \tag{3.6}$$

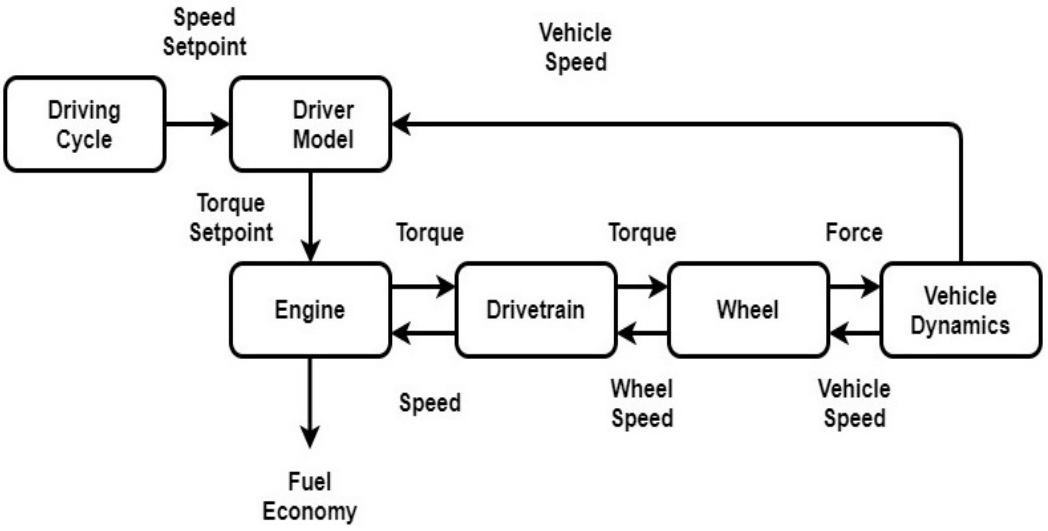

FIGURE 3.3: Forward vehicle simulator

3.2.3 Forward Modeling Approach

Eqn. (3.1) corresponds to forward vehicle simulator, in which acceleration i.e., $\frac{dv}{dt}$ is calculated based on the tractive force applied to move the vehicle for some distance. Speed of the vehicle is then calculated by integrating acceleration obtained in step one. Block diagram corresponds to forward vehicle simulator, as shown in Fig. 3.3.

3.3 Powertrain Limitation based Speed Guidance Model (PLSGM)

Both the backward and forward approaches have their strengths and weaknesses. Backward modeling approach is typically used for fuel consumption analysis over the given velocity trajectory with the assumption that trajectory is be exactly followed by the driver. Whereas, in forward approach, it is not possible to follow the exact profile, however error can be minimized through proper tuning of the driver block. Moreover, backward simulator completely ignores actuator and powertrain limitations with the assumption that the vehicle has the capacity to follow every trajectory being advised to it. This causes problem for the drive cycle, which may

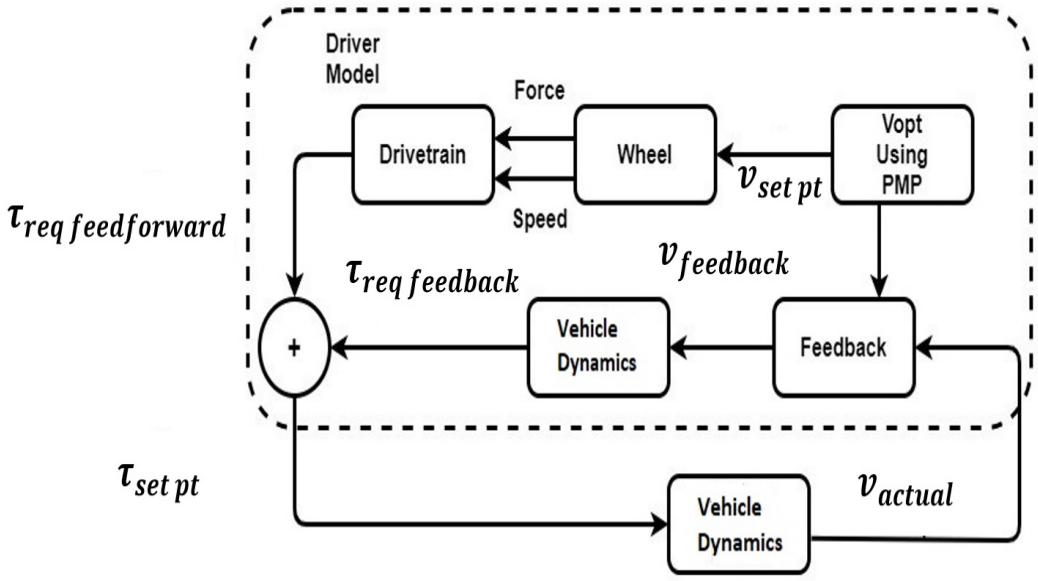

FIGURE 3.4: Powertrain Limitation based Speed Guidance Model (PLSGM)

require more power that a powertrain can deliver. On the other hand, forward simulators do not face such issues, because velocity is calculated from the tractive force, which can be saturated if the powertrain limitation exceeds. For this reason, forward simulators are used for the analysis of the system at saturation levels and also for the acceleration test of the vehicle.

PLSGM combines the advantages of both the simulators i.e., uses backward model to accurately follow the speed trajectory and uses forward model to manage powertrain limitations to avoid saturation of the actuators [5]. Block diagram of PLSGM is as shown in Fig. 3.4.

Refer to Fig. 3.4, where forward model, a driver block uses vehicle dynamics to calculate torque request feed forward. On the other hand another vehicle dynamic block uses actual speed profile to calculate the torque request feed backward. Combined torque effect is given back to vehicle model to reduce the error between actual and desired speed profile. Expressions of backward forward models are already mentioned in above sections. Combined expressions of torque i.e., τ and velocities v between forward and backward simulators are mentioned as:

$$\begin{aligned} \tau_{\text{set pt}} &= \tau_{\text{req feedforward}} + \tau_{\text{req feedback}} \\ v_{\text{feedback}} &= v_{\text{set pt}} - v_{\text{actual}} \end{aligned} \tag{3.7}$$

where $\tau_{\text{req feedforward}}$ is the torque request feed forward from the forward simulator and $\tau_{\text{req feedback}}$ is the torque feedback required to produce the desired velocity profile and $\tau_{\text{set pt}}$ is the torque set point to generate velocity of set or desired value. Similarly v_{feedback} is the velocity given to the feedback simulator or the desired velocity, $v_{\text{set pt}}$ is the velocity at the set points and v_{actual} is the actual velocity generated from the torque request using feed forward controller. Goal is to have minimum error between the actual velocity and feedback velocity.

3.4 Mathematical Model of Electric Vehicle

EV longitudinal dynamics are obtained using Eqn. (3.1). Position and velocity are the states of the system. Dividing Eqn. (3.1) by M on both sides and putting the values of F_{aero}, F_{grade} and F_{roll} from above section, longitudinal speed dynamics is expressed as:

$$\dot{v} \quad = h_1 \tau \eta^{\text{sign}(\tau)} - h_2 v^2 - h_0 - W \tag{3.8}$$

where

$$h_1 = \frac{\gamma}{mR_t}, \quad h_0 = g\sin(\theta(x(t))) - gC_r$$
$$h_2 = \frac{\rho A_f c_d}{2m}, \quad W = \frac{F_{brk}}{m} \tag{3.9}$$

Similarly position dynamic is simply the integral of velocity, expressed as:

$$\dot{x} = v \tag{3.10}$$

where sign(τ) is used to incorporate both accelerating and braking torques into the system [26]. In this thesis both linear and non-linear models of EV are used for separate scenarios [45]. For linear model, h_2 in Eqn. (3.8) is assumed to be zero [45]. Furthermore, road grade is kept constant during a trip, i.e., putting $\theta = 0$ in Eqn. (3.8).

TABLE 3.2: Description of symbols used in battery modeling

Symbol	Unit	Description
v_t	V	Terminal voltage
v_{oc}	V	Open circuit voltage
$I(t)$	A	Battery current
r_0	Ω	Internal resistance
P_{batt}	W	Battery power
Q_{norm}	whr	Nominal capacity
η_{col}	Unit less	Battery efficiency
SoC	Unit less	State of Charge
DoD	Unit less	Depth of Discharge
R_a	Ω	Electrochemical diffusion resistance
C_a	F	Electrochemical diffusion capacitance
R_i	Ω	Charging/discharging resistance
v_r	V	Voltage across R_i
v_a	V	Voltage across R_a
∇t_d	sec	Sampling time interval
P_{mech}	W	Motor power
η_m	Unit less	Motor efficiency

3.5 Mathematical Model of Battery

Battery plays a very critical role in the range extension of EV. As battery is the only source of power to the system and if its stored charge finishes during a trip, it can affect not only trip quality but also trip time etc. Variety of battery models are discussed to show the interaction with EVs [46]. Batteries face aging issues when used for long hours in EVs, as a result loss in terminal voltage and increase in internal resistance and hence reduction in vehicle performance. Latest research is focusing on finding the suitable battery models to predict the end life with given environmental conditions and velocity cycle, such as [47–51]. However, in short period of time, this aging factor does not play a significant role [5], hence not taken into account in this thesis.

In this thesis, dynamical model of EV is combined with battery to continuously monitor the battery remaining capacity and instant effect of selection of pedal

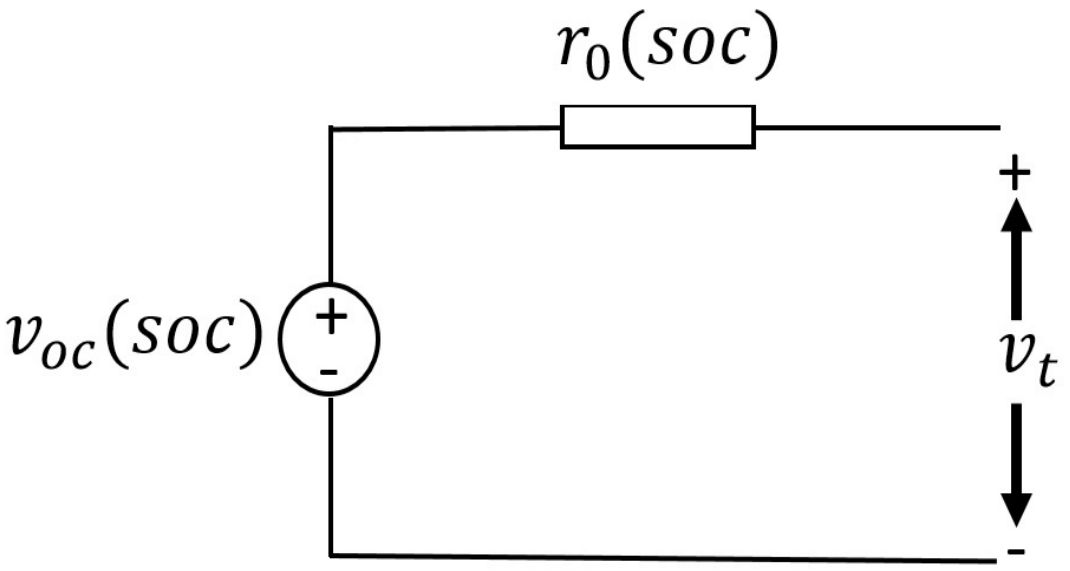

FIGURE 3.5: Zero order circuit based battery ideal model

position on battery to improve the range of EV and life of battery. Single order battery dynamics is considered in this thesis i.e., SoC, which is defined as the ratio between the instantaneous capacity to the nominal capacity. Two different models are considered in this thesis, which are:

1. Zero order ideal model
2. First order Thevenin model

3.5.1 Zero order Ideal Model

Circuit based model of the battery is as shown in Fig. 3.5, with internal resistance i.e., $r_0(soc)$ and open circuit voltage $v_{oc}(soc)$ as the two main variables to influence output voltage i.e, v_t. The mathematical model of zero order circuit based ideal model with manipulation of battery power expressions is used [52–55].
Output voltage is expressed as:

$$v_t = v_{oc}(soc) - I(t)r_0(soc) \tag{3.11}$$

where $I(t)$ is the current flowing through the battery and calculated using

$$P_{batt} = v_t I(t) = v_{oc} I(t) - r_0 I^2(t) \tag{3.12}$$

and expressed as:

$$I(t) = \frac{voc(soc)}{2r_0(soc)} - \sqrt{\frac{voc^2(soc)}{4r_0^2(soc)} - \frac{P_{batt}}{r_0(soc)}} \tag{3.13}$$

SoC dynamics is expressed as:

$$\dot{soc} = \frac{-I(t)}{Q_{norm}\eta_{col}^{sign(I(t))}} \tag{3.14}$$

where Q_{norm} is the nominal capacity of battery and η_{col} is the coulombic battery efficiency that depends upon current operating conditions i.e., temperature and current intensity [44].

SoC dynamics in terms of $v_{oc}(soc)$ and $r_0(soc)$ is expressed as:

$$\dot{soc} = \frac{1}{Q_{norm}\eta_{col}^{\text{sign}(I(t))}} \left[-\frac{voc(soc)}{2r_0(soc)} + \sqrt{\frac{voc^2(soc)}{4r_0^2(soc)} - \frac{P_{batt}}{r_0(soc)}} \right] \tag{3.15}$$

where P_{batt} is the battery electrical power and can be expressed as:

$$P_{batt} = v_{oc}(soc) I(t) - I(t)^2 r_0(soc) \tag{3.16}$$

Zero order ideal model is further divided into sub cases, which are

1. Constant r_0 and v_{oc}
2. SoC dependent r_0 and v_{oc}

3.5.1.1 Constant r_0 and v_{oc}

It is observed in Fig. 3.6 & 3.7 that major variations in both the variables are observed at the extreme values of SoC i.e., after 0.8 and before 0.2, while they

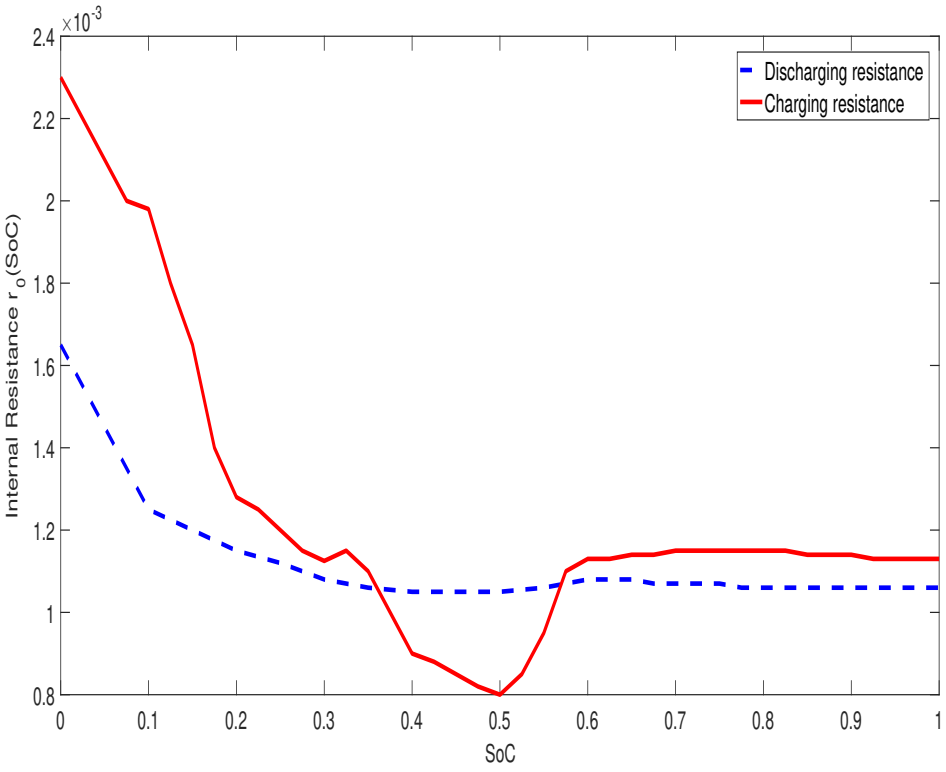

FIGURE 3.6: Internal resistance as a function of SoC

both stay close to constant values in the region between 0.8 and 0.2, hence constant values of r_0 and v_{oc} are considered to ease the calculation. Furthermore, $r_0(soc)$ and $v_{oc}(soc)$ are replaced by r_0 and v_{oc} respectively.

3.5.1.2 SoC dependent r_0 and v_{oc}

It has been observed that $r_0(soc)$ and $v_{oc}(soc)$ have direct relation and dependency on SoC and can be seen clearly in Fig. 3.6 & 3.7 respectively [56–58]. Detailed analysis of Fig. 3.6 & 3.7, show that when battery discharges, its resistance increases that causes increase in system losses and its output voltage decreases that causes decrease in battery output power [5, 37, 57, 59, 60]. This reason requires consideration of SoC dependent r_0 and v_{oc}.

Quartic equations are considered for v_{oc} and r_0 dependencies over SoC as mentioned in Eqn. (3.17).

$$v_{oc}(soc) = a_1(soc)^4 + a_2(soc)^3 + a_3(soc)^2 + a_4(soc) + a_5 \tag{3.17}$$

During discharging,

$$r_0(soc) = b_1(soc)^4 + b_2(soc)^3 + b_3(soc)^2 + b_4(soc) + b_5 \tag{3.18}$$

During charging,

$$r_0(soc) = c_1(soc)^4 + c_2(soc)^3 + c_3(soc)^2 + c_4(soc) + c_5 \tag{3.19}$$

Curve fitting tool is used to obtain the values of $a's$, $b's$ and $c's$, which are mentioned in v_{oc} and r_0 characteristics over SoC, as mentioned in Table. 3.3:

3.5.2 First order Thevenin Model

Detailed study of dynamic behaviour of lithium ion battery requires more accurate and reliable models, which not only increases the complexity of the system but

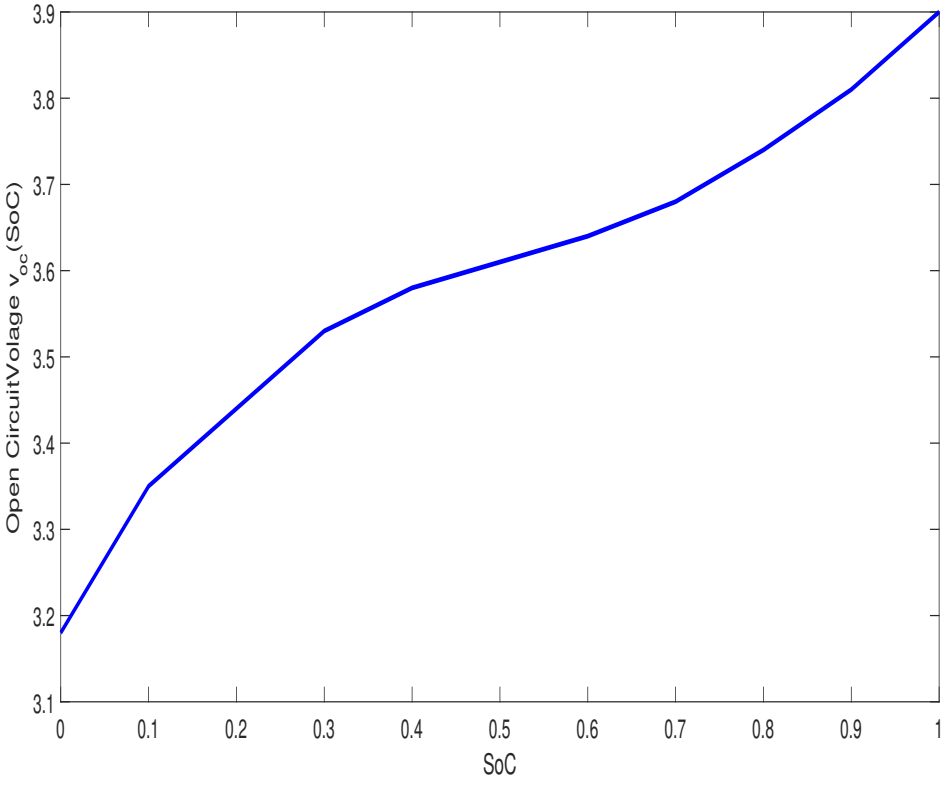

FIGURE 3.7: Open circuit voltage as a function of SoC

TABLE 3.3: Numerical values of co-efficients of quartic equation

Co-efficient	a_1	a_2	a_3	a_4	a_5
Value	-.67	2.8	-3.42	1.93	3.18
Co-efficient	b_1	b_2	b_3	b_4	b_5
Value	.0064	-.015	.012	-.0041	.0015
Co-efficient	c_1	c_2	c_3	c_4	c_5
Value	-.0063	.00625	.00506	-.00621	.00237

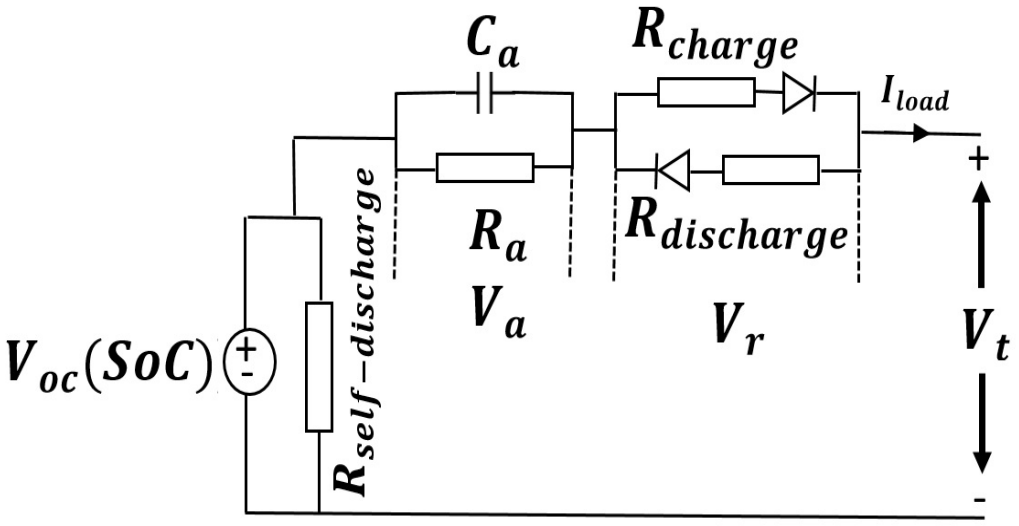

FIGURE 3.8: Circuit based battery First order Thevenin Model

also the computation time [39, 61]. Accuracy of the model increases by increasing number of resistor and capacitor (RC) networks, as shown in Fig. 3.8. First order Thevenin model is considered to cope with the trade-off between complexity and accuracy. Refer to Fig. 3.8, where $R_{self-discharge}$ represents the self losses during the period when charge is stored for a long time. $R_{self-discharge}$ increases 2% in every 10 months, so can be ignored whereas, R_a and C_a are the electrochemical diffusion resistance and capacitance respectively. R_{charge} and $R_{discharge}$ are the internal resistances of the battery during charging and discharging respectively and are already explained with detail in previous section.

Electrical behaviour of the battery is expressed as:

$$\dot{v}_a = \frac{-v_a}{R_a C_a} + \frac{I(t)}{C_a} \tag{3.20}$$

and

$$v_t = v_{oc} - v_a - v_r \tag{3.21}$$

where v_r is the voltage across R_i i.e., $R_{charge}/R_{discharge}$ and will be expressed differently during charging and discharging as:-

$$v_r = \begin{cases} I(t)R_{discharge} & \text{During discharging} \\ -I(t)R_{charge} & \text{During charging} \end{cases} \tag{3.22}$$

In this model, constant values of $r_0(soc)$ and $v_{oc}(soc)$ are considered based on the selected range of operation of SoC and to ease the calculations and are simply replaced with r_0 and v_{oc}. The discrete form of Eqn. (3.20) & (3.21) can be derived using zero order hold method (ZoH) [62] i.e., $H(z) = (1-z)^{-1}\mathcal{Z}(\mathcal{L}^{-1}\{\frac{H(s)}{s}\})$. where $H(s)$ is the Laplace transform [63], which will be calculated in next section to obtain $H(z)$ [64].

3.5.2.1 Laplace Transformation Method

By assuming $v_a = 0$ and by applying Laplace transformation to equation 3.20, we get:

$$sv_a(s) - v_a(0) = -\frac{1}{C_a R_a}v_a(s) + \frac{1}{C_a}I(s) \tag{3.23}$$

Procedure of getting Eqn. (3.23) from Eqn. (3.21) is explained in Appendix A.

$$H(s) = \frac{v_a(s)}{I(s)} = \frac{1}{C_a(s)(s + \frac{1}{R_a C_a})} \tag{3.24}$$

Discretized model using ZoH transformation and the corresponding solution is given as:-

$$H(z) = \frac{R_a(1 - e^{\frac{-\nabla t_d}{R_a C_a}})z^{-1}}{1 - z^{-1}e^{\frac{-\nabla t_d}{R_a C_a}}} \tag{3.25}$$

Transformation from Eqn. (3.24) to Eqn. (3.25) is explained in Appendix B with detail.

On taking inverse Z-transform of Eqn. (3.25), discrete form is written as:-

$$v_a^{k+1} = v_a^k e^{\frac{-\nabla t_d}{R_a C_a}} + R_a I(t)^k (1 - e^{\frac{-\nabla t_d}{R_a C_a}}) \tag{3.26}$$

where ∇t_d is the sampling interval and k is discrete time index and it is a non-negative integer number because estimation starts at $t = 0$ second.

P_{batt} in terms of P_{mech} is expressed as:

$$P_{batt}^k = \frac{P_{mech}^k}{\eta_m} = v_t^k I(t)^k = v_{oc}^k I^k - v_a^k I(t)^k - R_i^k I(t)^{2k} \tag{3.27}$$

Using quadratic formula, $I(t)^k$ is calculated and expressed as:

$$I(t)^k = \frac{v_{oc}^k}{2R_i^k} \left[\frac{v_a^k}{2R_i^k} - \sqrt{\frac{v_{oc}^{2(k)}}{4R_i^{2(k)}} - \frac{v_a^{2(k)}}{4R_i^{2(k)}} - \frac{v_a^k v_{oc}^k}{2R_i^{2(k)}} - \frac{P_{mech}^k}{\eta_m R_i^k}} \right] \tag{3.28}$$

where P_{mech} is:

$$P_{mech} = \frac{b_1 \tau v}{\eta_m} \tag{3.29}$$

where b_1 is the relation between linear velocity i.e., v and angular velocity i.e., ω, and expressed as:

$$b_1 = \frac{\gamma}{R_t} \tag{3.30}$$

SoC dynamics in discrete form is given as:-

$$soc^{k+1} - soc^k = \frac{-I(t)^k}{Q_{norm} \eta_{col}^{\text{sign}(I(t)^k)}} \tag{3.31}$$

Similarly DoD, is the Depth of Discharge and is the opposite of SoC and explains the used capacity, can be expressed as [65]:

$$DoD^{k+1} = 1 - SoC^{k+1} \tag{3.32}$$

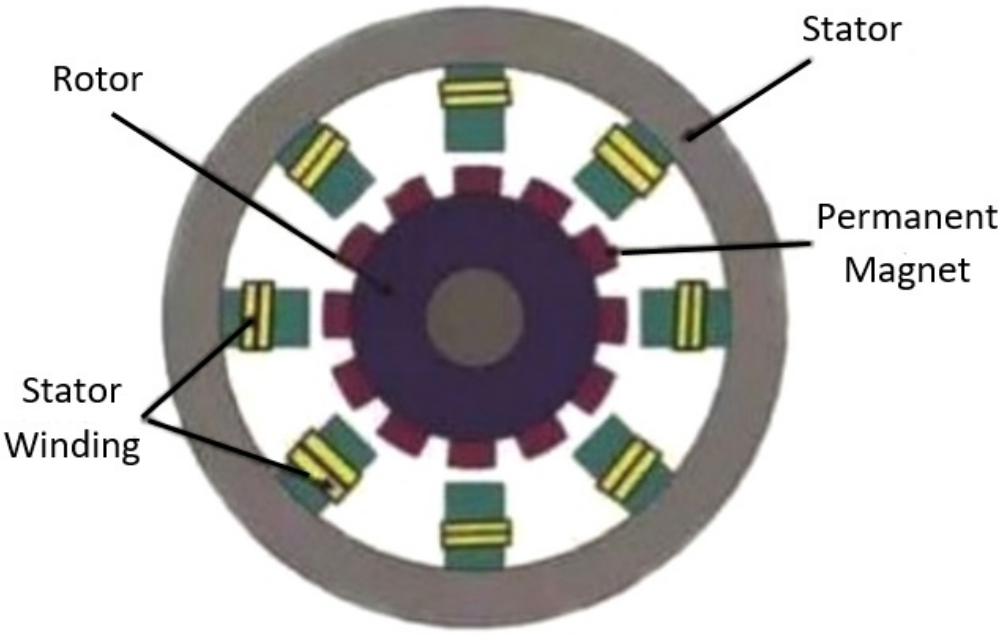

FIGURE 3.9: Basic working and components of PMSM [67]

3.6 Electric Motor (EM)

Electric Motor (EM) converts the electrical power coming from the battery to mechanical power or motor power, P_{mech}, through rectifier as shown in Fig. 3.11. Permanent Magnet Synchronous Motor (PMSM) is used here because of high speed and smooth torque requirements with low noise [66].

3.6.1 Permanent Magnet Synchronous Motor (PMSM)

PMSMs are the synchronous motors, which use permanent magnet to generate Electromotive Force (EMF), which is defined as the electric potential produced by changing the magnetic field. It contains rotor and stator, however instead of rotor windings, permanent magnet is used as rotor to generate magnetic field, as shown in Fig. 3.9. Furthermore, it provides stable output torque.

In this thesis, instead of using complete EM dynamics, its efficiency map is used [66]. Efficiency map is used to plot a contour of EM efficiency over torque and

angular speed breakpoints. It also describes the maximum efficiency for any torque/speed combination, which is used to find the feasibility of particular driving cycle using range of operating points. Efficiency map of used PMSM is as shown in Fig. 3.10, which shows the relation of τ vs ω with efficiency. Fig. 3.10 shows that there is a specific efficiency at every angular velocity vs torque breakpoints for both positive and negative values.

Based on the motor efficiency i.e., η_m is calculated from Fig. 3.10, the output of the battery is given to the EM and gets the output power as P_{mech}, shown in Fig. 3.11. If η_m is the motor efficiency, then it is expressed as:

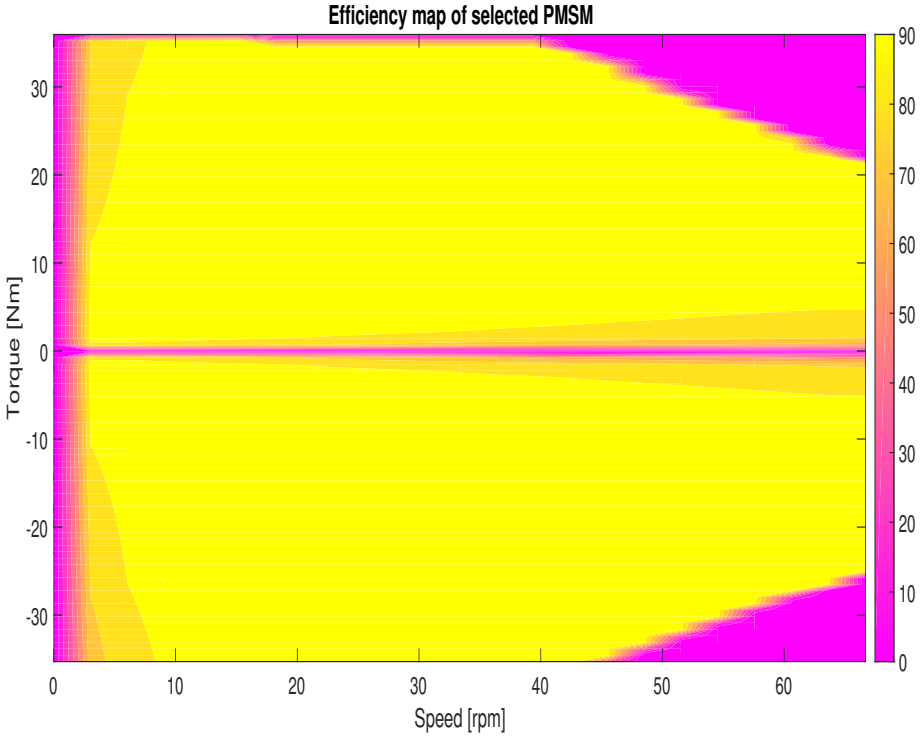

FIGURE 3.10: Efficiency map of used PMSM

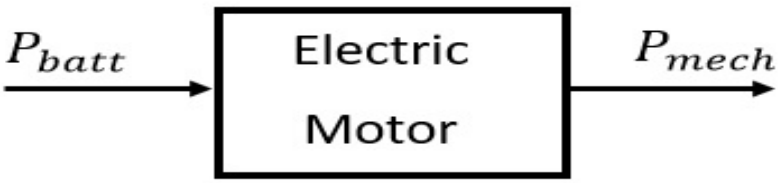

FIGURE 3.11: Relation between Battery Power and Motor Power

$$\eta_m = \begin{cases} \frac{P_{mech}}{P_{batt}} & \text{During motoring} \\ \frac{P_{batt}}{P_{mech}} & \text{During generation} \end{cases} \tag{3.33}$$

where, P_{mech} is already defined in Eqn. (3.29).

3.7 Chapter Summary

After the discussion on past efforts in range extension problem to EV and problem statement based on gap and research analysis in chapter 2, Chapter 3 mainly focuses on modeling of EV and battery. In the first part of this chapter, Mathematical modeling of EV based on energy analysis is discussed. Longitudinal dynamics of EV are derived with x and v as the states of the system. Furthermore, vehicle backward model for velocity tracking and forward model for powertrain limitations are discussed and derived. Modeling is extended to driver model based on Powertrain Limitation based Speed Guidance Model (PLSGM). In the second part of this chapter, two different mathematical models of battery are discussed. First zero order ideal model is discussed and secondly First order Thevenin model is discussed with SoC as the state of the system. Mathematical model of PMSM is discussed using its efficiency map.

Chapter 4

General Problem Formulation with Equality, Inequality and Interior Point Constraints

4.1 Introduction

Energy optimization during a trip can be achieved through different control techniques. OCP works on finding an admissible control trajectory $u : [ta, tb] \rightarrow \Omega \subseteq R^m$ that generates a corresponding state trajectory $x : [ta, tb] \rightarrow R^n$ such that the cost functional $J(u)$ is minimized. There are two major trajectory optimization strategies being applied in finding optimal trajectory problems; direct and indirect [68]. A direct technique works on finding direct numerical solutions by constructing a sequence of continually improving approximations to find the optimal solution, whereas, indirect method finds optimal solutions by analytically constructing and numerically solving the necessary and sufficient conditions of optimality [69].

DP provides the global optimal solution however, this technique suffers high computational time due to backward discretized model [18, 70]. PMP was proposed by Russian mathematician Lev Semenovich Pontryagin with his students in 1958 [71]. It can be regarded as one of the beginning of modern optimal control theory along

with DP [70, 72–74]. PMP works on finding the optimal control by satisfying the necessary conditions of optimality [6]. A control that is found using conditions of minimum principle is called extremal control. All extremal controls are not optimal however, optimal control is always an extremal. Several formulations of PMP exist and the use of particular design depends on the application [6, 72].

4.2 General Formulation of Pontryagin's Minimum Principle (PMP)

In this thesis, necessary conditions of optimality, also known as PMP, are used to find the optimal solution [72]. Different formulations are discussed, as:

1. The optimal control with fixed final state
2. The optimal control with free final state

4.2.1 The Optimal Control with Fixed Final State

The optimal control problem revolves around finding a piecewise continuous control $u : [t_0, t_f] \rightarrow \Omega$ such that the system with following constraints are satisfied. A Dynamic system is defined as:

$$\dot{x} = f(x(t), u(t), t) \tag{4.1}$$

where $t \in [t_0, t_f]$. Constraints on initial and final state are:

$$x(t_0) = x_0 \quad x(t_f) = x_f \tag{4.2}$$

with cost functional

$$J(u) = h(x(t_f), t_f) + \int_{t_0}^{t_f} L(x(t), u(t), t)dt \tag{4.3}$$

is minimized. $h(x(t_f), t_f)$ is the terminal cost and $L(x(t), u(t), t)$ is the running cost of the system.

Hamiltonian is formed as:

$$H(x(t), u(t), \lambda(t), \lambda_0(t)) = \lambda_0 L(x(t), u(t), t) + \lambda^T f(x(t), u(t), t) \tag{4.4}$$

Theorem 4.1. *Considering* $u^* : [t_0, t_f] \to \Omega$ *as optimal control, then there exist conditions, which need to be satisfied.*

$$\begin{aligned} \dot{x}(t) = \bigtriangledown_\lambda H = f(x^*(t), u^*(t), t) \\ x(t_0) = x_0 \\ x(t_f) = x_f \\ \lambda_0^*(t) = -\lambda \bigtriangledown_x H = -\left[\frac{\partial f}{\partial x}(x^*(t), u^*(t), t)\right]^T \lambda^*(t) \end{aligned} \tag{4.5}$$

If Hamiltonian $H(x^*(t), u(t), \lambda^*(t), \lambda_0^*(t),)$ *has global minimum then there exist additional condition*

$$H(x^*(t), u^*(t), \lambda^*(t), \lambda_0^*(t), t) \leq H(x^*(t), u(t), \lambda^*(t), \lambda_0^*(t), t) \tag{4.6}$$

If t_f *is free then there exists an additional condition*

$$H(x^*(t), u^*(t), \lambda^*(t), \lambda_0^*(t), t_f) = -\lambda_0^* \frac{\partial h(t_f)}{\partial t}(t_f) \tag{4.7}$$

Proof is given in [72].

4.2.2 The Optimal Control with Free Final State

Cost functional with free final state becomes:

$$J(u) = \int_{t_0}^{t_f} L(x(t), u(t), t) dt \tag{4.8}$$

$$H(x(t), u(t), \lambda(t), \lambda_0(t)) = \lambda_0 L(x(t), u(t), t) + \lambda^T f(x(t), u(t), t) \tag{4.9}$$

Theorem 4.2. *Considering $u^* : [t_0, t_f] \rightarrow \Omega$ as optimal control, then there exist conditions, which need to be satisfied [72].*

$$\begin{aligned} \dot{x}(t) = \bigtriangledown_\lambda H = f(x^*(t), u^*(t), t) \\ x(t_0) = x_0 \\ \lambda_0^*(t) = -\lambda \bigtriangledown_x H = -\left[\frac{\partial f}{\partial x}(x^*(t), u^*(t), t)\right]^T \lambda^*(t) \\ \lambda^* t_f = \bigtriangledown h(x^*(t_f), t_f) \end{aligned} \tag{4.10}$$

If Hamiltonian $H(x^*(t), u(t), \lambda^*(t), \lambda_0^*(t),)$ has global minimum with respect to $u \in \Omega$ then there exists condition

$$H(x^*(t), u^*(t), \lambda^*(t), \lambda_0^*(t), t) \leq H(x^*(t), u(t), \lambda^*(t), \lambda_0^*(t), t) \tag{4.11}$$

If t_f is free then there exists an additional condition

$$H(x^*(t), u^*(t), \lambda^*(t), \lambda_0^*(t), t_f) = -\lambda_0^* \frac{\partial h(x(t_f), t_f)}{\partial t}(t_f) \tag{4.12}$$

4.2.3 Necessary Conditions and Pontryagin's Minimum Principle

After the derivation of both fixed and free final value of state, the necessary conditions are defined as [6]:

$$\left.\begin{aligned} \dot{x}^* &= \frac{\partial H}{\partial \lambda}(x^*, u^*, \lambda^*, t) \\ \dot{\lambda}^* &= -\frac{\partial H}{\partial x}(x^*, u^*, \lambda^*, t) \\ 0 &= \frac{\partial H}{\partial u}(x^*, u^*, \lambda^*, t) \end{aligned}\right\} \text{for all } t \in [t_0, t_f] \tag{4.13}$$

These sets of necessary conditions of optimal control are called as PMP, as shown in Fig. 4.1 with sequence of steps as explained below.

1. Define cost functional.
2. Formulate Hamiltonian.

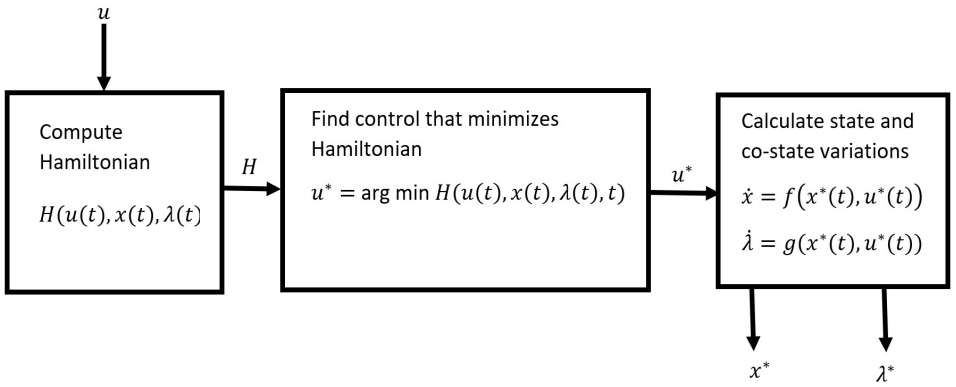

FIGURE 4.1: Flow of steps using PMP

3. Find control that minimizes Hamiltonian.

4. Find state and co-state variations.

5. Determine optimal state and co-state.

4.2.4 Boundary Conditions

Boundary conditions as discussed in previous section are state and time dependent i.e., fixed/free final state or fixed/free final time.

4.2.4.1 Two Point Boundary Value Problem (TPBVP)

Distributed conditions on both sides of the boundaries of the states are expressed as the boundary constraints on co-states as:

$$\dot{x}^* = f_1(x^*, u^*, \lambda^*, t)$$

$$\dot{\lambda}^* = f_2(x^*, u^*, \lambda^*, t) \tag{4.14}$$

$$x^*(t_0) = x_0 \tag{4.15}$$

$$\lambda^*(t_f) = \frac{\partial h}{\partial x}(x^*(t_f)) \tag{4.16}$$

if

$$x(t_f) = \text{fixed},\ \lambda(t_f) = \text{free} \tag{4.17}$$

TABLE 4.1: Boundary conditions using necessary conditions of optimality (PMP)

Problem	**Variables variations**	**Boundary conditions**
Fixed t_f Specified $x(t_f)$	$\delta x_f = \delta x(t_f) = 0$ $\delta t_f = 0$	$x^*(t_0) = x_0$ $x^*(t_f) = x_f$
Fixed t_f Free $x(t_f)$	$\delta x_f = \delta x(t_f)$ $\delta t_f = 0$	$x^*(t_0) = x_0$ $\frac{\partial h}{\partial x}(x^*(t_f)) - \lambda^*(t_f) = 0$
Free t_f Specified $x(t_f)$	$\delta x_f = 0$	$x^*(t_0) = x_0$ $x^*(t_f) = x_f$ $H(x^*t_f, u^*t_f, \lambda^*t_f, t_f)$ $+\frac{\partial h}{\partial t}(x^*(t_f), t_f) = 0$
Free t_f Free $x(t_f)$		$x^*(t_0) = x_0$ $\frac{\partial h}{\partial x}(x^*(t_f)) - \lambda^*(t_f) = 0$ $H(x^*t_f, u^*t_f, \lambda^*t_f, t_f)$ $+\frac{\partial h}{\partial t}(x^*(t_f), t_f) = 0$

where u^* is the control found in Eqn. (4.13).

Presence of specified values of either state or co-state at two boundaries i.e., t_0 and t_f make it a Two Point Boundary Value Problem (TPBVP) [75], which requires certain numerical iterative techniques to achieve these boundary conditions and are discussed in details in next section.

4.2.5 Numerical Iterative Techniques for TPBVP

These iterative techniques are used to satisfy these necessary conditions with some initial guess. The selection of a particular iterative method is based upon the final value of co-state, fixed or free. Two major classification of iterative techniques for this particular requirement are:

1. Shooting method
2. Gradient projection method

4.2.5.1 Shooting Method

Shooting method is an iterative technique used to find the solution of TPBVP for the case, where final value of state is fixed. In this case, there is no constraint on final value of it's co-state. Shooting method works in forward direction i.e., using an initial guess of a co-state to find the final value close to the desired specified value. If initial go close to the desired value, increment or decrement the previous initial guess will either come close to or go far away from the desired state value [5, 76, 77], as explained by a flowchart, shown in Fig. 4.2 and by following the steps explained below.

1. Initialize co-state i.e., $\lambda(0)$ with some initial guess.
2. Formulate Hamiltonian with respect to cost functional.
3. Find an optimal control with boundary conditions i.e., $x(t_f)$.

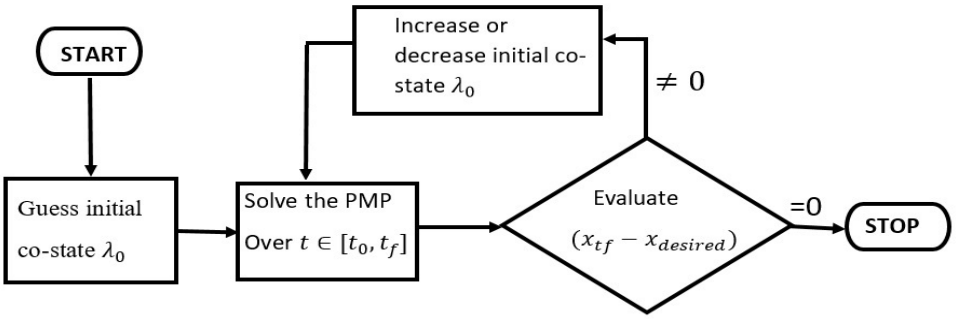

FIGURE 4.2: Flowchart of shooting method

4. If boundary conditions are satisfied within some reasonable range then quit the algorithm, otherwise adjusts initial conditions to restart the problem.

4.2.5.2 Gradient Projection Method

Gradient method is normally used to achieve the boundary conditions for the case in which final values of states are free, as in this case, the terminal boundary condition for the co-states are $\lambda(t_f) = \frac{\partial h}{\partial x}(x^*(t_f))$. To solve this problem, called gradient projection method is considered [6]. This approach solves the state equations forward in time and the co-state equations backward in time. The complete algorithm is summarized by the following steps and with flowchart in Fig. 4.3 [78].

1. Choose some random co-state boundary values i.e., λ_{t_f} and set the stopping criteria Δ_{max}.

2. Choose α between 0 and 1 and initialize iteration number $n = 1$ and set the stopping criteria ϵ_{max}.

3. Set $\Lambda^0(t) = 0$ for complete simulation time i.e., $t_0 < t \leq t_f$.

4. Solve the state equations forward in time.

5. Solve the co-state equation backward in time and update the effective co-state Λ^n :

$$\Lambda^n = (1 - \alpha)\lambda^{n-1} + \alpha\lambda^n$$

6. If $\epsilon = ||\Lambda^n - \lambda^{n||} < \epsilon_{max}$ then go to next step, otherwise again solve the state equations with new and updated effective co-state and repeat the procedure from step 4.

7. If $||x - x(T)|| < \Delta_{max}$ then quit the algorithm, otherwise again initialize the updated effective co-state and repeat the procedure from step 1.

The value of α is related to the convergence rate of the algorithm.

4.2.6 Interior Point Constraints

There are some other constraints, that do not exist on the boundaries e.g., at the start or end of trip, however, they occur at some intermediate points of a journey [22]. These constraints are called interior point constraints because of nature of their occurring time or maybe location as explained by example in Fig. 4.4. If the value of state is fixed at point where interior constraint has occurred, then that case can be solved using ordinary TPBVP e.g., Charging a vehicle during a trip, stopping at a signal during a red light. These both scenarios require velocity to be zero i.e., $v(t_i) = 0$ as shown in Fig. 4.3(a) and because of fixed velocity, its co-state can have any free value, as explained in Eqn. (4.17). However, if the value of velocity or another state is free e.g., traffic signal during green light, then this requires velocity of any value other than zero i.e., $v \neq 0$, as shown in Fig. 4.3(b). This scenario requires it's co-state to be of fixed value, as explained in Eqn. (4.14). This fixed value needs to be same at the end of $t = t_i$ and also at the start of $t = t_i$ [79]. This constraint on co-state cannot be handled using conventional TPBVP, as it can only solve the boundary constraints, as discussed in previous section. There is another iterative technique that can solve the problem including interior point constraints, known as Multi Point Boundary Value Problem (MPBVP).

4.2.6.1 Multi Point Boundary Value Problem

MPBVP is the extension of TPBVP along with continuity condition, which states that for a free value of state at some intermediate points of trip [80], it's co-state

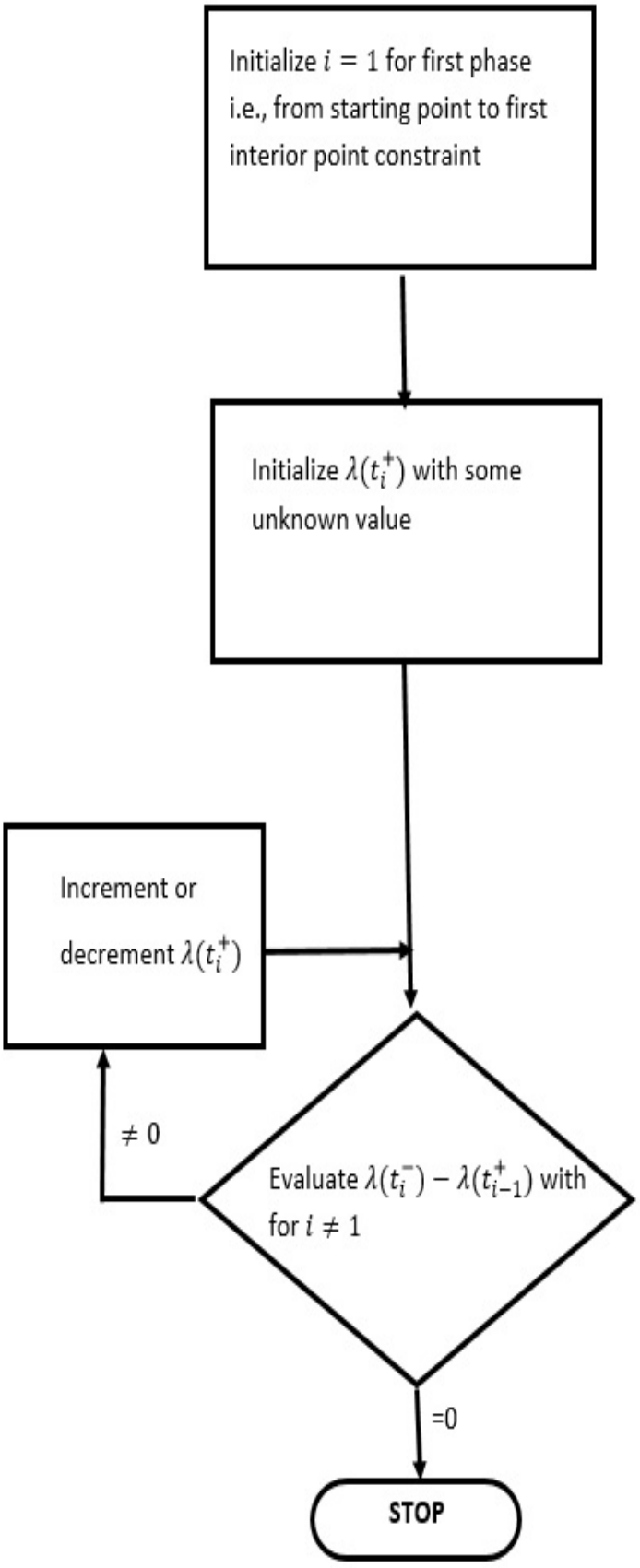

FIGURE 4.3: Flowchart of gradient method

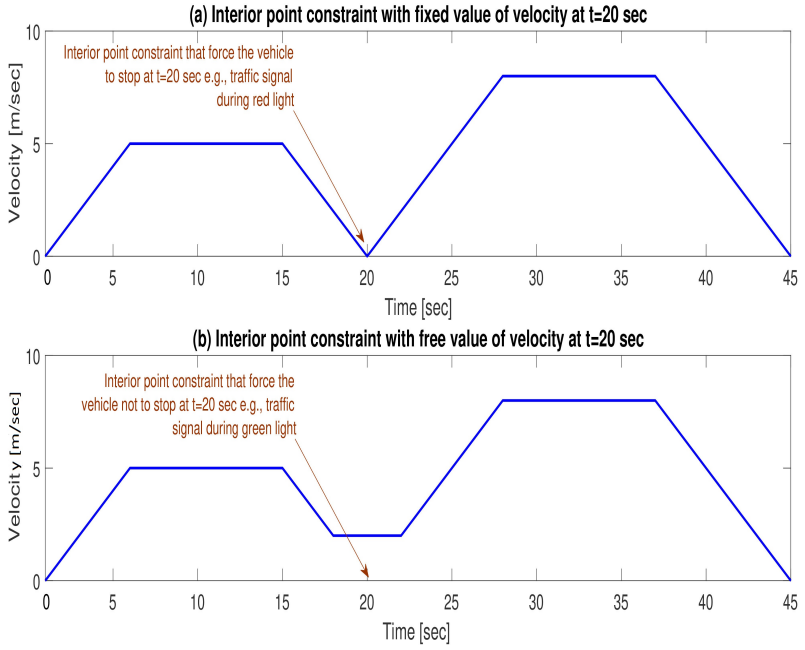

FIGURE 4.4: Scenario containing interior point constraint

must possess continuity just before and after the time a constraint occurs [79].This strategy converts the multi-phase problem into single phase. Mathematically it can be expressed as:

$$\lambda(t_i^+) \approx \lambda(t_i^-) \tag{4.18}$$

where t_i is some intermediate time at which constraint has occurred and t_i^+ is the instant just after a constraint has occurred and t_i^- is the instant just before a constraint has occurred.

4.2.7 Numerical Iterative Technique for MPBVP: Multiple Shooting Method

Multiple shooting method divides the problem into sub-phases, where a phase is a region between two interior point constraints [81]. Continuity of co-state is ensured using backward direction such that by adjusting the final value of co-state, its initial value becomes equal to the final value of co-state of previous phase. Moreover, final value of it's state at the junction point also becomes equal

to the desired value. Major steps of multiple shooting method are explained as below and in Fig. 4.5:

1. Transform the single phase trajectory into sub-phases.
2. Initialize the algorithm with some random value at the start of each sub-phase as unknown initial value of it's co-state i.e., $\lambda(t_0)$ to find final value of state and co-state.
3. Enforce continuity condition for required co-state at the phase junctions using final value of co-state $\lambda(t_{i^+})$ of next phase to find its initial value i.e., $\lambda(t_{i-1^-})$ of previous phase.

4.2.8 Inquality Constraints

Presence of inequality constraints, which are different from equality or boundary constraints, make the system more complex [82, 83]. However, there are certain limitations, which cannot be expressed as boundary, equality or interior point constraints e.g., current upper or lower bound in electrical devices, speed limits on the roads, etc.

4.2.8.1 Penalty Function Approach

System bounds can be handled once considered as inequality constraints in theory of optimal control. There are certain ways to tackle these constraints, out of which penalty function approach is one of the most adopted and reliable techniques [83–85]. Penalty function approach can be explained very easily by the example. There is a speed limit on the road of $70km/hr$. If a driver crosses the limit, he will pay a penalty of 50$. Penalty function approach works exactly the same way i.e., by converting the constrained optimization problem to unconstrained through the inclusion of artificially set penalty for violating the constraints. Mathematical

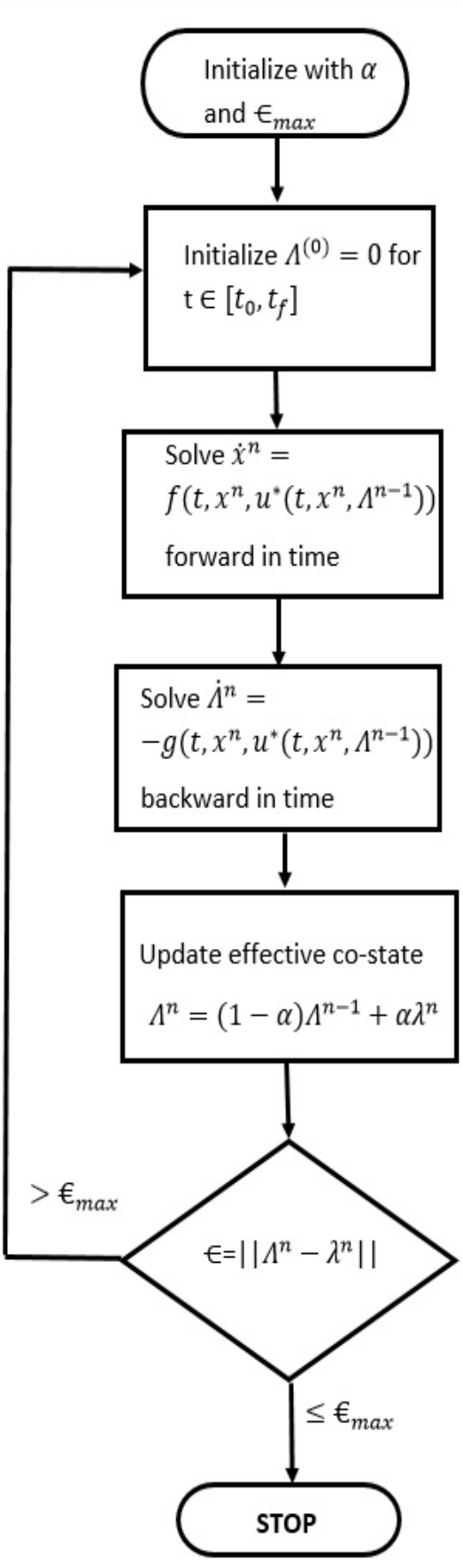

FIGURE 4.5: Flowchart of multiple shooting method

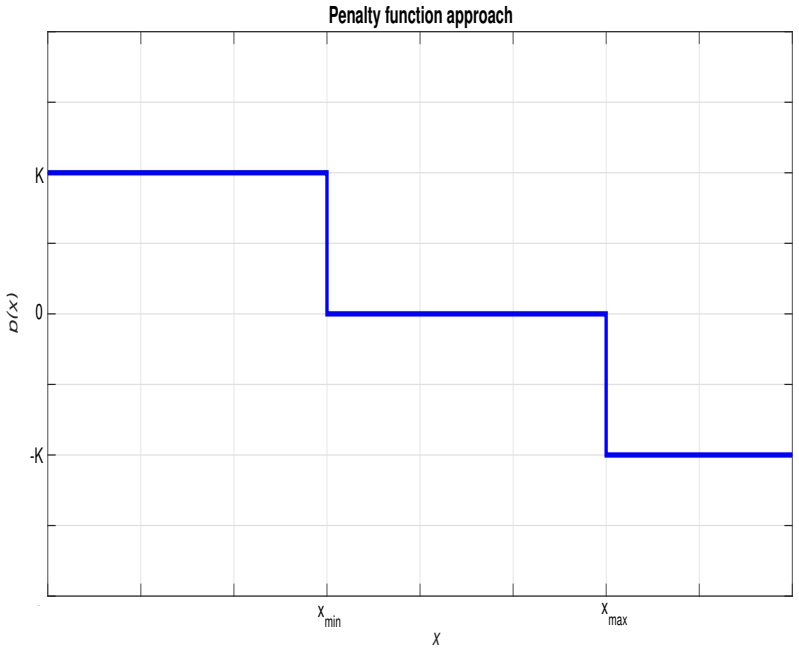

FIGURE 4.6: Penalty function approach

expression for the additive penalty function can be expressed as below and shown in Fig. 4.6.

$$P(x) = \begin{cases} 0 & \text{if} \quad x_{min} \leq x \leq x_{max} \\ K & \text{if} \quad x \leq x_{min} \\ -K & \text{if} \quad x \geq x_{max} \end{cases} \tag{4.19}$$

The value of K is determined using an iterative strategy or by hit and trial to ensure that the cost of Hamiltonian becomes high whenever the constrained trajectory hits the lower bound and becomes low when hits the upper bound and the penalty function is not active i.e., by adding a zero term to the Hamiltonian, when it stays within its allowable bounds.

4.3 Chapter Summary

In this chapter general formulation of PMP is discussed in details. Necessary conditions are derived for free and fixed final values of states and time. Furthermore concept of TPBVP is added to the problem of boundary constraints. Two different numerical iterative techniques are discussed i.e., shooting method and gradient

method. Problem is further extended to MPBVP and multiple shooting method for interior point constraints. Iterative algorithms are explained step by step for TPBVP and MPBVP. Penalty function approach is explained with an example for inequality constraints. These methods are applied in Chapter 5.

Chapter 5

Eco-driving Solution for Different Scenarios

5.1 Introduction

After the derivation of necessary conditions with initial, final, inequality and interior point constraints in chapter 4, this chapter focuses on eco-driving solutions for both unconstrained and constrained cases. Problem revolves around finding velocity profile that consumes optimal energy. Scenarios considered in this thesis are:

1. Unconstrained case.
2. Inclusion of zero order ideal battery model with charging/discharging limits and free final velocity.
3. Inclusion of zero order ideal battery model with charging/discharging limits and fixed final velocity.
4. Solution with traffic signals as interior point constraints.
5. Solution with traffic signals as interior point constraints and speed limits on the route.

6. Solution with traffic signals and SoC dependent v_{oc} and r_0.

7. Solution with traffic signals and leading vehicle constraints in an urban environment.

5.2 Unconstrained Case

In this case, simplest of the scenario is considered with only linear longitudinal dynamics of EV. Linear model of EV is considered with $h_2 = 0$ in Eqn. (3.8). No battery dynamics are considered in this case. Problem is formulated as:

$$\begin{cases} x(t_0) = 0 \;\; x(t_f) = D \\ v(0) = 0 \;\; v(t_f) = 0 \end{cases} \tag{5.1}$$

where $x(t_0)$ and $x(t_f)$ are the initial and final positions of EV respectively with D as the desired final position. Similarly $v(t_0)$ and $v(t_f)$ are the initial and final velocities respectively. Cost functional J is defined as:

$$J = \int_{t_0}^{t_f} \frac{b_1 \tau v}{\eta_m} \tag{5.2}$$

Goal of the problem in Eqn. (5.1) with cost functional in Eqn. (5.2) is to find the optimal velocity profile that consumes optimal battery energy with fixed initial and final positions and velocities of EV.

Hamiltonian of cost functional J is expressed using the procedure explained in Eqn. (4.9) and longitudinal linear dynamics as mentioned in Eqn. (3.8) & (3.10).

$$H = \frac{b_1 \tau v}{\eta_m} + \lambda_1(v) + \lambda_2(h_1 \tau \eta^{\text{sign}(\tau)} - h_0 - W) \tag{5.3}$$

Next step is to find optimal controls that minimize the Hamiltonian as defined above. There are two optimal controls i.e., accelerating and braking torques i.e., τ^+ and τ^- respectively. τ^+ is applied when sign(τ) is considered positive and τ^- is applied when sign(τ) is considered negative.

Accelerating torque is obtained as:

$$\tau^{+} = \frac{\partial H}{\partial \tau} = \frac{b_1 v}{\eta_m} + \lambda_2 h_1 \eta \tag{5.4}$$

Similarly braking torque is expressed as:

$$\tau^{-} = \frac{\partial H}{\partial \tau} = \frac{b_1 v}{\eta_m} + \frac{\lambda_2 h_1}{\eta} \tag{5.5}$$

Position state equation is expressed as:

$$\dot{x} = \frac{\partial H}{\partial \lambda_1} = v \tag{5.6}$$

Velocity state equation is expressed as:

$$\dot{v} = \frac{\partial H}{\partial \lambda_2} = h_1 \tau \eta^{\text{sign}(\tau)} - h_0 - W \tag{5.7}$$

Position co-state i.e., λ_1 is expressed as:

$$\dot{\lambda_1} = -\frac{\partial H}{\partial x} = 0 \tag{5.8}$$

Velocity co-state i.e., λ_2 is expressed as:

$$\dot{\lambda_2} = -\frac{\partial H}{\partial v} = -\frac{b_1 \tau}{\eta_m} - \lambda_1 \tag{5.9}$$

From the Table. 3.1, with fixed final values of states, its co-states will have free final values, if the terminal cost is zero i.e., $h(x(t_f), t_f) = 0$.

Numerical Iterative Technique:

In this case, as the final values of position and velocity are fixed, so with zero terminal cost, final values of their co-states are free i.e., they have no restriction. In this case shooting method is used, where with any initial guess on both co-states i.e., $\lambda_{1,2}(t_0)$ will take close to the desired location and final velocity close to zero. If the initial guess do not take close to the desired final values of states, increment or decrement the initial co-state values to achieve the close desired final states in next few iterations.

5.3 Inclusion of Zero Order Ideal Battery Model with Charging/Discharging Limits and Free Final Velocity

Battery acts as the sole source of electrical power to the system however, due to its limited capacity, it acts as one of the main components in deciding the range of EV. Moreover, battery life gets affected by many factors, out of which charge and discharge the battery beyond certain limits, accelerate its degradation process [86]. This limit is added using the inequality constraints to the optimization problem. Zero order ideal battery dynamic model as explained by Eqn. (3.14) is used in this case along with EV dynamics as explained in Eqn. (4.9). *SoC* dynamics for zero order ideal battery is expressed as [45]:

$$\dot{soc} = \frac{-I(t)}{Q_{norm}\eta_{col}^{\text{sign}(I(t))}} \tag{5.10}$$

where $I(t)$ is the current flowing through the battery and expressed as:

$$I(t) = \frac{v_{oc}}{2r_0} - \sqrt{\frac{v_{oc}^2}{4r_0^2} - \frac{P_{batt}}{r_0}} \tag{5.11}$$

Problem is formulated as:

$$\begin{cases} x(0) = 0 \;\; x(t_f) = D \\ v(0) = 0 \\ soc_{min} \leq soc \leq soc_{max} \end{cases} \tag{5.12}$$

Goal is to to reach the fixed destination using velocity profile that consumes optimal energy with fixed initial velocity, while keeping battery *SoC* within charging and discharging limits. Charging and discharging constraint is applied to limit the battery from getting fully charged and discharged. When the battery discharges beyond 20% and gets charged more than 80%, its output gets reduced. However, for this case, to ease the computation, r_0 and v_{oc} are taken as constant values.

Cost functional is same as defined in Eqn. (5.2). Corresponding Hamiltonian is expressed as:

$$H = \frac{b_1 \tau v}{\eta m} + \lambda_1 v + \lambda_2 (h_1 \tau \eta^{sign(\tau)} - h_2 v^2 - h_0 - W) + (\lambda_3 + P(SoC))(\frac{-I(t)}{Q_{norm} \eta_{col}^{sign(I(t))}}) \quad (5.13)$$

where $P(soc)$ is the penalty function to keep SoC within desired limits, as explained by Eqn. (4.19).

Accelerating torque, τ^+ is expressed as:

$$\tau^+ = \frac{\partial H}{\partial \tau} = \frac{f_1}{f_2} \quad (5.14)$$

where f_1 is expressed as:

$$f_1 = (\lambda_3 b_1 v + P(soc) b_1 v)^2 - (b_1 v v_{oc} Q_{norm} \eta_{col})^2 - (\lambda_2 h_1 \eta_m Q_{norm} \eta_{col} \eta v_{oc})^2 - (2 b_1 v \lambda_2 h_1 \eta_m Q_{norm}^2 \eta_{col}^2 v_{oc}^2) \quad (5.15)$$

Similarly f_2 is expressed as:

$$f_2 = -(4 r_0 b_1^3 v^3 Q_{norm}^2) - (4 r_0 Q_{norm}^2 \eta_m \eta_{col}^2 b_1 v \lambda_2^2 h_1^2 \eta^2) - (8 r_0 Q_{norm}^2 \eta_{col}^2 b 1^2 v^2 \lambda_2 h_1 \eta) \quad (5.16)$$

Braking torque, τ^- is expressed as:

$$\tau^- = \frac{\partial H}{\partial \tau} = \frac{f_3}{f_4} \quad (5.17)$$

where f_3 and f_4 are expressed as:

$$f_3 = (\lambda_3 b_1 v + P(soc) b_1 v)^2 - \frac{(b_1 v v_{oc} Q_{norm})}{\eta_{col}^2} - (\lambda_2 h_1 \eta_m Q_{norm} \eta_{col} \eta v_{oc})^2 - (2 b_1 v \lambda_2 h_1 \eta_m Q_{norm}^2 \eta_{col}^2 v_{oc}^2) \quad (5.18)$$

$$f_4 = -(4 r_0 b_1^3 v^3 Q_{norm}^2) - (\frac{4 r_0 Q_{norm}^2 \eta_m b_1 v \lambda_2^2 h_1^2}{\eta^2 \eta_{col}^2}) - (\frac{8 r_0 Q_{norm}^2 b_1^2 v^2 \lambda_2 h_1}{\eta \eta_{col}^2}) \quad (5.19)$$

In this case, nonlinear EV dynamics are considered as by Hamiltonian in (5.13):

$$\dot{x} = \frac{\partial H}{\partial \lambda_1} = v \tag{5.20}$$

$$\dot{v} = \frac{\partial H}{\partial \lambda_2} = h_1 \tau \eta^{\text{sign}(\tau)} - h_0 - h_2 v^2 - W \tag{5.21}$$

Similarly, co-state equations are given as:

$$\dot{\lambda}_1 = -\frac{\partial H}{\partial x} = 0 \tag{5.22}$$

$$\dot{\lambda}_2 = \frac{\partial H}{\partial v} = -\frac{b_1 \tau}{\eta m} - \lambda_1 + (\lambda_3 b_1 \tau + P(soc) b_1 \tau) \frac{1}{2\eta_m r_0 Q_{norm} \eta_{col}^{sign(I(t))} \sqrt{\frac{v_{oc}^2}{r_0^2} - \frac{b_1 \tau v}{\eta_m r_0}}} \tag{5.23}$$

$$\dot{\lambda}_3 = -\frac{\partial H}{\partial soc} = 0 \tag{5.24}$$

Numerical Iterative Technique:

In this case, as the final value of position is fixed, while final values of velocity and SoC are free. Shooting method with initial guess of position co-state $\lambda_1(t_0)$ will give the final value of position state because of free value of position co-state. Whereas, $\lambda_{2,3}(t_f) = 0$ will move in backward direction because of their fixed final values and zero terminal cost.

Complete algorithm is summarized by the following major steps.

1. Initialize position co-state i.e., λ_1 with some stopping criteria Δ_{max} for final value of states.
2. Select α between 0 and 1 with iteration number $n = 1$ and set the second stopping criteria ϵ_{max} for final value of co-states.
3. Set $\Lambda^0(t) = 0$ for $0 < t \leq T$.

4. Solve the three state equations and position co-state equation forward in time.

5. Solve the velocity and SoC i.e., $\lambda_{2,3}$ co-state equations backward in time and update the effective co-state $\Lambda^n_{2,3}$:
   $\Lambda^n_{2,3} = (1-\alpha)\lambda^{n-1}_{2,3} + \alpha\lambda^n_{2,3}$

6. If $\epsilon = ||\Lambda^n_{2,3} - \lambda^{n||}_{2,3} < \epsilon_{max}$ satisfies then move forward otherwise, again solve the state equations with updated effective co-state and repeat the procedure from step 4.

7. If $||x - x(t_f)|| < \Delta_{max}$ satisfies then quit the algorithm, otherwise start with new initial guess of position co-state and repeat the procedure from step 1 with new value of α.

The value of α is related to the convergence rate of the algorithm.

5.4 Inclusion of Zero Order Ideal Battery Model with Charging/Discharging Limits and Fixed Final Velocity

In this case, along with initial velocity, the final velocity of EV is also fixed i.e., $v(t_f) = 0$. Optimal controls, states and co-state equations are the same as derived in previous scenario.
Problem becomes [55]:

$$\begin{cases} x(0) = 0 \;\; x(t_f) = D \\ v(0) = 0 \;\; v(t_f) = 0 \\ soc_{min} \leq soc \leq soc_{max} \end{cases} \tag{5.25}$$

The basic difference between problem defined in Eqn. (5.1) & Eqn. (5.13) is the numerical iterative technique to achieve the boundary conditions due to fixed

final velocity. In this case, as the final values of position and velocity are fixed, while final value of SoC is free. Shooting method with initial guess on position and velocity co-states $\lambda_{1,2}(t_0)$ will give the final value of position and velocity states. However, with $\lambda_3(t_f) = 0$, steepest gradient method will move the SoC in backward direction. The complete algorithm is summarized as:

1. Initialize position and SoC co-states with some random guess i.e., $\lambda_{1,2}(t_0)$ and some stopping criteria Δ_{max} for the final values of states.
2. Select α between 0 and 1 and set the iteration number $n = 1$ and stopping criteria ϵ_{max} for SoC co-state final value.
3. Set $\Lambda^0(t) = 0$ for $0 < t \leq T$.
4. Solve the three state equations, position and velocity co-state equations forward in time.
5. Solve SoC co-state equation i.e., λ_3 backward in time and update effective co-state $\Lambda_3^n := (1-\alpha)\lambda_3^{n-1} + \alpha\lambda_3^n$
6. If $\epsilon = ||\Lambda_3^n - \lambda_3^{n||} < \epsilon_{max}$ satisfies then move forward otherwise again solve the state equations with updated effective co-state and repeat the procedure.
7. If $||x - x(t_f)||\&||v - v(t_f)|| < \Delta_{max}$ satisfies then quit the algorithm, otherwise start with new initial guess.

The value of α is related to convergence rate of the algorithm.

5.5 Solution with Traffic Signals as Interior Point Constraints

Interior point constraints are those constraints that do not occur at the boundaries, rather they appear at some intermediate points of trip, as explained in previous chapter. They pose an adverse effect on numerical technique, as they cannot be

handled using TPBVP. Cost functional is same as defined in Eqn. (5.2). Traffic signals are considered as interior point constraints. Goal is to cross these signals during their green duration i.e., when driver does not need to stop there.

Goal is to find optimal velocity profile that can reach a signal during their green light time and following other constraints. Traffic signals timings are assumed to be known in advance using V2I communication protocol. Initial and final velocity and positions are fixed along with fixed signals locations.

Problem formulation for this case is expressed as [87]:

$$\begin{cases} x(t_0) = 0 \;\; x(t_i) = x_i \;\text{ and }\; x(t_f) = D \\ v(t_0) = 0 \;\; v(t_f) = 0 \\ soc_{min} \leq soc \leq soc_{max} \end{cases} \tag{5.26}$$

Hamiltonian with interior point and other constraints is expressed as:

$$\begin{aligned} H = & \left[\left(\frac{b_1 \tau v}{\eta_m} \right) + (\lambda_1 v) + \left(\lambda_2 (h_1 \tau \eta^{\text{sign}(\tau)} - h_2 v^2 - h_0 - W) \right) \right. \\ & + \left((\lambda_3)(\frac{-I(t)}{Q_{norm} \eta_{col}^{\text{sign}(I(t))}}) \right) + \left(\frac{\beta_1}{2} (x(t_f) - x_{des,t_f})^2 \right) \\ & + \left(\mu_1 (\max(0, SoC_{min} - SoC)^2 + \max(0, SoC - SoC_{max})^2) \right) \\ & \left. + \left(\frac{\beta_2}{2} v(t_f)^2 \right) + \left(\frac{\rho_i}{2} \sum_{i=1}^{5} (x_{ti} - x_{des,ti})^2 \right) \right] \end{aligned} \tag{5.27}$$

where μ_1 is the penalty factor to keep SoC between desired bounds. $\lambda_{1,2,3}$ are the three co-states. $\frac{\beta_1}{2}(x(t_f) - x_{des,t_f})^2$ is the position terminal constraint and $\frac{\beta_2}{2} v(t_f)^2$ is the velocity terminal constraint. $\frac{\rho_i}{2} \sum_{i=1}^{5} [(x_{ti} - x_{des,ti})^2]$ are the 5 interior point constraints that show 5 traffic signals on the route.

Accelerating torque i.e., τ^+, is the optimal control that minimizes Hamiltonian, when sign(η) and sign($I(t)$) are positive.

It is expressed as

$$\begin{aligned} \tau^+ = & \left[\frac{b_1 v}{4 r_0 \eta_m v_{oc}^2} \right] - \left[\left(\frac{\lambda_3^2 b_1 v}{Q_{norm}^2 \eta_m \eta_{col}^2} \right) \right. \\ & \left. \left(\frac{1}{(\frac{b_1 v}{\eta_m})^2 + (\frac{\lambda_2 h_1}{\eta^2}) + (\frac{2 b_1 v \lambda_2 h_1}{\eta})} \right) \right] \end{aligned} \tag{5.28}$$

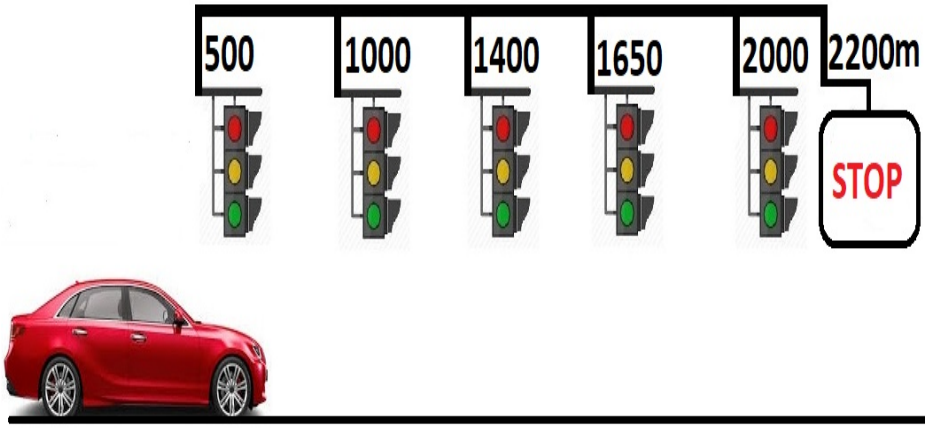

FIGURE 5.1: Location of Five Signals with Destination Point

Similarly braking torque i.e., τ^- is the optimal control that minimizes Hamiltonian, when sign(η) and sign($I(t)$) are negative. It is expressed as

$$\tau^- = \left[\frac{b_1 v}{4r_0\eta_m v_{oc}^2}\right] - \left[\left(\frac{\lambda_3^2 b_1 v \eta_{col}^2}{Q_{norm}^2 \eta_m}\right) \left(\frac{1}{(\frac{b_1 v}{\eta_m})^2 + (\lambda_2 h_1 \eta^2) + (2b_1 v \lambda_2 h_1 \eta)}\right)\right] \tag{5.29}$$

Co-state equations are obtained as:

$$\dot{\lambda}_1 = -\frac{\partial H}{\partial x} = -\beta_1(x(t_f) - x_{des,t_f}) - \rho_i \sum_{i=1}^{5}(x_{ti} - x_{des,ti}) \tag{5.30}$$

$$\dot{\lambda}_2 = -\frac{\partial H}{\partial v} = \left[\left(-\frac{b_1\tau}{\eta_m}\right) - \lambda_1 + 2\lambda_2 h_2 v - \beta_2 v(t_f) + \left(\frac{\lambda_3 b_1 \tau}{\eta_m r_0 Q_{norm} \eta_{col}^{\text{sign}(I(t))} (\frac{v_{oc}^2}{4r_0^2} - \frac{b_1 \tau v}{\eta_m r_0})^{\frac{1}{2}}}\right)\right] \tag{5.31}$$

with constant values of r_0 and v_{oc}, $\dot{\lambda}_3$ comes out to be

$$\dot{\lambda}_3 = -\frac{\partial H}{\partial soc} = [2\mu_1(\max(0, soc_{min} - soc)) - 2\mu_2(\max(0, soc - soc_{max}))] \tag{5.32}$$

State equations are same as expressed in previous scenario.

Refer to Fig. 5.1, which shows the exact position of each traffic signal on the route and explains that this is the scenario related to multi-phase problem, where phase

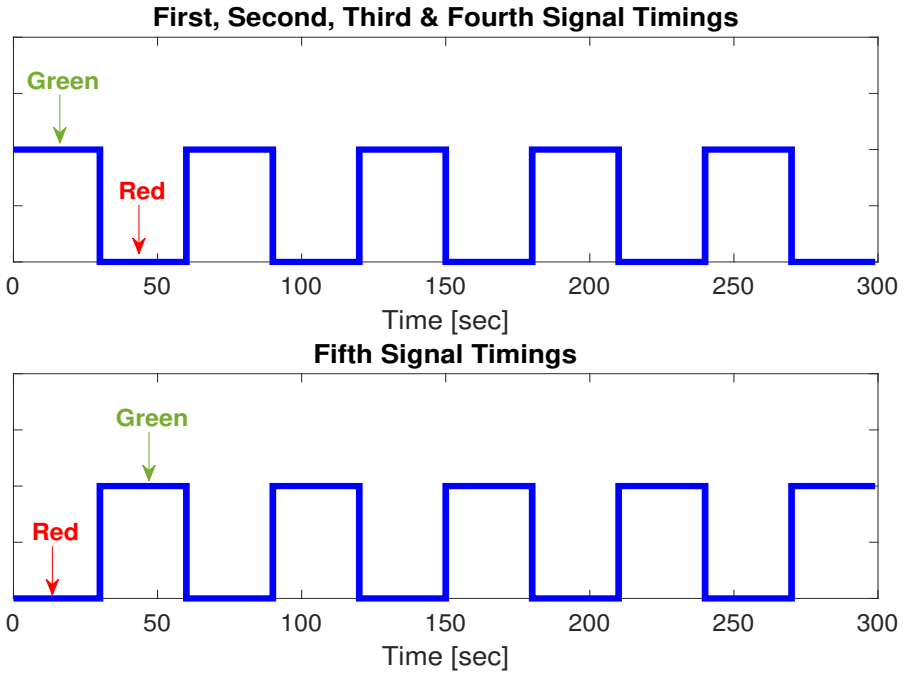

FIGURE 5.2: Green and Red Duration of five signals on the route

is a region from starting point to first traffic signal and so on. Main objective is to cross these signals when they are green. Major steps to decide the reaching time at a coming signal are:-

1. Get a distance between upcoming signal and current location i.e., dis.
2. Get information about signal red and green time using V2I protocols.
3. Calculate optimal velocity i.e., v_{opt} for the unconstrained case.
4. Assume it as unconstrained case that is no signal is there and calculate time to reach at signal location using optimal velocity as calculated in previous step using $t = \frac{dis}{v_{opt}}$.
5. If calculated time i.e., t can take to the signal during green light and also other constraints are followed, then follow the route otherwise take next green as the updated t.

Signals timings can be easily available using different V2I protocols. Fig. 5.2 shows the green and red light timings of five signals. Green light duration of five

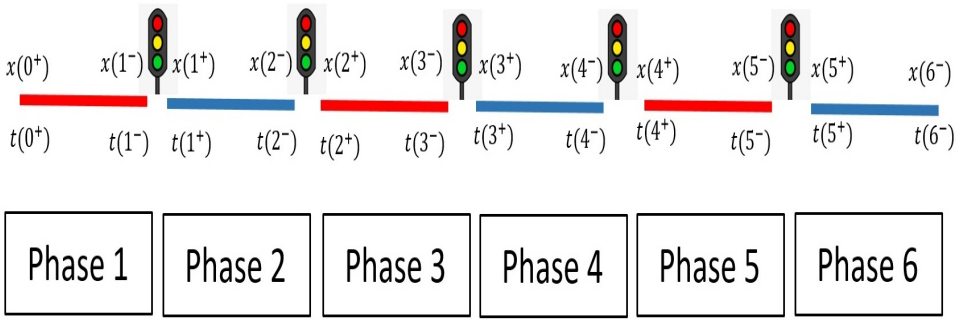

FIGURE 5.3: Continuity at the Junctions (Five traffic signals) for Multi-phase Problem

TABLE 5.1: Continuity Condition at the Junction Points

Junction No	**Continuity Condition**
Junction 1	$\lambda_{2,3}(t_1^-) \approx \lambda_{2,3}(t_1^+)$
Junction 2	$\lambda_{2,3}(t_2^-) \approx \lambda_{2,3}(t_2^+)$
Junction 3	$\lambda_{2,3}(t_3^-) \approx \lambda_{2,3}(t_3^+)$
Junction 4	$\lambda_{2,3}(t_4^-) \approx \lambda_{2,3}(t_4^+)$
Junction 5	$\lambda_{2,3}(t_5^-) \approx \lambda_{2,3}(t_5^+)$

signals are mentioned in seconds in Eqn. (5.33).

$$\begin{aligned} \text{signal1} &= [...60-90, 120-150, 180-210, ...] \\ \text{signal2} &= [...60-90, 120-150, 180-210, ...] \\ \text{signal3} &= [..120-150, 180-210, 240-270..] \\ \text{signal4} &= [..120-150, 180-210, 240-270..] \\ \text{signal5} &= [..150-180, 210-240, 270-300..] \end{aligned} \tag{5.33}$$

As explained in previous chapter that MPBVP adds another condition to TPBVP, which ensures smoothness and continuity of co-state with free final value of its state just before and after the junction i.e., where an interior constraint has occurred, known as continuity or corner condition. In this scenario, velocity and SoC are free at the junction points, so their co-states must possess continuity at the signals. Fig. 5.3 and Table. 5.1 explain the MPBVP with continuity condition at the junction points. To achieve, continuities of the two co-states at the junctions, multiple shooting technique is used. Steps of multiple shooting technique are:

1. Transform the single phase trajectory into sub-phases.

2. Initialize the algorithm with some random value at the start of each sub-phase as unknown initial value of position co-state i.e., $\lambda(t_0)$ to find final value of position.

3. Enforce continuity condition for velocity and SoC co-states at the phase junctions using final values of their co-states i.e., $\lambda_{2,3}(t_{i^+})$ of next phase to find its initial values i.e., $\lambda_{2,3}(t_{i-1^-})$ of previous phase.

5.5.1 Complete Algorithm

Complete algorithm is summarized as:

1. Initialize the algorithm with $i = 0$.

2. Increment i by 1.

3. Choose initial value of λ_1 and define location of ith signal $x(t_{i^-,des})$.

4. Choose α between 0 and 1 with iteration number i.e., $n = 1$ and some stopping criteria ϵ_{max} for co-states.

5. Set $\Lambda^0(t) = 0$ for $t_{i-1^+} < t \leq t_{i^-}$.

6. Define initial values of all the states to solve the state equations and first co-state equation forward in time.

7. Define final value of velocity and SoC co-states to solve the $\lambda_{2,3}$ backward in time and update effective co-state $\Lambda^n = (1-\alpha)\Lambda^{n-1} + \alpha\lambda^n$.

8. Check if $\epsilon = ||\Lambda^n - \lambda^n|| < \epsilon_{max}$ satisfies then go to step 10 for satisfying co-state convergence for $i = 1$ and for $i = 2, 3, 4, 5, 6$ go to step 9 for continuity condition. If $\epsilon = ||\Lambda^n - \lambda^n|| \not< \epsilon_{max}$ do not satisfy for co-states convergence, go back to step 7 with updated effective co-state.

9. If $\lambda_{2,3}(t_{i^+}) \approx \lambda_{2,3}(t_{i^-})$ satisfies, go to next step, otherwise go back to step 7.

10. If $x(t_{i^-}) = x(t_{i^-,des}) < \Delta_{max}$ satisfies then move to next step either to terminate the algorithm or to move to next junction. Otherwise, repeat the procedure until continuity achieved.

11. If $i = 6$, stop the algorithm, otherwise repeat the procedure.

Value of α will help in converging the scheme as fast as possible.

5.6 Solution with Traffic Signals as Interior Point Constraints and Speed Limits on the Route

Speed limits are applied on the roads for safety purposes. Traffic rules are made to facilitate the public not only sitting in the cars but also for the pedestrians. These speed limits play very critical role when looking from energy consumption perspective as well. Therefore, in this scenario along with traffic signals and battery constraints, speed limits are also considered. Problem becomes:

$$\begin{cases} x(t_0) = 0 \;\; x(t_i) = x_i \;\text{ and }\; x(t_f) = D \\ v(t_0) = 0 \;\; v(t_f) = 0 \\ soc_{min} \leq soc \leq soc_{max} \\ v_{min} \leq v \leq v_{max} \end{cases} \tag{5.34}$$

Hamiltonian with all these constraints is expressed as:

$$\begin{aligned} H = \Bigg[& \left(\frac{b_1 \tau v}{\eta_m}\right) + (\lambda_1 v) + \left(\lambda_2 (h_1 \tau \eta^{\text{sign}(\tau)} - h_2 v^2 - h_0 - W)\right) \\ & + \left((\lambda_3)(\frac{-I(t)}{Q_{norm}\eta_{col}^{\text{sign}(I(t))}})\right) + \left(\frac{\beta_1}{2}(x(t_f) - x_{des,t_f})^2\right) \\ & + \left(\mu_1(\max(0, v_{min} - v)^2 + \max(0, v - v_{max})^2)\right) \\ & + \left(\mu_2(\max(0, soc_{min} - soc)^2 + \max(0, soc - soc_{max})^2)\right) \\ & + \left(\frac{\beta_2}{2} v(t_f)^2\right) + \left(\frac{\rho_i}{2} \sum_{i=1}^{5} (x_{ti} - x_{des,ti})^2\right) \Bigg] \end{aligned} \tag{5.35}$$

where μ_1 and μ_2 are the penalty factors to keep v and SoC between defined bounds. $\frac{\beta_1}{2}(x(t_f) - x_{des,t_f})^2$ is the terminal position constraint and $\frac{\beta_2}{2}v(t_f)^2$ is the velocity terminal constraint. $\frac{\rho_i}{2}\sum_{i=1}^{5}[(x_{ti} - x_{des,ti})^2]$ are the interior point constraints that show 5 traffic signals on the route.

Accelerating torque i.e., τ^+, is expressed as:

$$\tau^+ = \left[\frac{b_1 v}{4r_0\eta_m v_{oc}^2}\right] - \left[\left(\frac{\lambda_3^2 b_1 v}{Q_{norm}^2\eta_m\eta_{col}^2}\right) \left(\frac{1}{(\frac{b_1 v}{\eta_m})^2 + (\frac{\lambda_2 h_1}{\eta^2}) + (\frac{2b_1 v\lambda_2 h_1}{\eta})}\right)\right] \tag{5.36}$$

Similarly braking torque i.e., τ^- is the optimal input that maximizes Hamiltonian, when sign(η) and sign($I(t)$) are negative.

It is expressed as

$$\tau^- = \left[\frac{b_1 v}{4r_0\eta_m v_{oc}^2}\right] - \left[\left(\frac{\lambda_3^2 b_1 v\eta_{col}^2}{Q_{norm}^2\eta_m}\right) \left(\frac{1}{(\frac{b_1 v}{\eta_m})^2 + (\lambda_2 h_1\eta^2) + (2b_1 v\lambda_2 h_1\eta)}\right)\right] \tag{5.37}$$

Co-state equations are obtained as:

$$\dot{\lambda}_1 = -\frac{\partial H}{\partial x} = -\beta_1(x(t_f) - x_{des,t_f}) - \rho_i\sum_{i=1}^{5}(x_{ti} - x_{des,ti}) \tag{5.38}$$

$$\begin{aligned}\dot{\lambda}_2 = -\frac{\partial H}{\partial v} = \Bigg[\left(-\frac{b_1\tau}{\eta_m}\right) - \lambda_1 + 2\lambda_2 h_2 v - \beta_2 v(t_f) \\ + \left(\frac{\lambda_3 b_1\tau}{\eta_m r_0 Q_{norm}\eta_{col}^{\text{sign}(I(t))}(\frac{v_{oc}^2}{4r_0^2} - \frac{b_1\tau v}{\eta_m r_0})^{\frac{1}{2}}}\right) \\ + (2\mu_1(\max(0, v_{min} - v)) - 2\mu_1(\max(0, v - v_{max})))\Bigg]\end{aligned} \tag{5.39}$$

$$\begin{aligned}\dot{\lambda}_3 = -\frac{\partial H}{\partial soc} = [2\mu_2(\max(0, soc_{min} - soc)) \\ -2\mu_2(\max(0, soc - soc_{max}))]\end{aligned} \tag{5.40}$$

State equations are same as expressed in previous scenario.

Complete algorithm adds another step to the procedure explained in previous case that speed limits constraint also need to be followed using the penalty function.

5.7 Solution with Traffic Signals and SoC Dependent v_{oc} and r_0

In previous cases, constant values of v_{oc} and r_0 were assumed, however, for realistic scenario, v_{oc} and r_0 are SoC dependent and this dependency needs to be considered to see the change in battery losses and output power [87].
Traffic signal timings are as mentioned in Eqn. (5.41).

$$\begin{aligned}
\text{signal1} &= [..90-120, 150-180, 210-240..] \\
\text{signal2} &= [..120-150, 180-210, 240-270..] \\
\text{signal3} &= [..210-240, 270-300, 330-360..] \\
\text{signal4} &= [..240-270, 300-330, 360-390..] \\
\text{signal5} &= [..150-180, 210-240, 270-300..]
\end{aligned} \tag{5.41}$$

Problem for this case is formulated as:

$$\begin{cases}
x(0) = 0 \;\; x(t_i) = x_i \;\text{ and }\; x(t_f) = D \\
v(0) = 0 \;\; v(t_f) = 0 \;\text{ for case 2: }\; v(t_i) = 0 \\
soc_{min} \leq soc \leq soc_{max} \\
v_{min} \leq v \leq v_{max}
\end{cases} \tag{5.42}$$

Hamiltonian for this case is defined as:

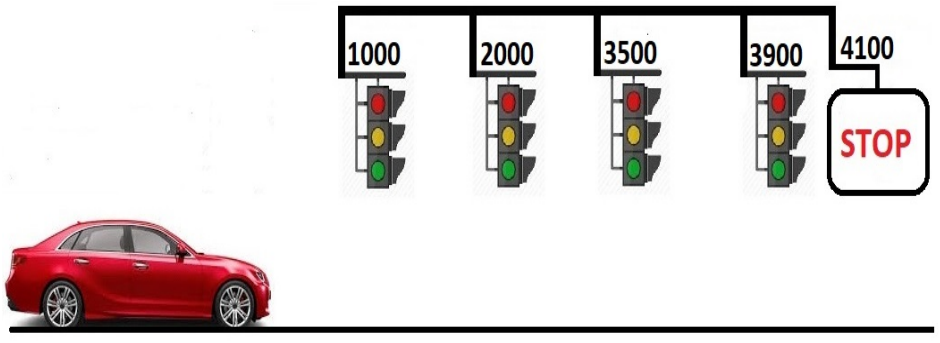

FIGURE 5.4: Location of four signals with destination point

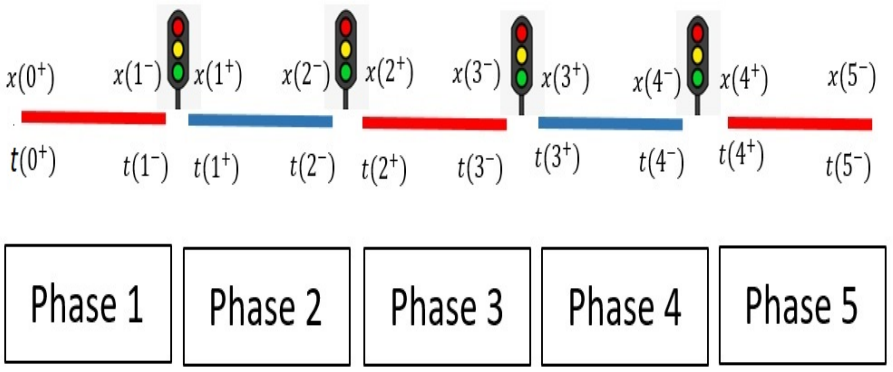

FIGURE 5.5: Continuity at the Junctions (Four traffic signals) for Multi-phase Problem

$$
\begin{aligned}
H = & \left[\left(\frac{b\tau v}{\eta_m}\right) + (\lambda_1 v) + \left(\lambda_2(h_1\tau\eta^{\text{sign}(\tau)} - h_2 v^2 - h_0 - W)\right)\right. \\
& + \left((\lambda_3)(\frac{-I(t)}{Q_{norm}\eta_{col}^{\text{sign}(I(t))}})\right) + \left(\frac{\beta_1}{2}(x(t_f) - x_{des,t_f})^2\right) \\
& + \left(\mu_1(\max(0, v_{min} - v)^2 + \max(0, v - v_{max})^2)\right) \\
& + \left(\mu_2(\max(0, soc_{min} - soc)^2 + \max(0, soc - soc_{max})^2)\right) \\
& \left. + \left(\frac{\beta_2}{2}v(t_f)^2\right) + \left(\frac{\rho_i}{2}\sum_{i=1}^{4}(x_{ti} - x_{des,ti})^2\right)\right]
\end{aligned} \tag{5.43}
$$

Optimal accelerating and braking torques are expressed as:

$$
\begin{aligned}
\tau^+ = & \left[\frac{bv}{4r_0(soc)\eta_m v_{oc}^2(soc)}\right] - \left[\left(\frac{\lambda_3^2 bv}{Q_{norm}^2\eta_m\eta_{col}^2}\right)\right. \\
& \left.\left(\frac{1}{(\frac{bv}{\eta_m})^2 + (\frac{\lambda_2 h_1}{\eta^2}) + (\frac{2bv\lambda_2 h_1}{\eta})}\right)\right]
\end{aligned} \tag{5.44}
$$

$$
\begin{aligned}
\tau^- = & \left[\frac{bv}{4r_0(soc)\eta_m v_{oc}^2}\right] - \left[\left(\frac{\lambda_3^2 bv\eta_{col}^2}{Q_{norm}^2\eta_m}\right)\right. \\
& \left.\left(\frac{1}{(\frac{v}{\eta_m})^2 + (\lambda_2 h_1\eta^2) + (2bv\lambda_2 h_1\eta)}\right)\right]
\end{aligned} \tag{5.45}
$$

Co-state equations i.e., position λ_1, velocity λ_2 and SoC λ_3 are expressed as:

$$
\dot{\lambda}_1 = -\frac{\partial H}{\partial x} = -\beta_1(x(t_f) - x_{des,t_f}) - \rho_i\sum_{i=1}^{4}(x_{ti} - x_{des,ti}) \tag{5.46}
$$

$$\dot{\lambda}_2 = -\frac{\partial H}{\partial v} = \Bigg[\left(-\frac{b\tau}{\eta_m}\right) - \lambda_1 + 2\lambda_2 h_2 v - \beta_2 v(t_f) + \left(\frac{\lambda_3 b\tau}{\eta_m r_0(soc) Q_{norm} \eta_{col}^{\text{sign}(I(t))} (\frac{v_{oc}^2(soc)}{4r_0^2(soc)} - \frac{b_1 \tau v}{\eta_m r_0(soc)})^{\frac{1}{2}}}\right) + (2\mu_1(\max(0, v_{min} - v)) - 2\mu_1(\max(0, v - v_{max})))\Bigg] \tag{5.47}$$

$$\dot{\lambda}_3 = -\frac{\partial H}{\partial soc} = [2\mu_2(\max(0, soc_{min} - soc)) - 2\mu_2(\max(0, soc - soc_{max}))] - \lambda_3 f_5(soc) + \lambda_3 f_6(soc) \tag{5.48}$$

where $f_5(soc)$ and $f_6(soc)$ are defined as:

$$f_5(soc) = \frac{\frac{\partial(\frac{v_{oc}(SoC)}{2r_0(SoC)})}{\partial soc}}{2Q_{norm}\eta_{col}^{\text{sign}(I(t))}} \tag{5.49}$$

$$f_6(soc) = \frac{\frac{\partial\sqrt{\frac{voc^2(soc)}{4r_0^2(soc)} - \frac{P_{batt}}{r_0(soc)}}}{\partial soc}}{2Q_{norm}\eta_{col}^{\text{sign}(I(t))}\frac{voc(soc)}{2r_0(soc)} - \sqrt{\frac{voc^2(soc)}{4r_0^2(soc)} + \frac{P_{batt}}{r_0(soc)}}} \tag{5.50}$$

Numerical iterative algorithm is used as explained in previous scenario.

5.8 Solution with Traffic Signals and Leading Vehicle Constraints in an Urban Environment

In previous cases, urban traffic environment were not considered to ease the computation. In this case, traffic is considered both as single and multiple leading vehicles on the route. Goal is to find an optimal velocity profile while keeping safe distance ahead with leading vehicles and following other constraints. Problem is formulated as:

$$\begin{cases} x(t_0) = 0, \;\; x(t_i) = x_i \;\; x(t_f) = D, \\ v(t_0) = 0 \;\text{ and }\; v(t_f) = 0 \\ soc_{min} \leq soc \leq soc_{max}, \\ v_{min} \leq v \leq v_{max} \\ x \leq (x_{lead} - x_{safe}) \end{cases} \tag{5.51}$$

where i indicates i^{th} traffic signal with t_i as timing constraint on i^{th} traffic signal, which can be any value between green light duration of i^{th} traffic signal. x_{lead} is fixed for single leading vehicle but for the case of multiple leading vehicles, it changes continuously, vehicle that get close to host EV, becomes the leading vehicle.

Hamiltonian for the scenarios is expressed as:

$$\begin{aligned} H = \tfrac{b_1\tau v}{\eta m} + \lambda_1 v + \lambda_2(h_1\tau\eta^{\text{sign}(\tau)} - h_2v^2 - h_0 - W) - \lambda_3\left[\tfrac{I_{load}(t)}{Q_{norm}\eta_{col}^{\text{sign}(I(t))}}\right] \\ +\tfrac{\beta_1}{2}(x(t_f) - x_{des,t_f})^2 + \mu_1(\max(0, v_{min} - v)^2) + \max((0, v - v_{max})^2)) \\ +\mu_2(\max(0, soc_{min} - soc)^2) + \max(0, soc - soc_{max})^2) + \tfrac{\beta_2}{2}v(t_f)^2 \\ +\tfrac{\rho_i}{2}\textstyle\sum_{i=1}^{5}[(x_{ti} - x_{des,ti})^2] + \mu_3(\max(0, x - (x_{lead} - x_{safe})^2)) \end{aligned} \tag{5.52}$$

Accelerating and braking torques are expressed as:

$$\tau^+ = \frac{\partial H}{\partial \tau} = 0 = \frac{b_1 v}{4r_0\eta_m v_{oc}^2} - \frac{\lambda_3^2 b_1 v}{Q^2\eta_m\eta_{col}^2\left[\frac{b_1^2v^2}{\eta_m^2} + 2b_1v\lambda_2h_1\eta + \lambda_2^2h_1^2\eta^2\right]} \tag{5.53}$$

$$\tau^- = \frac{\partial H}{\partial \tau} = 0 = \frac{b_1 v}{4r_0\eta_m v_{oc}^2} - \frac{\lambda_3^2 b_1 v}{\frac{Q^2\eta_m}{\eta_{col}^2}\left[\frac{b_1^2v^2}{\eta_m^2} + \frac{2b_1v\lambda_2h_1}{\eta} + \frac{\lambda_2^2h_1^2}{\eta^2}\right]} \tag{5.54}$$

Co-state equations are obtained as:-

$$\begin{aligned} \dot{\lambda}_1 = -\frac{\partial H}{\partial x} = -\beta_1(x(t_f) - x_{des,t_f}) - \rho_i\sum_{i=1}^{5}[(x_{ti} - x_{des,ti})] \\ +2\mu_3(max(0, x - (x_{lead} - x_{safe}))) \end{aligned} \tag{5.55}$$

$$\begin{aligned} \dot{\lambda}_2 = -\frac{\partial H}{\partial v} = -\frac{b_1\tau}{\eta m} - \lambda_1 + 2\lambda_2h_2v + \frac{\lambda_3 b_1\tau}{\eta_m r_0 Q\eta_{col}^{\text{sign}(I_{load}(t))}\left[\frac{v_{oc}^2}{4r_0^2} - \frac{b_1\tau v}{\eta_m r_0}\right]^{\frac{1}{2}}} \\ +2\mu_1[max(0, v_{min} - v)] - 2\mu_1[max(0, v - v_{max})] - \beta_2 v(t_f) \end{aligned} \tag{5.56}$$

SoC co-state with constant v_{oc} and r_0 becomes:

$$\dot{\lambda}_3 = -\frac{\partial H}{\partial soc} = 2\mu_2[max(0, soc_{min} - soc)] - 2\mu_2[max(0, soc - soc_{max})] \tag{5.57}$$

5.8.1 Simulation of Urban Mobility (SUMO)

In this scenario, traffic signals timings are assumed to be known in advance and route from Jinnah Avenue to Fasial Mosque is selected with five traffic signals is considered. SUMO is an open source traffic simulation software, which is used for the traffic and signals forecasting on the selected route. Traffic signals timings are set as 50% duty cycle. Fig. 5.6 shows the SUMO view map of selected route with zoomed view of traffic signals. Single and multiple vehicles are running on the the selected route, which is formulated as leading vehicle constraint.

5.8.2 Numerical Iterative Technique

Refer to Fig. 5.7, that shows location of five traffic signals along with multiple leading vehicles. Location of traffic signals in this problem is different from the one discussed in previous case. This is because in this case real route from Jinnah Avenue to Faisal Mosque, Islamabad, Pakistan is considered. Five traffic signals

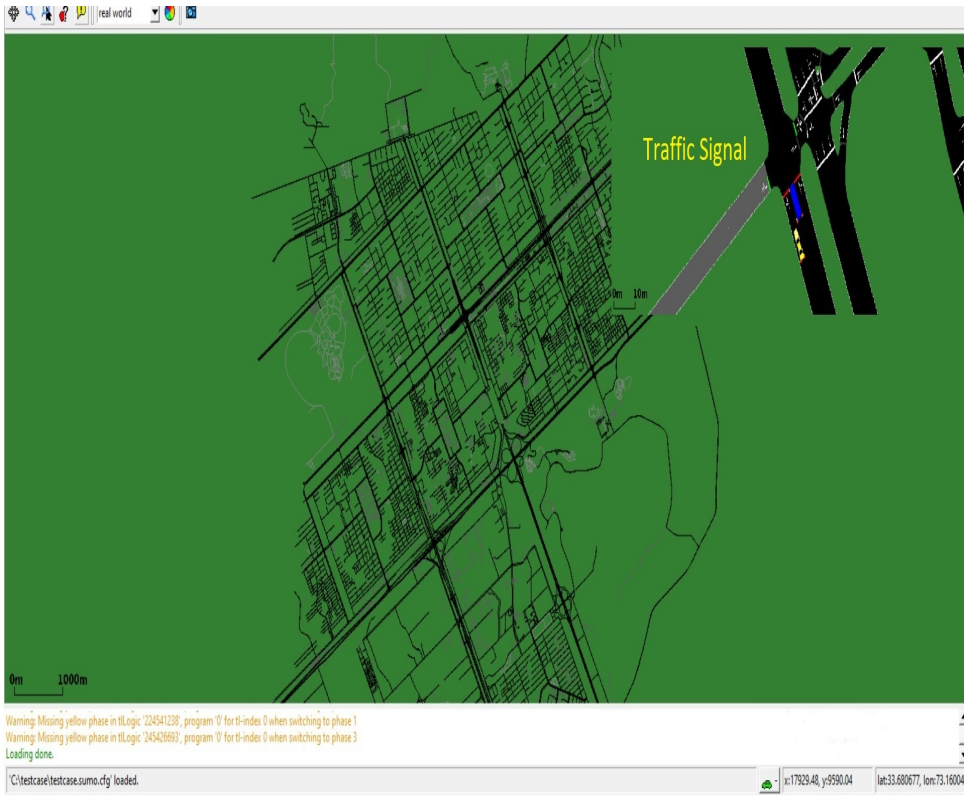

FIGURE 5.6: SUMO map view of selected route with traffic signals

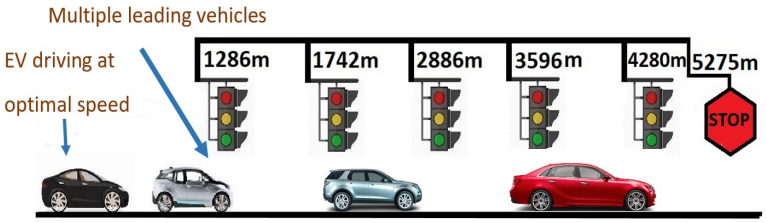

FIGURE 5.7: Locations of traffic signals with multiple leading vehicles along the route

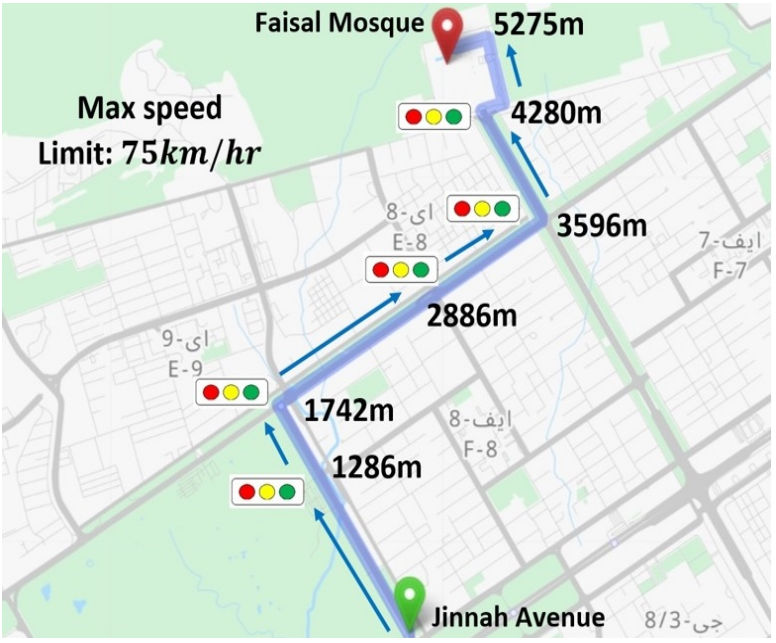

FIGURE 5.8: Google map view of selected route with traffic signals, starting and ending locations

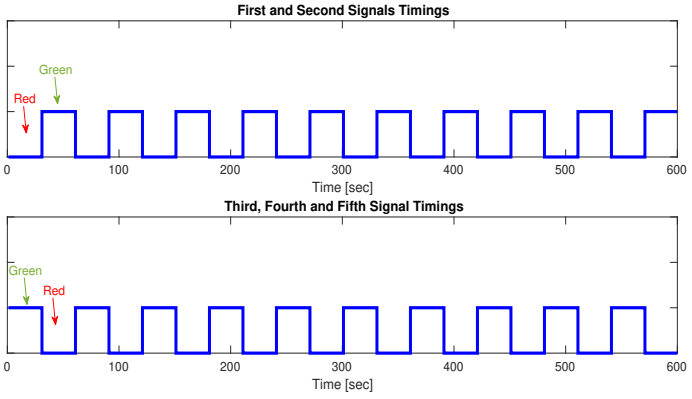

FIGURE 5.9: Signal timings of the five signals on the route

are present on the route so five interior point constraints are present. Fig. shows the Google map view of the selected route with traffic signals, start and end positions. Signal timings are as mentioned in Eqn. (5.58).

$$\begin{aligned}
\text{Signals } 1 &= [....31-60, 91-120, 151-180, 211-240....] \\
\text{Signals } 2 &= [....31-60, 91-120, 151-180, 211-240....] \\
\text{Signals } 3 &= [..301-330, 361-390, 421-450, 481-510..] \\
\text{Signals } 4 &= [..301-330, 361-390, 421-450, 481-510..] \\
\text{Signals } 5 &= [..301-330, 361-390, 421-450, 481-510..] \qquad (5.58)
\end{aligned}$$

Complete algorithm is explained as:

1. Initialize the algorithm with $i = 0$.
2. Increment i by 1.
3. Select $\lambda_1(t_0)$ and measure i^{th} signal location as $x(t_{i^-,des})$.
4. Select α with $n = 1$ and convergence stopping criteria for co-states ϵ_{max}.
5. Set effective co-state i.e., $\Lambda^0(t) = 0$ between starting time to signal's reaching time as $t_{i-1^+} < t \leq t_{i^-}$.
6. Define initial values of all the three states to solve the state equations and first co-state equation forward in time.
7. Define final value of second and third co-states to solve the $\lambda_{2,3}$ backward in time and update effective co-state $\Lambda^n = (1-\alpha)\Lambda^{n-1} + \alpha\lambda^n$.
8. Check if $\epsilon = ||\Lambda^n - \lambda^n|| < \epsilon_{max}$ satisfies then go to step 10 for $i = 1$ to further satisfy the boundary conditions of states and for $i = 2, 3, 4, 5, 6$ go back to 9 to satisfy the continuity condition of co-states. If $\epsilon = ||\Lambda^n - \lambda^n|| \not< \epsilon_{max}$, go back to step 7 to re-start the procedure with new updated effective co-state.
9. If $\lambda_{2,3}(t_{i^+}) \approx \lambda_{2,3}(t_{i^-})$ satisfies, go to step 10, otherwise go to step 7.
10. If $x(t_{i^-}) = x(t_{i^-,des}) < \Delta_{max}$ then return step 11, otherwise return to step 7.
11. If $i = 6$, terminate algorithm, otherwise repeat procedure for next signal.

5.8.3 Smoothing of Chattering in Optimal Results

It is observed in this case that the presence of traffic as multiple or single leading vehicle constraint causes fast switching in torque profiles, which may not look good from driver's perspective. Furthermore fast switching in torque profile consumes more energy. Second order low pass butterworth filter with cutoff frequency of $270Hz$, is used to smooth out these torque profiles [88]. Frequency response of a transfer function of this filter is as shown in Fig. 5.10 with transfer function is as mentioned below. Denominator co-efficients of a designed filter are mentioned in Table. 5.2. Filtering is applied after the calculation of optimal results because of offline nature of considered problem, procedure is highlighted in Fig. 5.11.

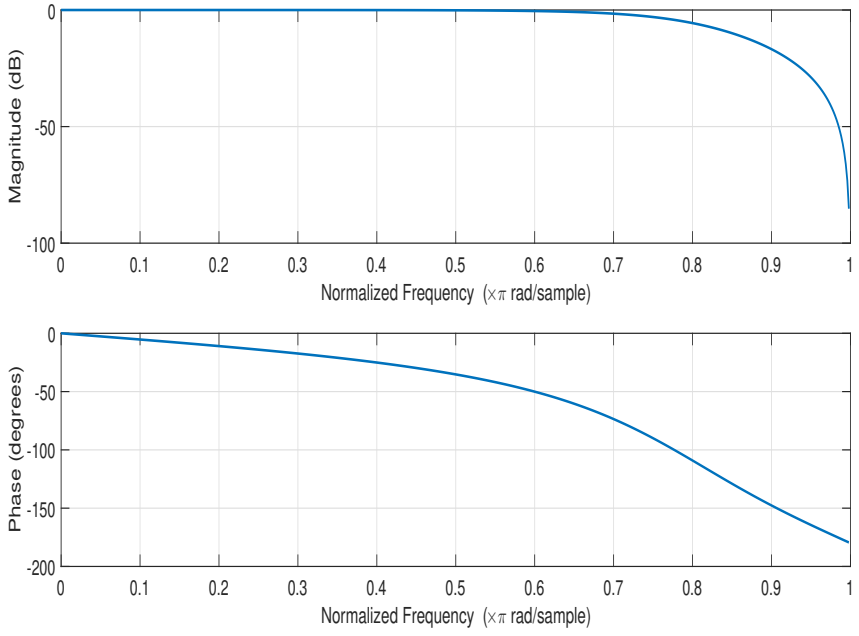

FIGURE 5.10: Frequency response of 2^{nd} order low pass Butterworth filter

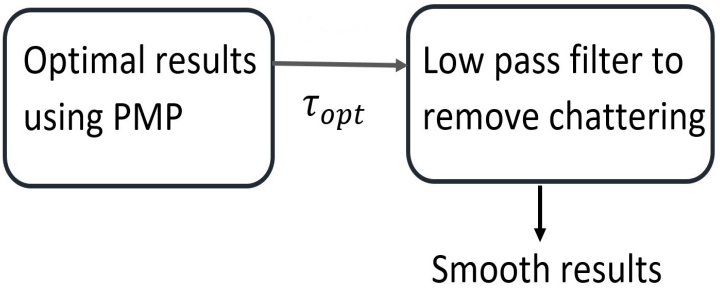

FIGURE 5.11: Smoothing algorithm for torque profiles

TABLE 5.2: Co-efficients of denominator of 2^{nd} order lowpass filter

Co-efficients	b_0	b_1	b_2
Values	.5690	1.138	.5690

$$H(s) = \frac{1.75s^2 + 1.65s + .5858}{s^2 + 2s + 1} \tag{5.59}$$

5.9 Different Modes of Optimal Torque

Vehicle starts off the journey with maximum power and then continues the trip with smooth velocity. When the surrounding vehicles are near by, it adjusts its speed and when the destination is about to come, it starts reducing the speed and applies the brakes to stop. Optimal torque is selected based on accelerating and braking torques numerical values and are further bounded by motor maximum accelerating and braking torques as τ_M and τ_m respectively. Selection of particular mode is based upon the calculated values of τ^+ and τ^-, as explained below.

$$\tau_{opt} = \begin{cases} \tau^+ & \text{if } \tau^+ > 0, \tau^- > 0 \\ 0 & \text{if } \tau^+ < 0, \tau^- > 0 \\ \tau^- & \text{if } \tau^+ < 0, \tau^- < 0 \end{cases} \tag{5.60}$$

$$W(t) = \begin{cases} 0 & \text{if } \lambda_2 > 0, I(t) < 0 \\ W & \text{if } \lambda_2 < 0, I(t) > 0 \end{cases} \tag{5.61}$$

$$\tau_{opt} = \begin{cases} \tau_M & \text{if } \tau_{opt} \geq \tau_M \\ \tau_m & \text{if } \tau_{opt} \leq \tau_m \end{cases} \tag{5.62}$$

Six possible optimal torque modes are considered, which are listed as:-

1. First mode i.e., Maximum Acceleration (MA)

2. Second mode i.e., Acceleration (A)
3. Third mode i.e., Coasting (C)
4. Fourth mode i.e., Deceleration (D)
5. Fifth mode i.e., Maximum Deceleration (MD)
6. Sixth mode i.e., Braking (B)

5.9.1 Maximum Acceleration (MA)

During this mode, accelerating torque i.e., τ^+ goes to maximum level in positive side but due to applied upper limit on actuator, it can only go to level of τ_M. On the other hand, braking torque i.e., τ^- in this mode also stays on the positive side. Optimal torque and brake for this mode become

$$\begin{aligned} \tau_{opt} &= \tau_M \\ W_{opt} &= 0 \end{aligned} \tag{5.63}$$

5.9.2 Acceleration (A)

Once the trip has passed through the initial phase, EV switches to accelerating mode. During this mode, accelerating torque i.e., τ^+ becomes less than τ_M, but remains on positive side. Optimal torque and brake for this mode become

$$\begin{aligned} \tau_{opt} &= \tau^+ \\ W_{opt} &= 0 \end{aligned} \tag{5.64}$$

5.9.3 Coasting (C)

During this mode, accelerating mode τ^+ switches from positive to negative side with braking torque i.e., τ^- remains on positive side. Optimal torque and brake

for this mode become

$$\begin{aligned} \tau_{opt} &= 0 \\ W_{opt} &= 0 \end{aligned} \tag{5.65}$$

5.9.4 Deceleration (D)

During this mode, EV switches from C to D mode. Both accelerating and braking torques go to negative side. Optimal torque and brake during this mode become

$$\begin{aligned} \tau_{opt} &= \tau^{-} \\ W_{opt} &= 0 \end{aligned} \tag{5.66}$$

5.9.5 Maximum Deceleration (MD)

Braking torque keeps going in negative side and when it gets close to saturation limit i.e., τ_m but cannot cross it, it indicates the fifth mode has started. Optimal torque and brake for this mode become

$$\begin{aligned} \tau_{opt} &= \tau_m \\ W_{opt} &= 0 \end{aligned} \tag{5.67}$$

5.9.6 Braking (B)

During the entire accelerating mode of operation, velocity co-state remains on the negative side but once it goes on the positive side i.e., $\lambda_2 > 0$, braking mode has started. As a result, battery starts charging using regenerative braking mechanism. Optimal control values for this mode are

$$\begin{aligned} \tau_{opt} &= \tau_m \\ W_{opt} &= W \end{aligned} \tag{5.68}$$

These modes will be clearly observed in optimal torque trajectories for every case.

5.10 Chapter Summary

Using the general formulation of necessary conditions of optimality from Chapter 4, Chapter 5 focuses on the derivation of Hamiltonian, state, optimal control and co-state equations for different scenarios. Scenarios included unconstrained case, boundary conditions for final values of position, velocity and SoC, inequality constraints for charging/discharging and road speed limits, interior point constraints for traffic signals, SoC dependent r_0 and v_{oc} and leading vehicle constraints for the inclusion of safe gap in urban traffic. Furthermore, six different modes of optimal torque during accelerating and braking phase are discussed in details.

Chapter 6

Simulation and Results

6.1 Unconstrained case

In this scenario, unconstrained case is considered. Final position and velocity are fixed. Six possible modes of optimal torques are considered, as explained in chapter 5. Fig. 6.1 shows the states of EV with Fig. 6.1(a) shows the position profile of EV and Fig. 6.1(b) shows the optimal velocity profile achieved using PMP. Boundary conditions are as mentioned in Table. 6.1. Fig. 6.2 shows the optimal torque profile with six different modes and energy consumption during a trip. It can be seen clearly that from start, EV first followed the trip with maximum accelerating mode and then it converts to an accelerating mode i.e., with comparatively smooth velocity profile. Once the EV has achieved certain comfort zone, it then converts to coasting mode i.e. close to constant velocity and when the destination is about to come, it first converts to deceleration followed by maximum deceleration. Finally at the end brakes are applied to stop at final destination and during this mode, energy consumption is on the negative side, i.e., regenerative braking mechanism means energy is giving back to the system. Fig. 6.3(a)&(b) show the position and velocity co-states respectively. Moreover, velocity co-state remains on the negative side throughout the operation apart from the braking phase. Energy consumption for EV during a trip is as mentioned in Table. 6.1.

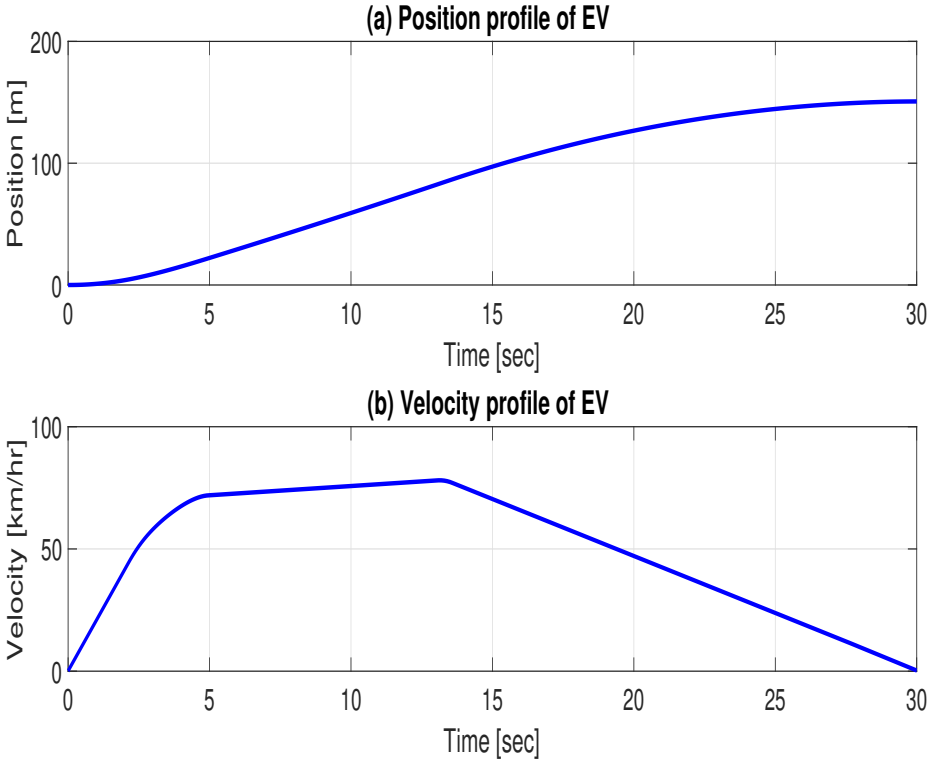

FIGURE 6.1: States of EV for unconstrained case

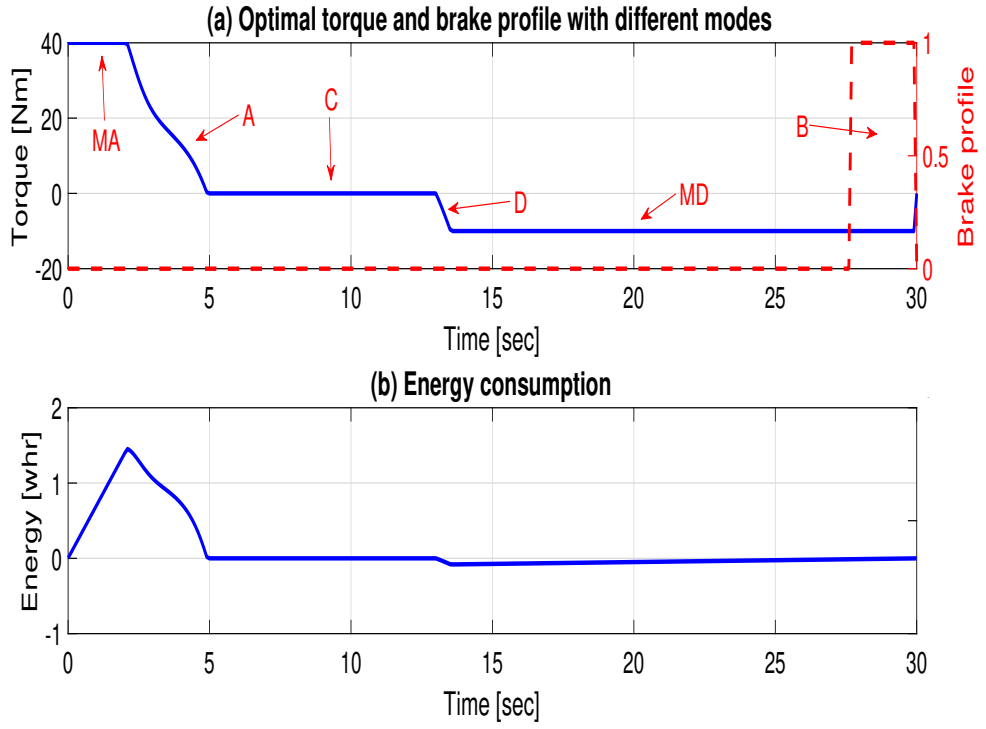

FIGURE 6.2: Optimal torque and brake profile with energy consumption during a trip

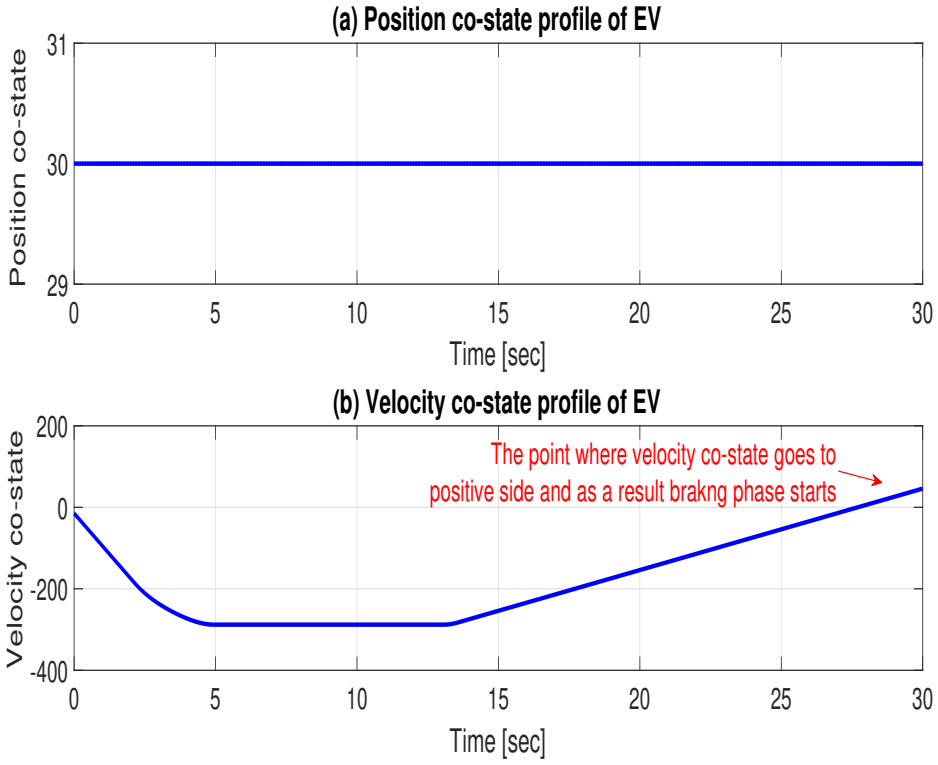

FIGURE 6.3: Co-states of EV for unconstrained case

TABLE 6.1: Boundary conditions and energy consumption for unconstrained case

Variables	Values
x_f	150m
v_f	0
$\lambda_1(t_f)$	free
$\lambda_2(t_f)$	free
Energy consumption	33wh

6.2 Inclusion of Zero Order Ideal Battery Model with Charging/Discharging Limits and Free Final Velocity

In this scenarios, battery dynamics are integrated with EV dynamics. The major reason for considering battery dynamics is to enhance the range of EV. Moreover

constraints are applied on battery SoC to limit the charging/discharging, which indirectly improves its life. Fig. 6.4 shows the position profile of EV. Fig. 6.5 shows the optimal velocity followed by EV and SoC of battery. It can be seen clearly that when the velocity increases, SoC decreases i.e., battery discharges and when the velocity of EV decreases during braking, SoC increases i.e., battery charges. Optimal torque profile with five optimal modes and energy consumption during a trip, are as shown in Fig. 6.6. It can be observed, as there is not brake applied during a trip hence no energy recovery is observed in Fig. 6.6(b). Final position is fixed, while final velocity and SoC are free, as mentioned in Table. 6.12. Fig. 6.7 shows the co-states of EV with Fig. 6.7(b) shows that final value of velocity co-state is zero and that is because of free final velocity. Fig. 6.7(a)&(c) shows the position and SoC co-states respectively. It can be seen that both position and SoC co-states have constant values due to $\dot{\lambda_1}$ and $\dot{\lambda_3}$, as expressed in Eqn. (5.22) & (5.24) respectively.

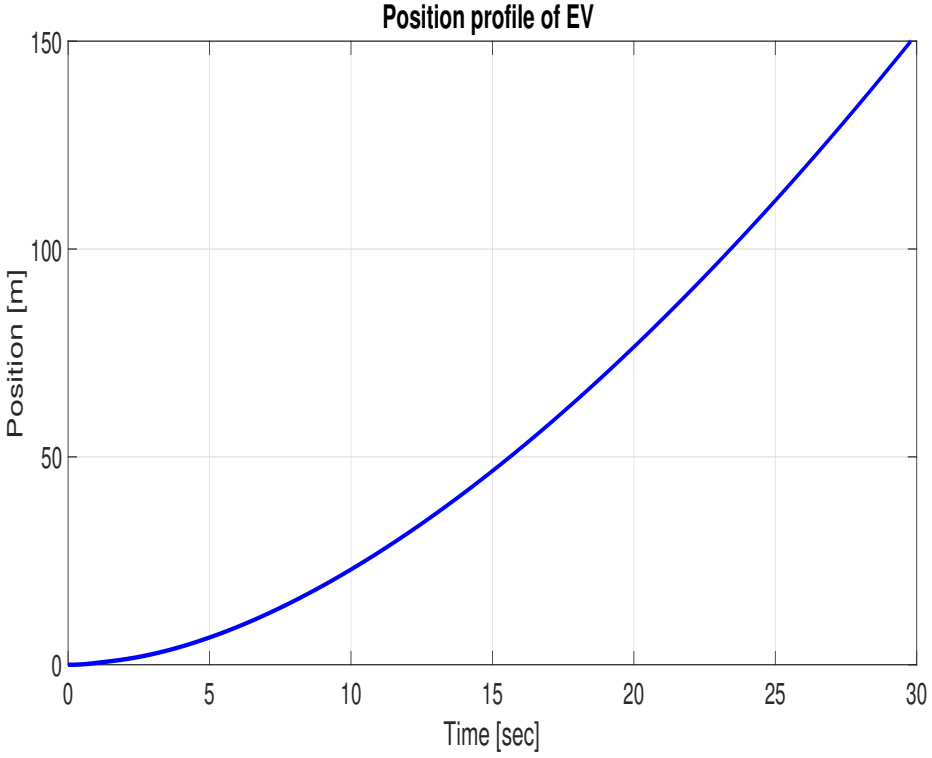

FIGURE 6.4: Position profile of EV for constrained SoC case

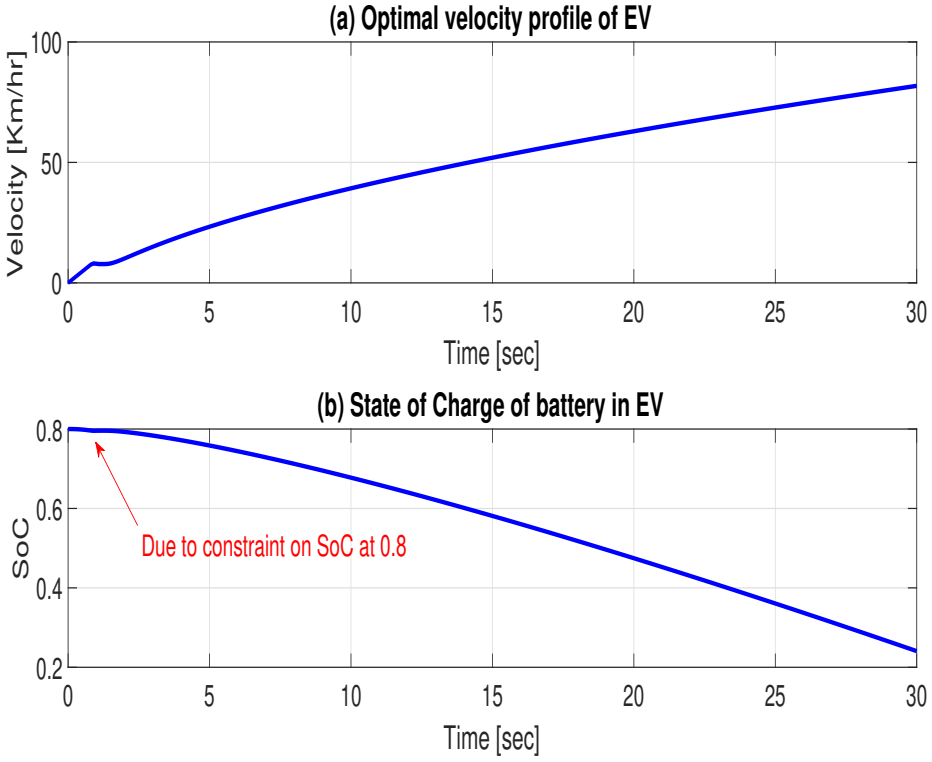

FIGURE 6.5: Velocity and SoC profiles of EV for constrained SoC case

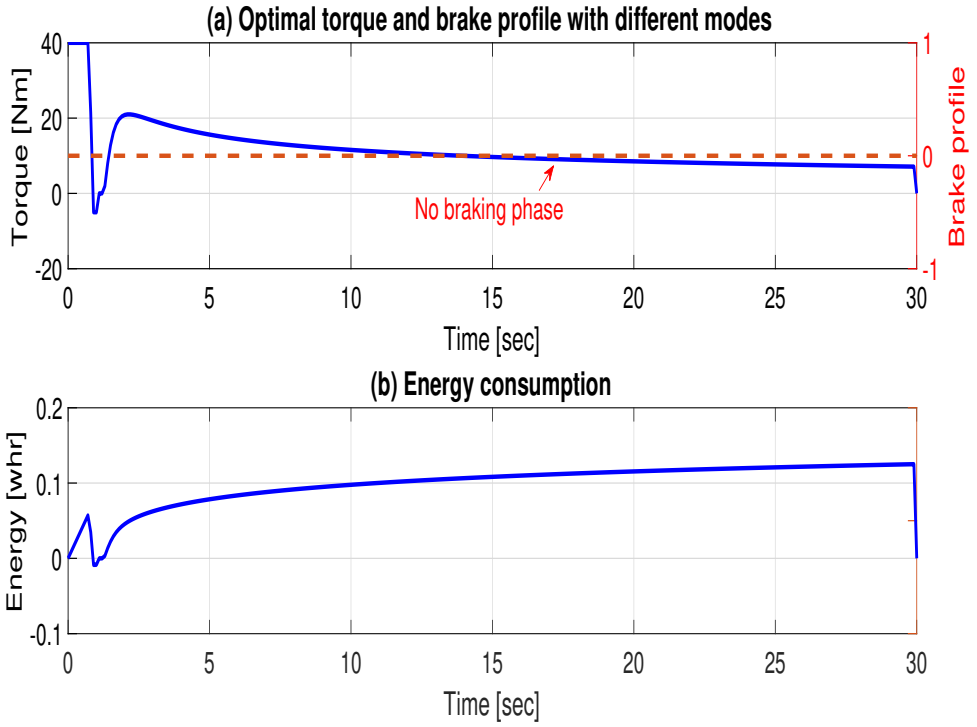

FIGURE 6.6: Optimal torque profile with energy consumption of EV for constrained SoC case

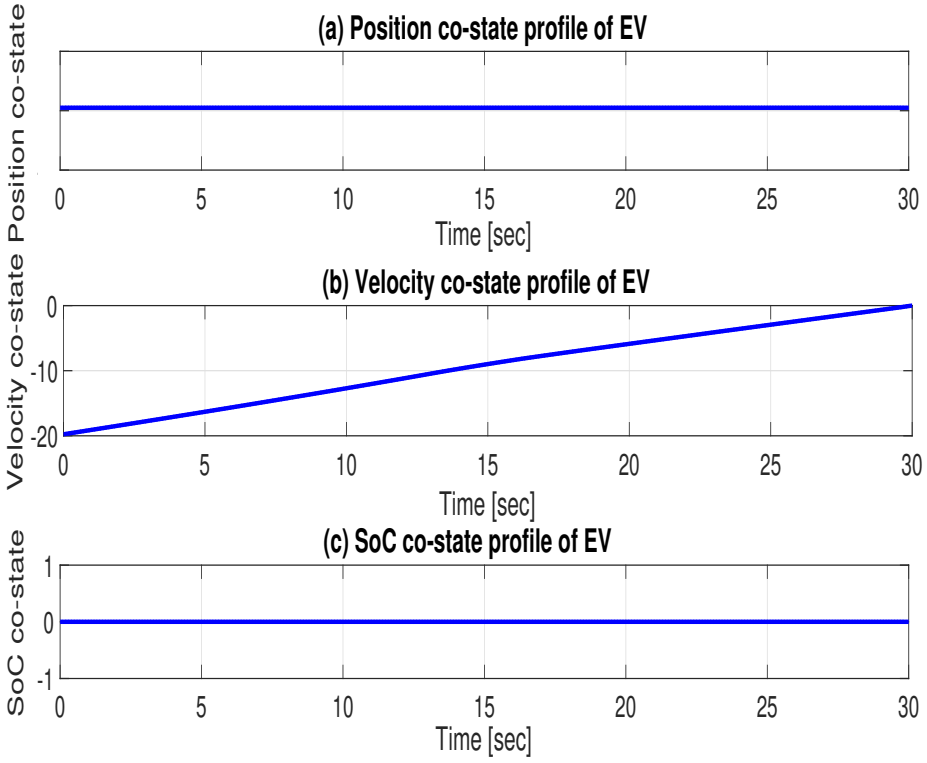

FIGURE 6.7: Co-states of EV for constrained SoC case

TABLE 6.2: Boundary conditions, inequality constraints, battery size and energy consumption for SoC charging limits with free final velocity

Variables	Values	Variables	Values
x_{t_f}	150m	$\lambda_2(t_f)$	0
$\lambda_1(t_f)$	free	$\lambda_3(t_f)$	free
$SoCmin$	0.2	SoC_{max}	0.8
Battery size	50wh	Energy consumption	30wh

6.3 Inclusion of Zero Order Ideal Battery Model with Charging/Discharging Limits and Fixed Final Velocity

This scenario is the extension of previous case with the difference that the final value of velocity is fixed, as mentioned in Table. 6.3 along with other boundary conditions, which are same from previous case. Final position of EV is fixed,

as shown in Fig. 6.8. Similar to previous case, when velocity of EV increases, its battery experiences discharging phase through the reduction in SoC. During the coasting phase, almost no difference is observed in SoC, while during the braking phase, its SoC gets increased i.e., by charging the battery, also known as regenerative braking mechanism, as shown in Fig. 6.10(a)&(b). Fig. 6.11 shows the co-states of EV, with Fig. 6.11(a)&(c) show the position and SoC co-states which remained constant throughout the operation and due to the values of $\dot{\lambda_1}$ & $\dot{\lambda_3}$ in Eqn. (5.22) & (5.24) respectively. Fig. 6.11(b) is the pictorial representation of velocity co-state, which has final value free due to the fixed final velocity. Moreover, it can be seen clearly that velocity co-state goes to positive side, once the brakes are applied.

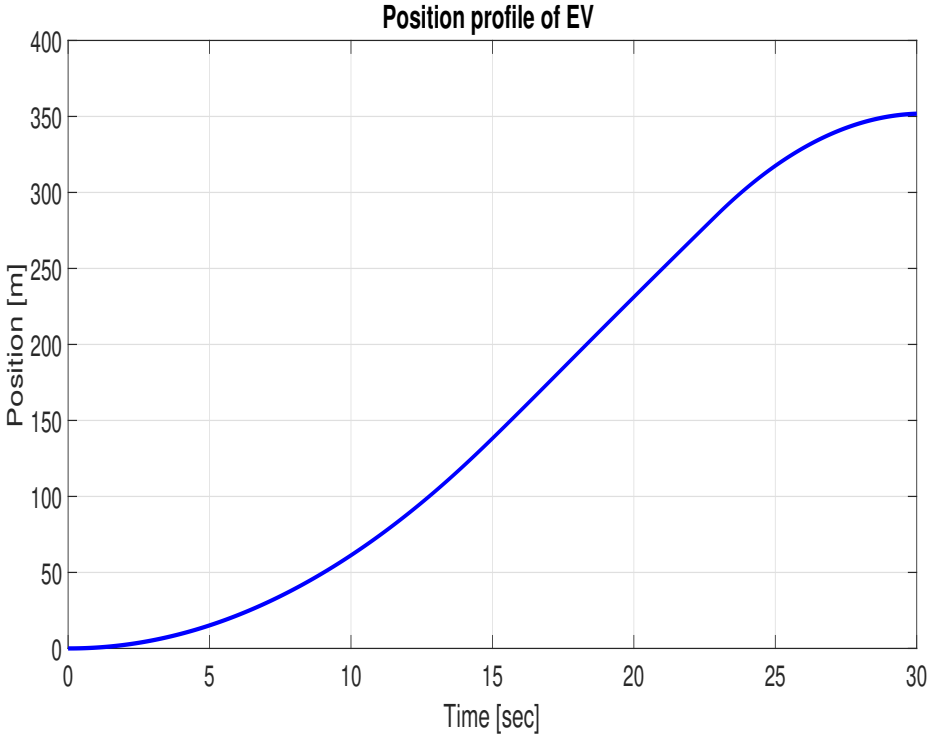

FIGURE 6.8: Position profile of EV for constrained SoC with fixed final velocity case

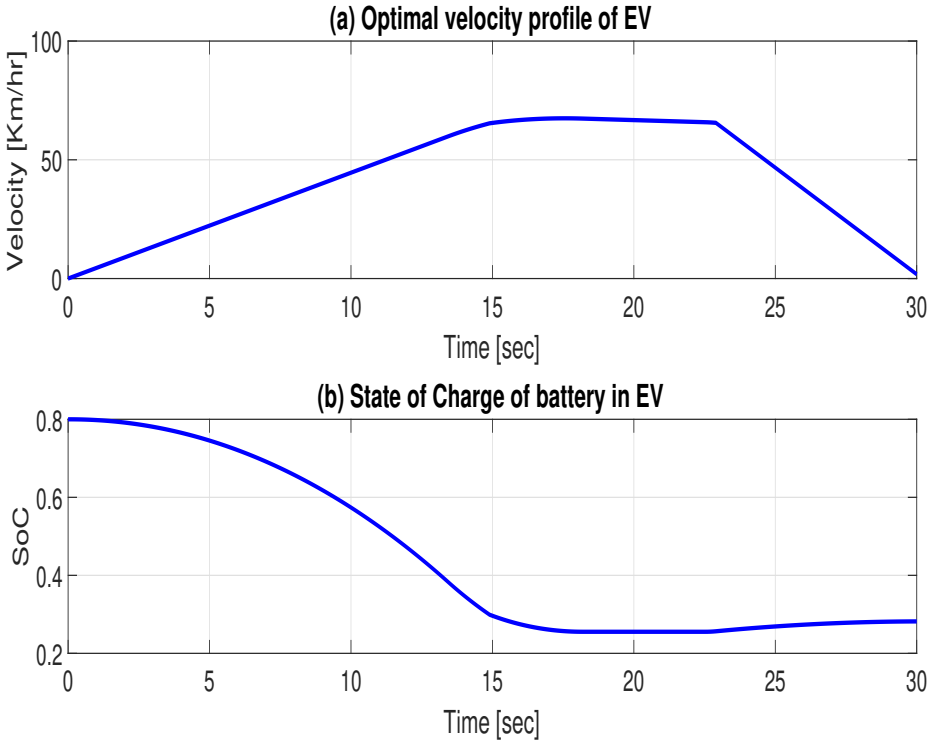

FIGURE 6.9: Velocity and SoC profiles of EV for constrained SoC with fixed final velocity case

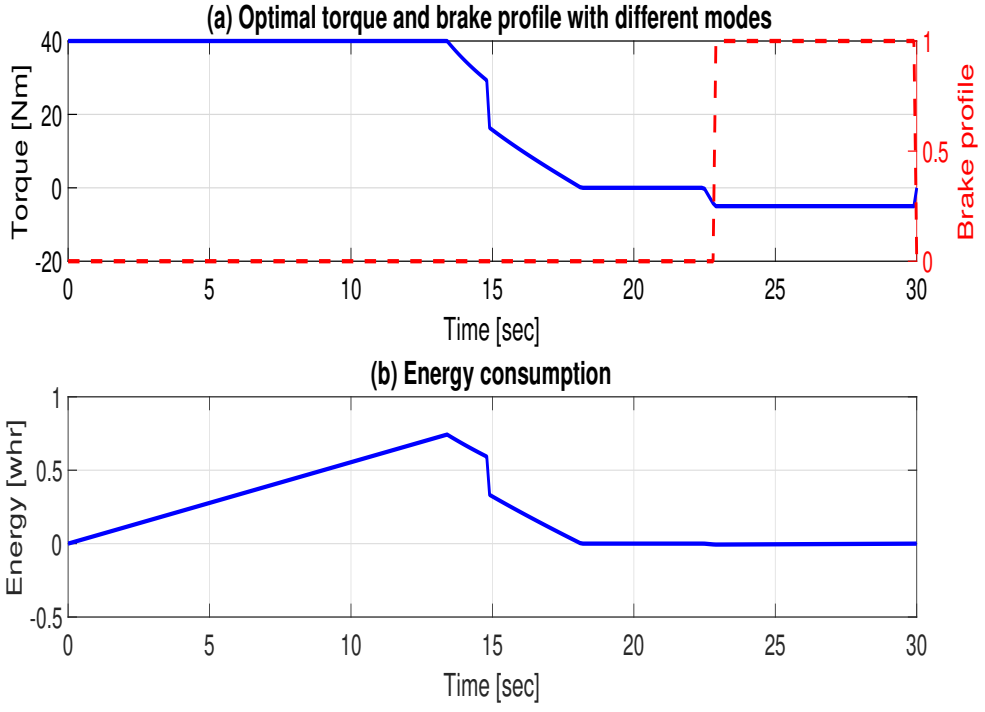

FIGURE 6.10: Optimal torque and brake profile with energy consumption of EV for constrained SoC with fixed final velocity case

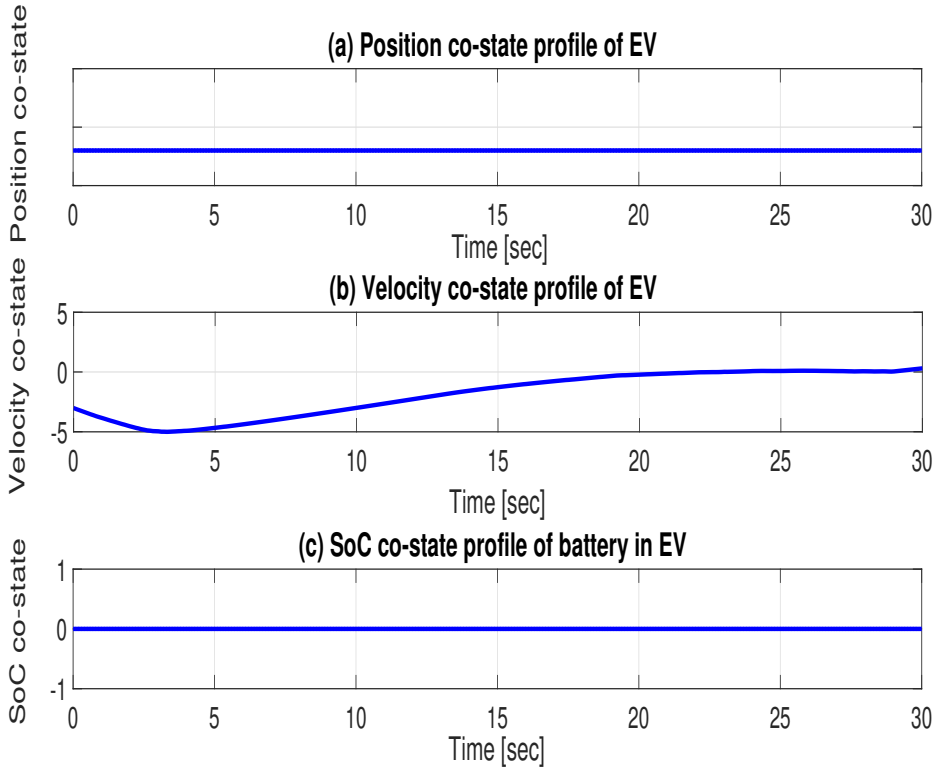

FIGURE 6.11: Co-states of EV for constrained SoC with fixed final velocity case

TABLE 6.3: Boundary conditions, inequality constraint, battery size and energy consumption for SoC charging limits with fixed final velocity

Variables	Values	Variables	Values
x_0	0	x_{t_f}	350m
v_0	0	v_{t_f}	0
SoC_{t_f}	free	$\lambda_1(t_f)$	free
$SoCmin$	0.2	SoC_{max}	0.8
$\lambda_2(t_f)$	free	$\lambda_2(t_f)$	free
Battery size	100wh	Energy consumption	62wh

6.4 Solution with Traffic Signals as Interior Point Constraints

In this scenario, along with other constraints of previous scenario, traffic signals are added as interior point constraints. Boundary conditions with inequality constraints are as mentioned in Table. 6.4. Location of every traffic signal is as

TABLE 6.4: Boundary conditions, inequality constraints and battery size for interior points scenario

Variables	**Values**	**Variables**	**Values**
x_0	0	x_{t_f}	5300m
v_0	0	v_{t_f}	0
x_{t_i}	fixed	v_{t_i}	free
SoC_{t_f}	free	$\lambda_3(t_f)$	free
$SoCmin$	0.2	SoC_{max}	0.8
$\lambda_1(t_f)$	free	$\lambda_2(t_f)$	free
Battery size	5.5kwh	$\lambda_{2,3}(t_i)$	continuous

mentioned in Eqn. (5.22). Fig. 6.12 shows the position profile of EV with Fig. 6.13(a) shows the optimal velocity profile. It can be seen clearly that EV velocity does not go to zero at the signals due to green duration, when compared with their timing signals from Eqn. (5.33) and Fig. 5.2. Exact reaching time of EV at every traffic signal is as mentioned in Table. 6.5. Fig. 6.13(b) shows the SoC of the battery installed in EV, which shows that it charges only at the end of the route, while no charging is observed during the signals locations, which was one of the main goals of this work. Similarly Fig. 6.15 shows the optimal torque and brakes profile with energy consumption, that explains more clearly that no braking phase is observed during a trip.

EV has crossed these signals through coasting phase. Fig. 6.14 shows the co-states of the system, with Fig. 6.13(a) shows the position co-state, while Fig. 6.14(b)&(c) show the velocity and SoC co-states respectively. Major point to be noted in all the three co-state profiles is that there occur discontinuities at the junctions in case of position co-state, while no discontinuities occur at the junctions in case of velocity and SoC co-states. Exact comparison of values of λ_2 at every junction using MPBVP and TPBVP is as mentioned in Table. 6.6 with constant λ_3. Furthermore, energy consumption comparison using the two strategies i.e., MPBVP and TPBVP is as mentioned in Table. 6.7. Fig. 6.16 shows the used EM efficiency through the use of optimal torque and velocity break points. Furthermore, average efficiency using efficiency map for the scenario is ~ 93. .

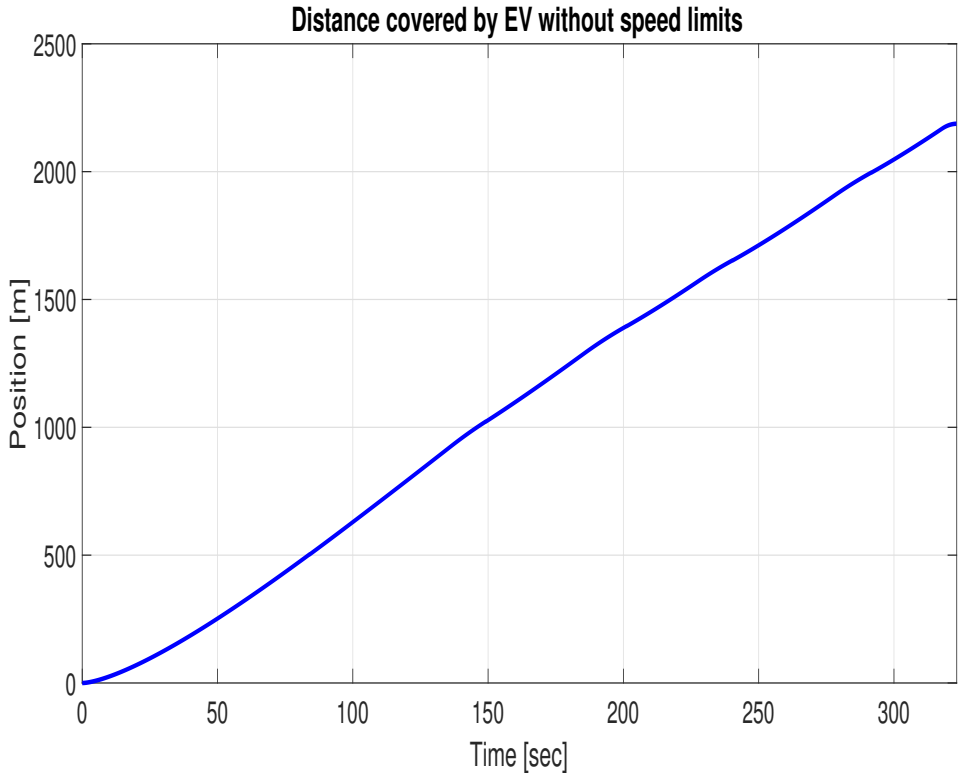

FIGURE 6.12: Position profile of EV with interior point constraints

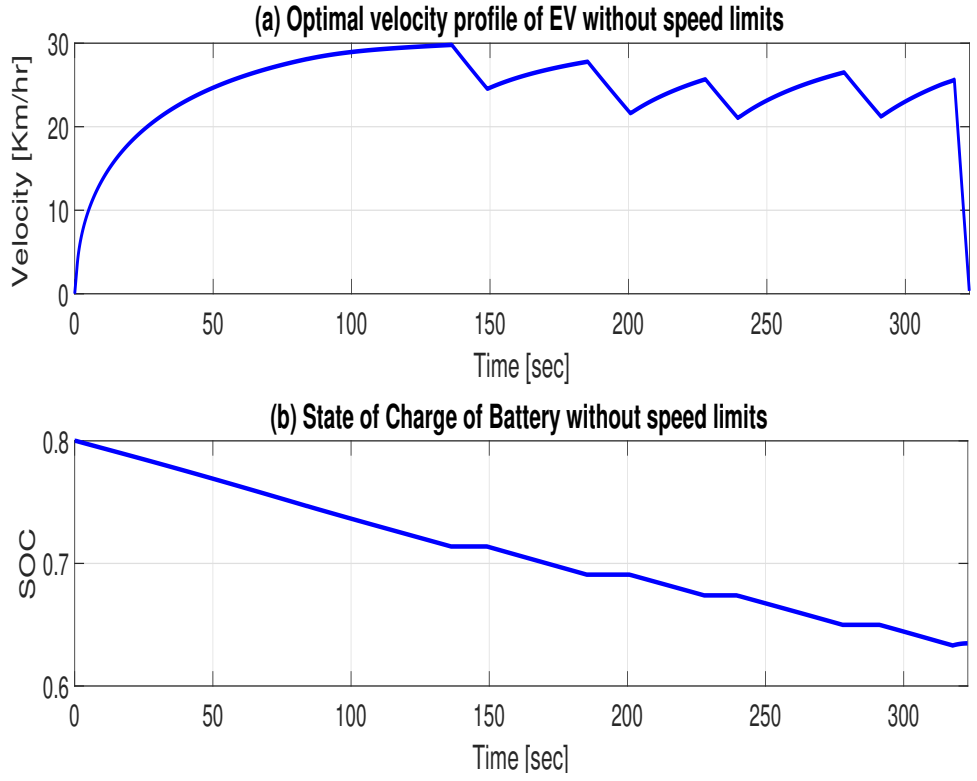

FIGURE 6.13: Velocity and SoC profiles of EV with interior point constraints

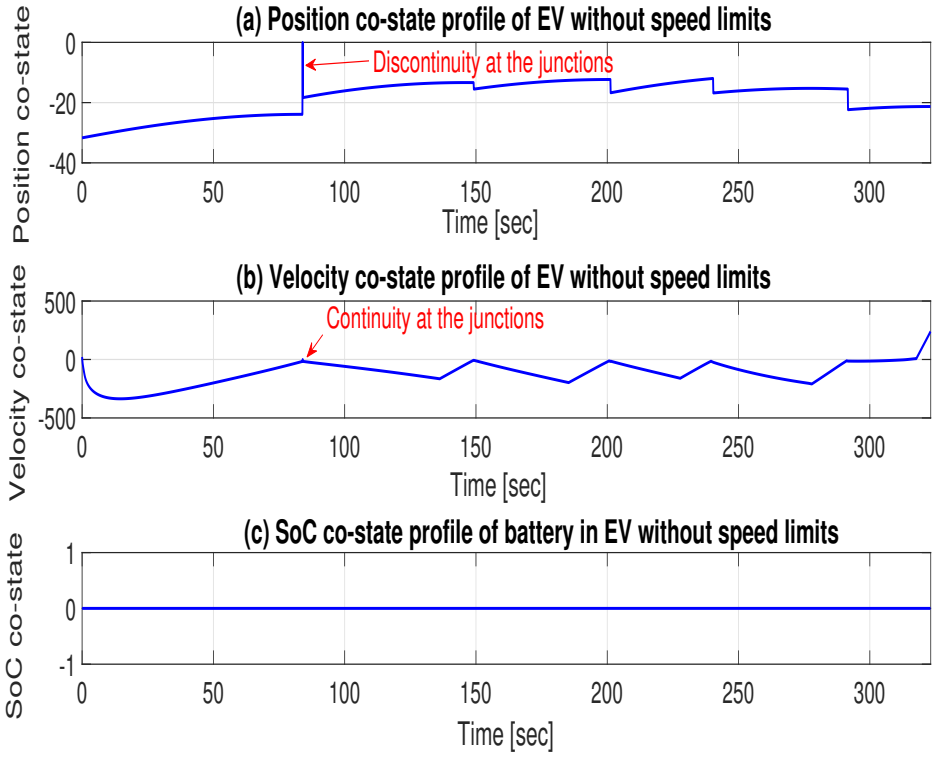

FIGURE 6.14: Co-states of EV with interior point constraints

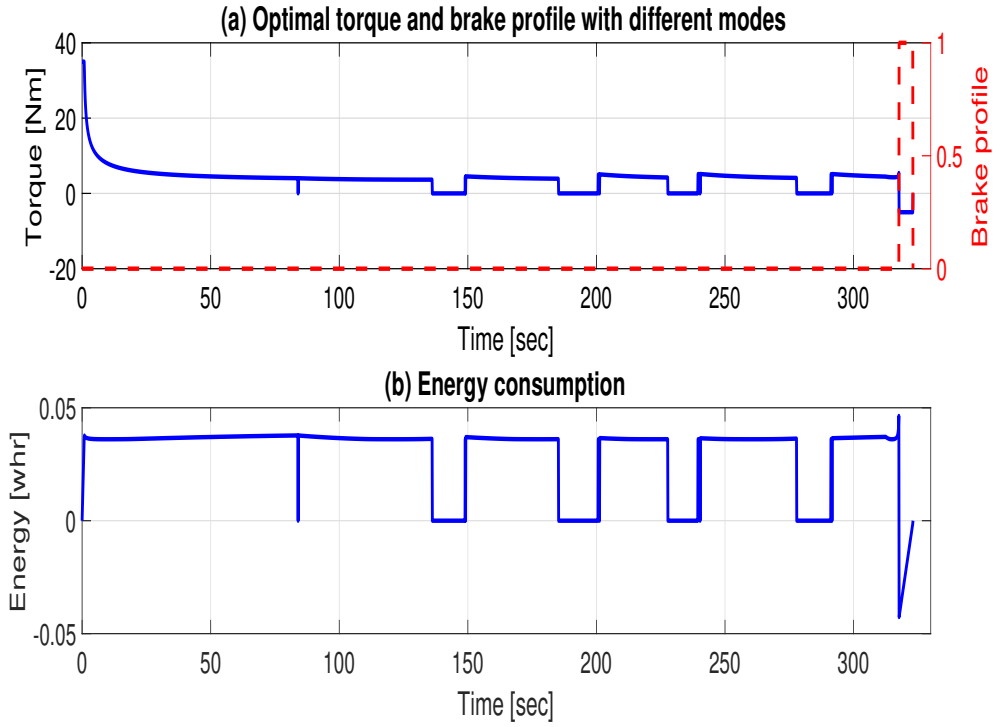

FIGURE 6.15: Optimal torque and brake profile with energy consumption of EV with interior point constraints

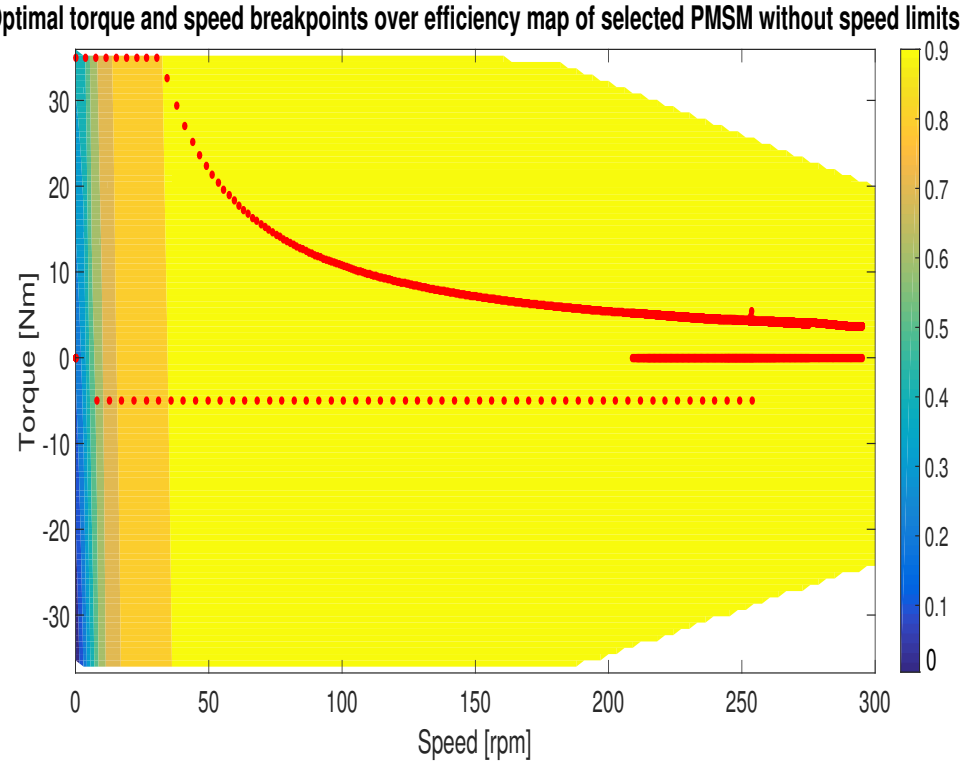

FIGURE 6.16: Efficiency map with optimal torque and speed breakpoints

TABLE 6.5: Reaching time of EV at the signals

Signal No	**Time [sec]**
1	83
2	146
3	201
4	241
5	292

TABLE 6.6: Comparison of co-state values at the junctions between MPBVP and TPBVP

MPBVP		**TPBVP**	
$\lambda_2(t_i^-)$	$\lambda_2(t_i^+)$	$\lambda_2(t_i^-)$	$\lambda_2(t_i^+)$
-25	-25.32	-7.01	-14.41
-8.22	-8.15	-11.5	-45.85
-17	-16.1	-17.12	-21.26
-23	-22.17	-23.14	-32.13
-13.7	-13.8	-13.11	-83.7

TABLE 6.7: Energy consumption comparison

MPBVP	TPBVP
95.08wh	96.8wh

6.5 Solution with Traffic Signals as Interior Point Constraints and Speed Limits on the Route

In this scenario, speed limits are added to the previous scenario. Boundary conditions, inequality constraints and interior point constraints are as mentioned Table. 6.4. Moreover, speed limits for different phases are mentioned in Table. 6.8. Fig. 6.17 shows the position profile with location of traffic signals and destination point. Fig. 6.18 shows the optimal velocity profile with speed limits and SoC of the battery. Fig. 6.19 shows the co-states of the system, with position co-state that faces discontinuities at the junctions due to fixed locations of signals in Fig. 6.19(a). Fig. 6.19(b) shows the velocity co-state with continuities at the junctions using MPBVP and multiple shooting method. Exact values of velocity co-state λ_2 at the junctions are mentioned in Table. 6.9. Fig. 6.20 shows the optimal torque and brake profile with different modes and energy consumption during a trip. Fig. 6.20(a)&(b) shows that no braking and energy recovery phase is observed throughout the operation apart from end point of trip. All the signals are crossed by EV during their green duration, with exact reaching time is as mentioned in Table. 6.10. Furthermore, energy consumption comparison during a trip is as mentioned in Table. 6.11. Fig. 6.21 shows the used EM efficiency through the use of optimal torque and velocity break points with achieved average efficiency is $\sim 93\%$.

TABLE 6.8: Speed limits in every phase

Phase No	$\mathbf{v_{min}(km)}$	$\mathbf{v_{max}(km)}$
Phase 1	10	26.5
Phase 2	18.5	30
Phase 3	18.5	26.5
Phase 4	15	26.5
Phase 5	15	26.5
Phase 6	0	30

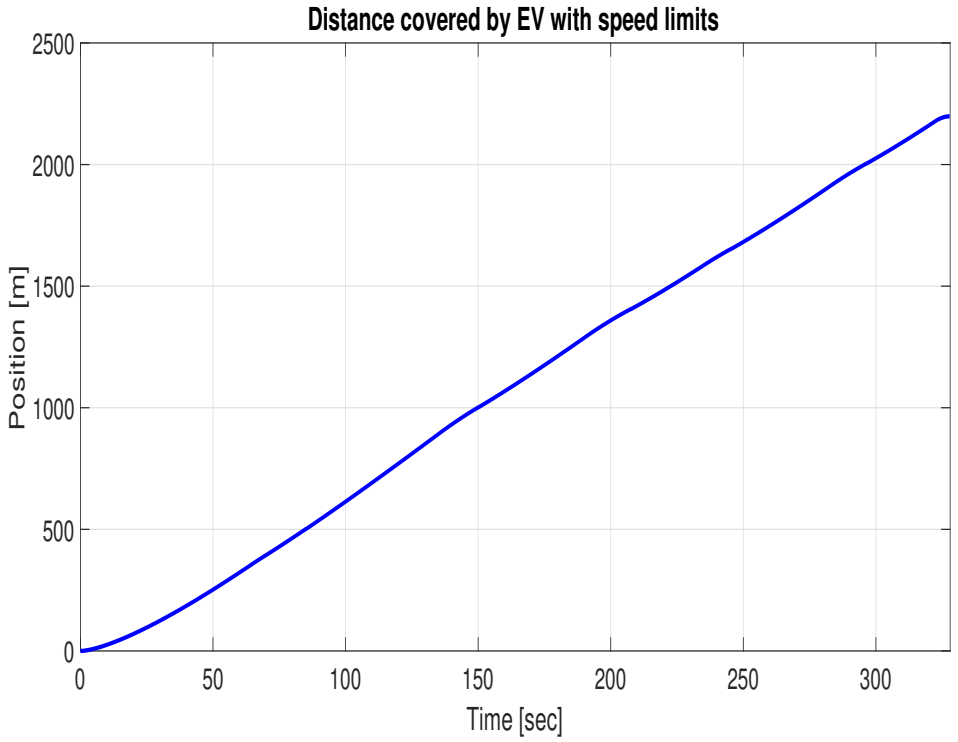

FIGURE 6.17: Position profile of EV with interior point constraints and speed limits

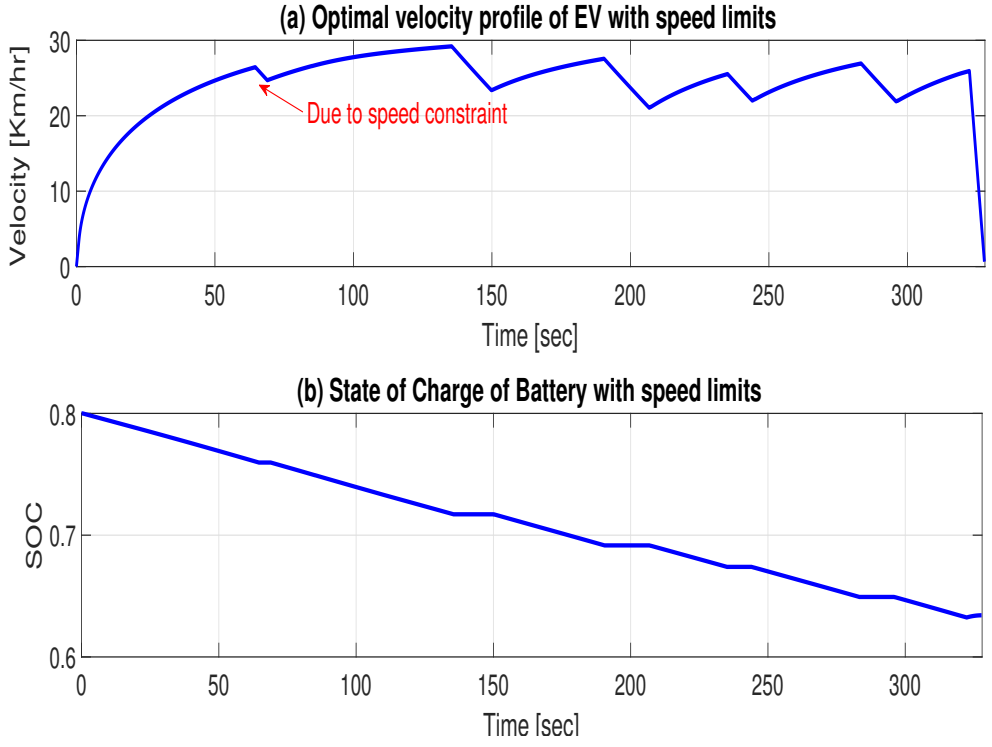

FIGURE 6.18: Velocity and SoC profiles of EV with interior point constraints and speed limits

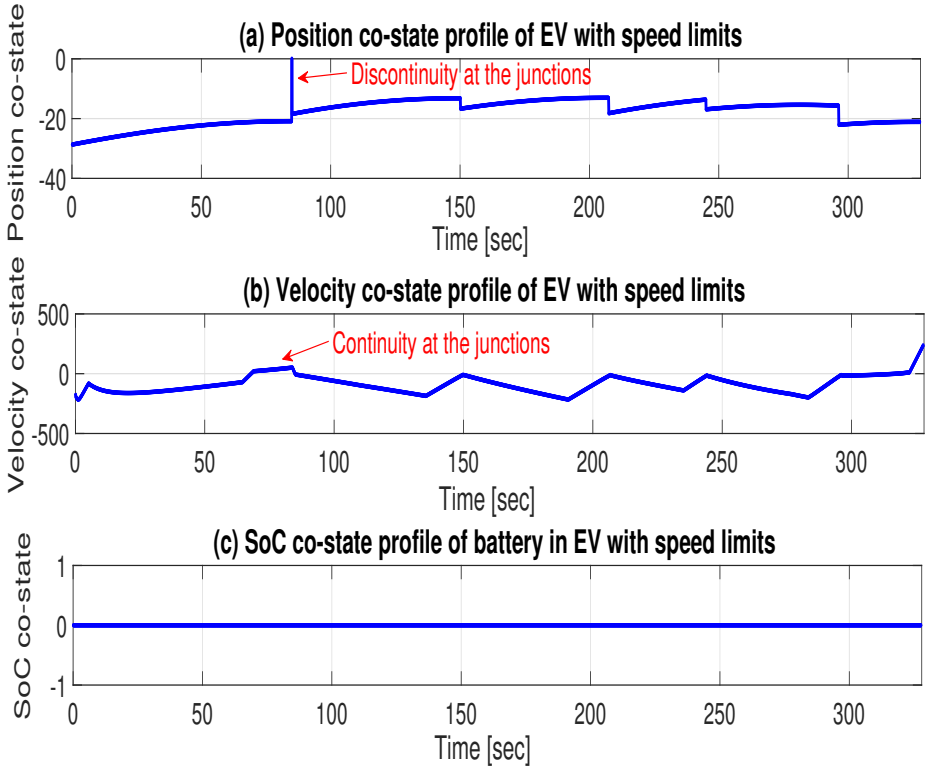

FIGURE 6.19: Co-states of EV with interior point constraints and speed limits

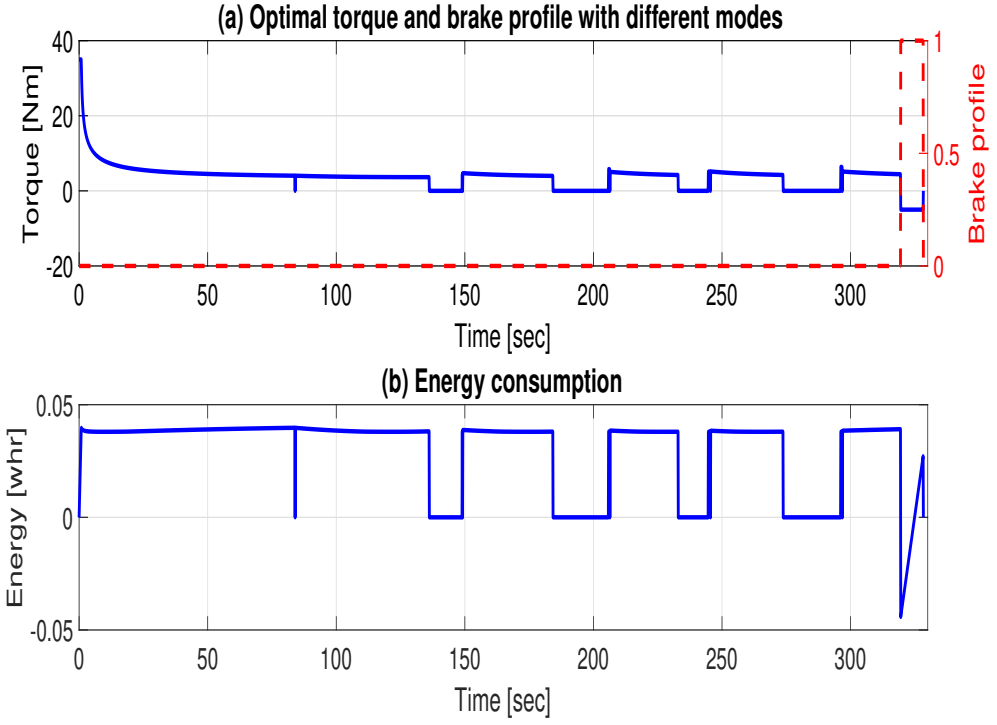

FIGURE 6.20: Optimal torque and brake profile with energy consumption of EV with interior point constraints and speed limits

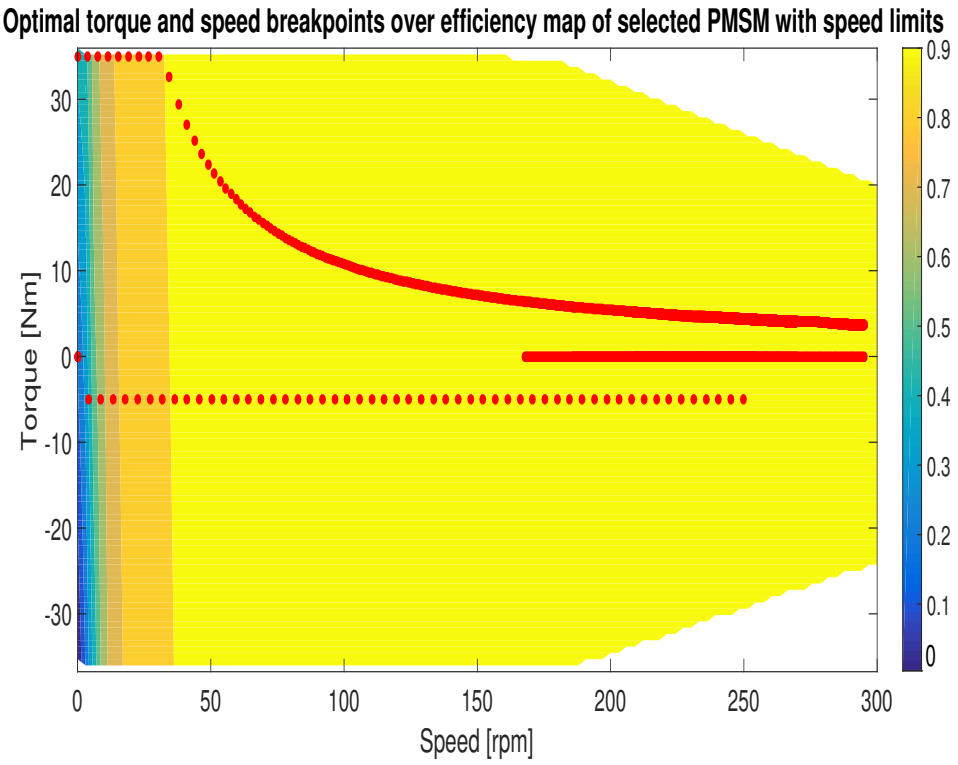

FIGURE 6.21: Efficiency map with optimal torque and speed breakpoints and speed limits

TABLE 6.9: Velocity co-state values at the junctions

$\lambda_2(t_i^-)$	$\lambda_2(t_i^+)$
-7.01	-7.942
-12.57	-12.93
-17.65	-17.8
-23.14	-23.41
-13.47	-13.37

TABLE 6.10: Reaching time at the signals with speed limits

Signal No.	**Time [sec]**
1	85
2	150
3	207.2
4	244.7
5	295.9

TABLE 6.11: Energy consumption

Energy consumption	95.4wh

6.6 Solution with Traffic Signals and SoC Dependent v_{oc} and r_0

In this scenario, internal resistance r_0 and open circuit voltage v_{oc} are taken as the function of SoC. Fig. 6.22 shows the position profile of EV with traffic signals and final position. Fig. 6.23 shows the optimal velocity profile with SoC of the battery. Again in this scenario, EV has successfully crossed all the signals during their green duration and following continuity condition. Fig. 6.25 shows the optimal torque and braking profile with energy consumption during a trip. Fig. 6.26 shows the change in r_0 and v_{oc} in (a) and (b) respectively. It shows that once battery discharges, its output power gets reduces by reduction in v_{oc} and increase in r_0 that show losses. In these figures, it is not clearly observable as the selected range of SoC is very small due to the applied eco-driving strategy. Table. 6.13 shows the energy consumption comparison with and without using eco-driving strategy. Fig. 6.27 shows the used EM efficiency map with average efficiency is $\sim 92.4\%$.

TABLE 6.12: Velocity co-state values and reaching time at the signals for SoC dependent v_{oc} and r_0

Signal No.	$\lambda_2(t_i^-)$	$\lambda_2(t_i^+)$	**Reaching time**
1	-8.714	-8.739	105.2
2	-15.3	-15.29	193
3	-.25	-.20	331.1
4	-.008	-.0002	374.7

TABLE 6.13: Energy consumption comparison between EV using eco-driving strategy and vehicle without eco-driving assistance for SoC dependent v_{oc} and r_0

EV with eco-driving assistance	184wh
Vehicle without eco-driving assistance	217wh

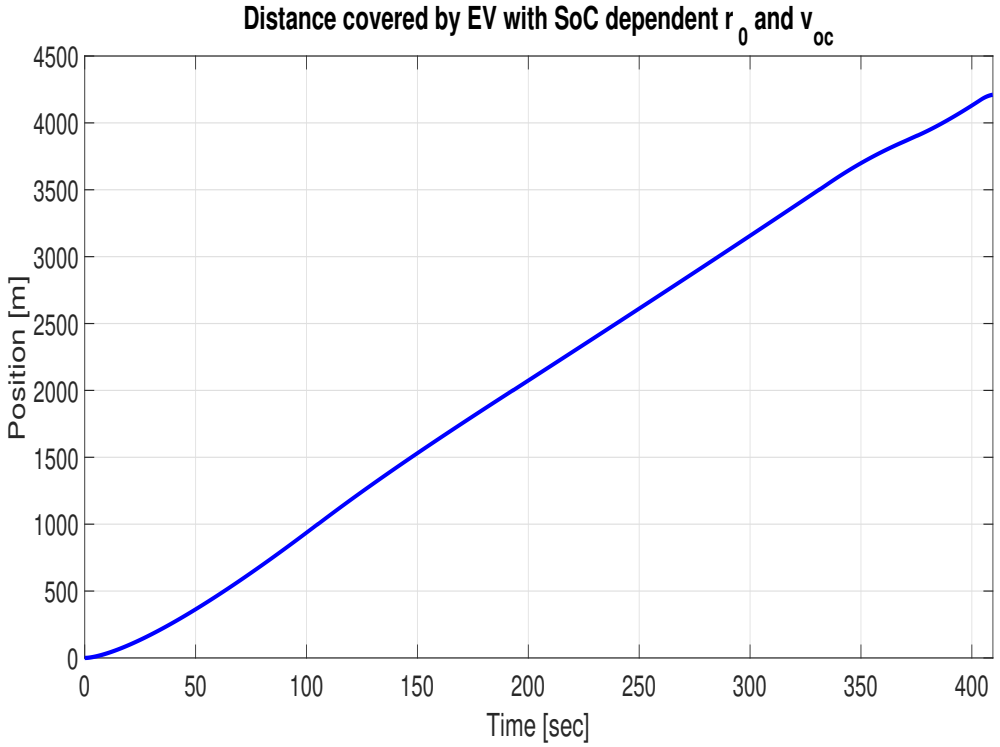

FIGURE 6.22: Position profile of EV with interior point constraints and SoC dependent v_{oc} and r_0

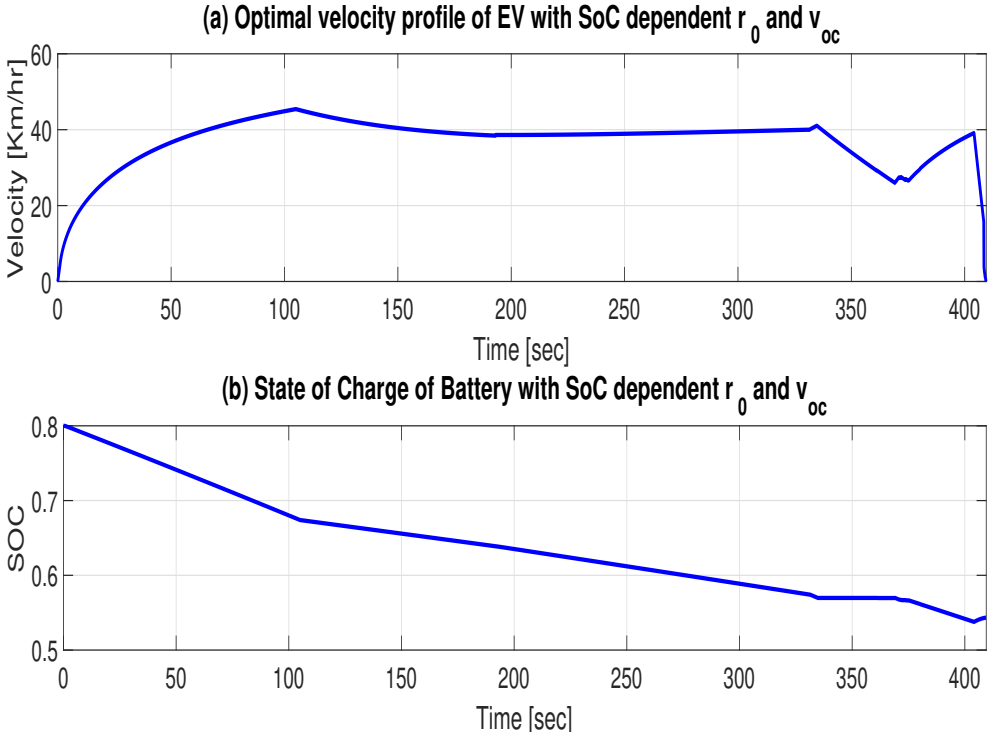

FIGURE 6.23: Velocity and SoC profiles of EV with interior point constraints and SoC dependent v_{oc} and r_0

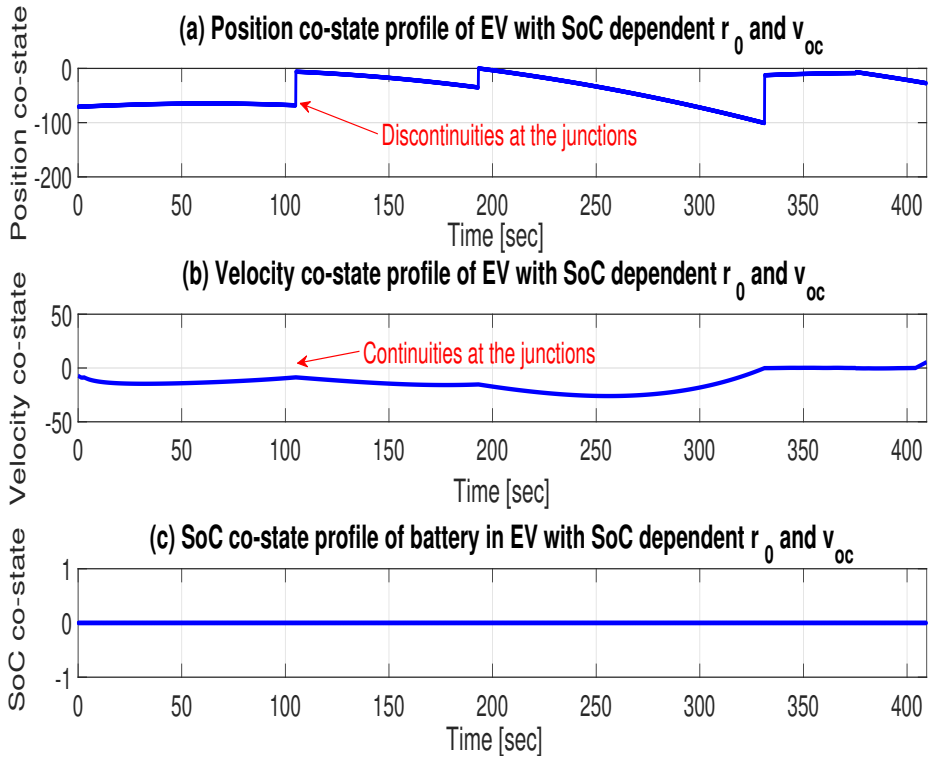

FIGURE 6.24: Co-states of EV with interior point constraints and SoC dependent v_{oc} and r_0

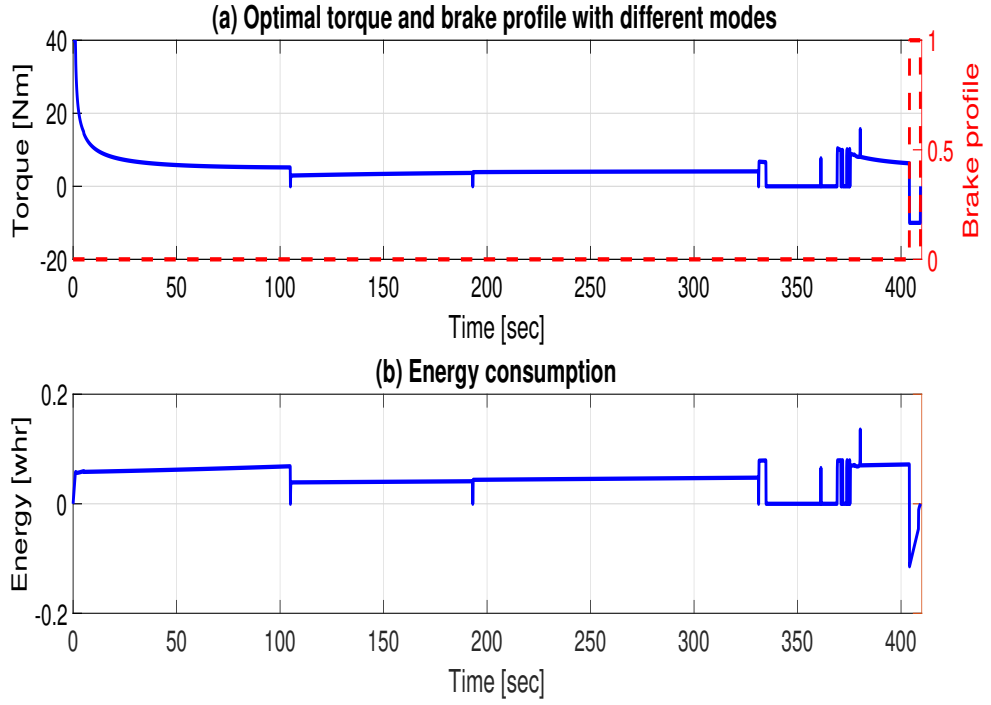

FIGURE 6.25: Optimal torque and brake profile with energy consumption of EV with interior point constraints and SoC dependent v_{oc} and r_0

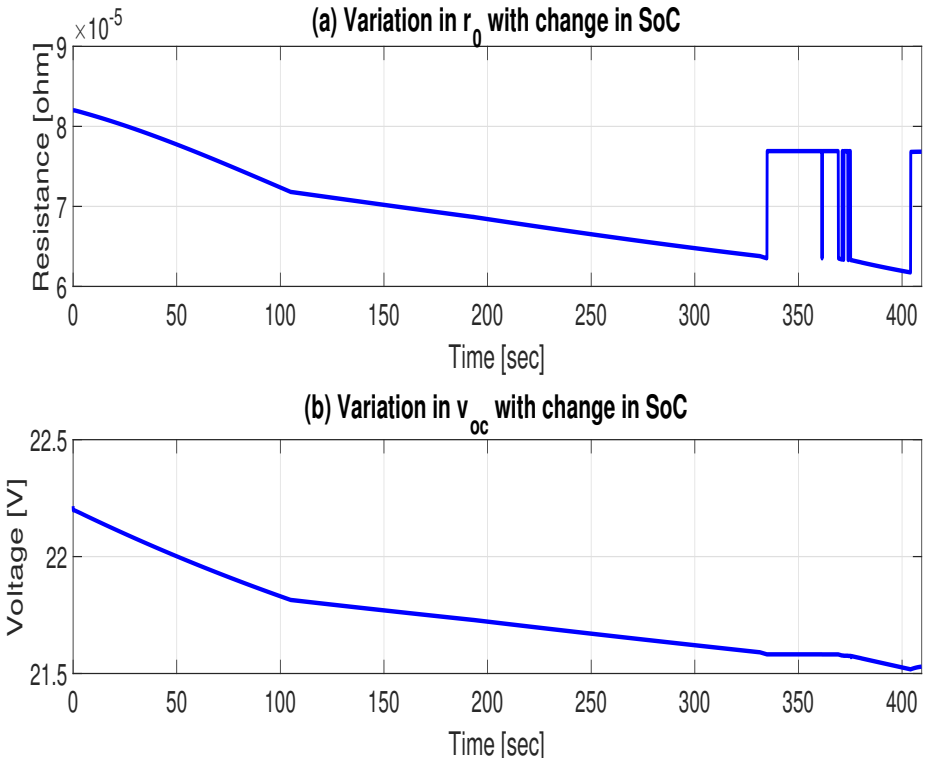

FIGURE 6.26: Change in r_0 and v_{oc} as a function of SoC

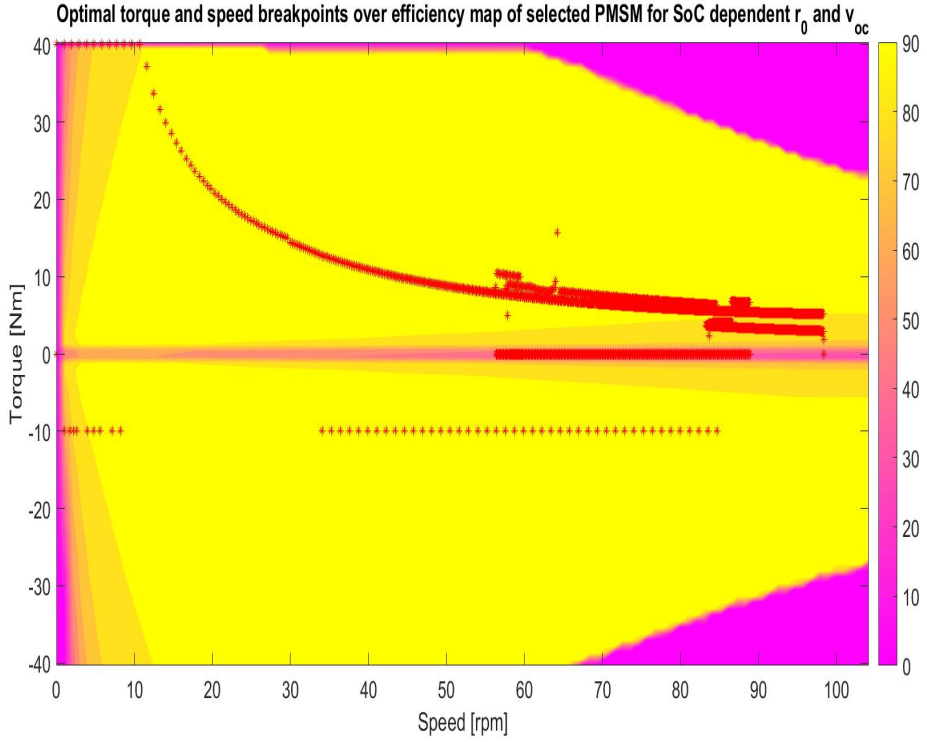

FIGURE 6.27: Efficiency map with optimal torque and speed breakpoints with SoC dependent v_{oc} and r_0

6.7 Solution with Traffic Signals and Leading Vehicle Constraints in an Urban Environment

In the previous scenarios, traffic signals, charging/discharging limits, speed constraints and boundary conditions were considered however, it was assumed that there was no traffic on the road. In this scenario, urban traffic is considered to get close approximation to real environment. Two environments are considered in this scenario, one is with single vehicle on the route and other is with multiple vehicles. Traffic problem is considered and solved as leading vehicle constraint. If a single vehicle is present on the route, then it is the only leading vehicle and safe gap must need to be maintained but if multiple vehicles are running on the road then the vehicle which gets close to EV with eco-driving assistance, becomes the leading vehicle for that instant of time. Fig. 6.28 (a) and (b) show positions profile of EV with eco-driving assistance and their leading vehicles without eco-driving assistance for both the scenarios. Fig. 6.28(a) shows results of single leading vehicle scenario, while Fig. 6.28(b) shows multiple leading vehicles scenario.
Fig. 6.29 shows the distance ahead and gap between EV and leading vehicles. Fig. 6.29(a) shows the gap with single leading vehicle whereas, Fig. 6.29(b) shows gap for the closest vehicle for multiple leading vehicles scenario. One important thing to be noticed in Fig. 6.29 that for both the scenarios minimum safe gap of $5m$ is violated at some points, however without collision EV has recovered through switching from acceleration to coasting mode. Fig. 6.30 & Fig. 6.31 show the achieved velocities using PMP with both backward EV simulator and PLSGM. Moreover, SoC and DoD for both the scenarios are shown in Fig. 6.30 and Fig. 6.31 (b) & (c) respectively with 5.5kwh of battery capacity, as used in previous cases of problem with traffic signals. It can be seen observed that EV using PLSGM has followed the advised velocities with great accuracy and without powertrain saturation. In similar ways, Fig. 6.32 & Fig. 6.33 show leading vehicle velocities with battery's SoC and DoD. Velocities comparison show that proposed approach of eco-driving assistance in Fig. 6.30 & Fig. 6.31 use very less braking

TABLE 6.14: Co-state values comparison at the junction points between single and multiple leading vehicles

	Single leading vehicle				**Multiple leading vehicles**			
Signal	$\lambda_2(t_i^-)$	$\lambda_2(t_i^+)$	$\lambda 3(t_i^-)$	$\lambda 3(t_i^+)$	$\lambda_2(t_i^-)$	$\lambda_2(t_i^+)$	$\lambda 3(t_i^-)$	$\lambda 3(t_i^+)$
$i = 1$	-5	-5.92	8.2	8.2	5.25	5.24	6.5	6.5
$i = 2$	-20.5	-22.28	8.2	8.2	-5.4	-5.42	6.5	6.5
$i = 3$	-10	-11.02	8.2	8.2	-2.3	-2.33	6.5	6.5
$i = 4$	-5	-6.18	8.2	8.2	-1	-1.71	6.5	6.5
$i = 5$	-3.5	-5.72	8.2	8.2	$-.65$	$-.68$	6.5	6.5

action as compared to different *Stop&Go* approach of leading vehicles as shown in Fig. 6.32 & Fig. 6.33.

Moreover, it can be observed clearly that EV using eco-driving strategy has successfully reached every signal during their green light duration, as mentioned in Table. 6.15. Fig. 6.34 shows optimal torque profiles which is calculated using PMP for both the scenarios. Optimal torque profiles switches from one mode to other with braking mode at the end of trip. Fig. 6.35 shows the three co-states for both the scenarios. Position co-states face discontinuities at the junctions, which is acceptable because of fixed signals location. Velocities and *SoC* are not fixed at the junctions, therefore continuity of their co-states are required and hence achieved, as mentioned in Table. 6.14. Fig. 6.36 shows the comparison in charging rates between EV with eco-driving assistance and leading vehicles without eco-driving. Table. 3.7 shows the energy consumption, charging rates and DoD comparison between EV with eco-driving assistance and their leading vehicles without eco-driving strategies. Moreover, while looking at the discharged battery's status through *SoC* in Fig. 6.30, Fig. 6.31, Fig. 6.32 & Fig. 6.33, It can be observed easily that using eco-driving strategy 5 to 20% less battery is used as compared to leading vehicles without eco-driving assistance. Fig. 6.38 & Fig. 6.38 show the efficiency map with achieved efficiency is $\sim$ 94%. Furthermore, energy consumption during a trip for both the scenarios are shown in Fig. 6.37.

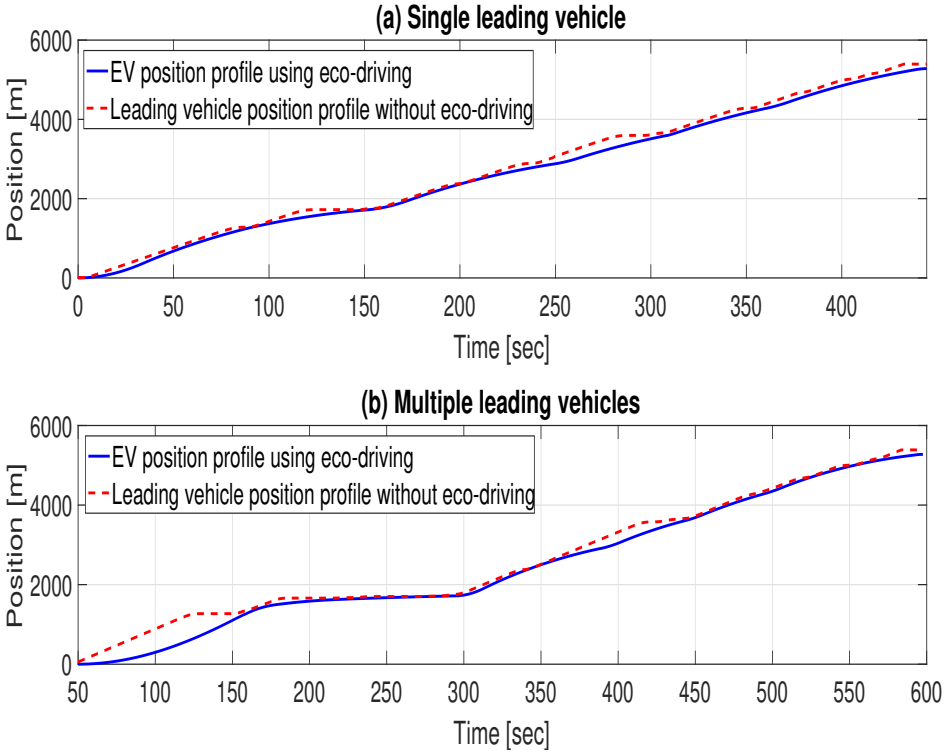

FIGURE 6.28: Position profiles of EV and leading vehicles (single and multiple leading vehicles on the route)

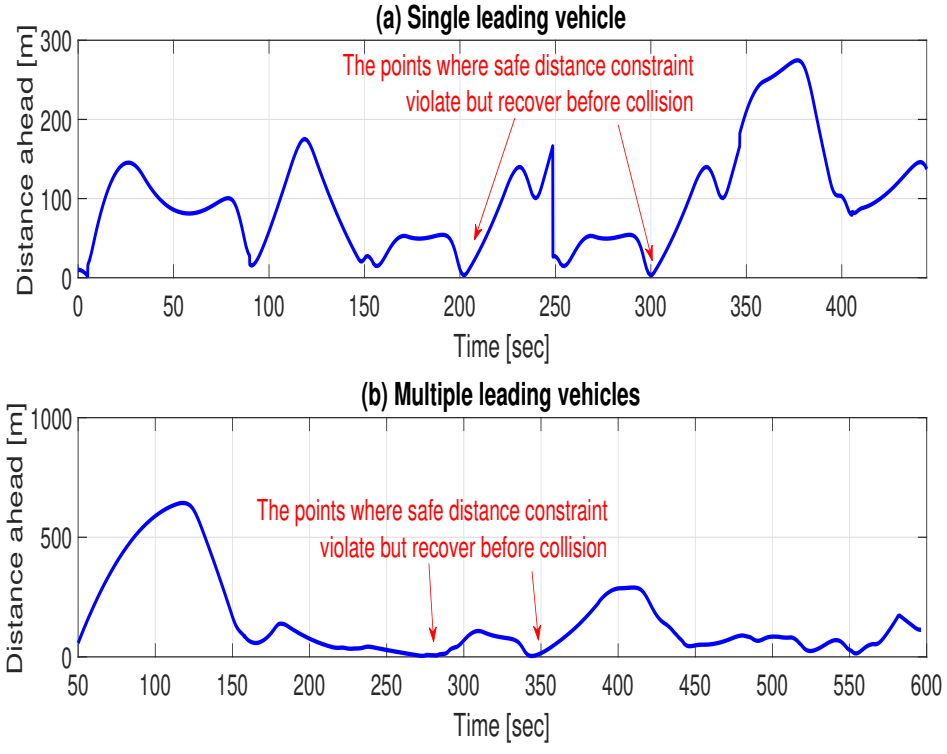

FIGURE 6.29: Distance ahead with leading vehicles (single and multiple leading vehicles on the route)

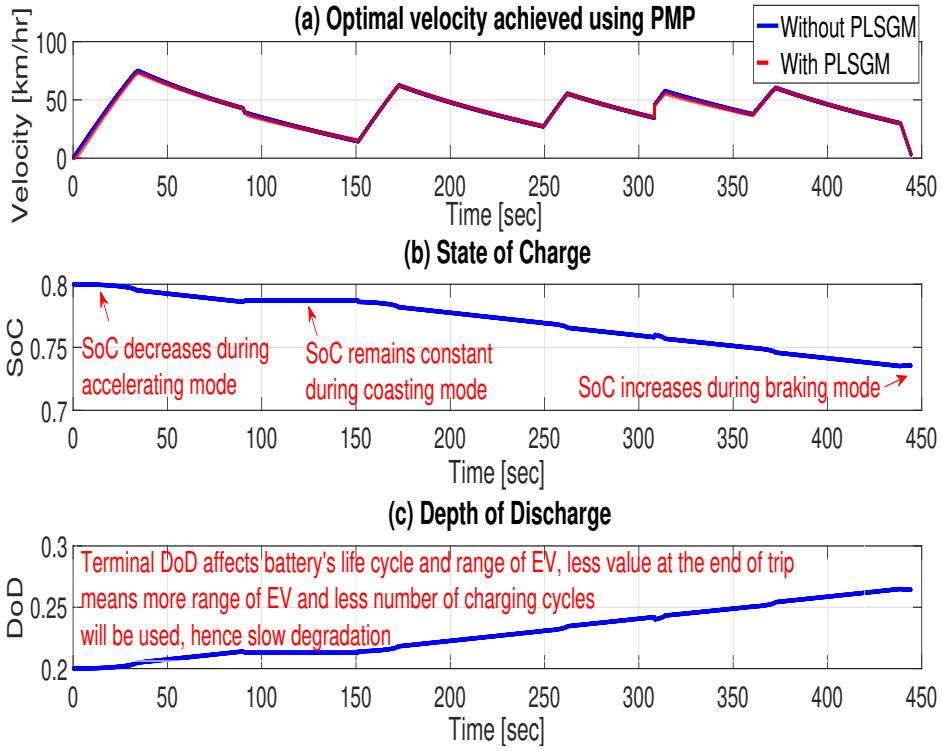

FIGURE 6.30: Optimal Velocity (Backward and PLSGM), SoC and DoD with single leading vehicle on the route

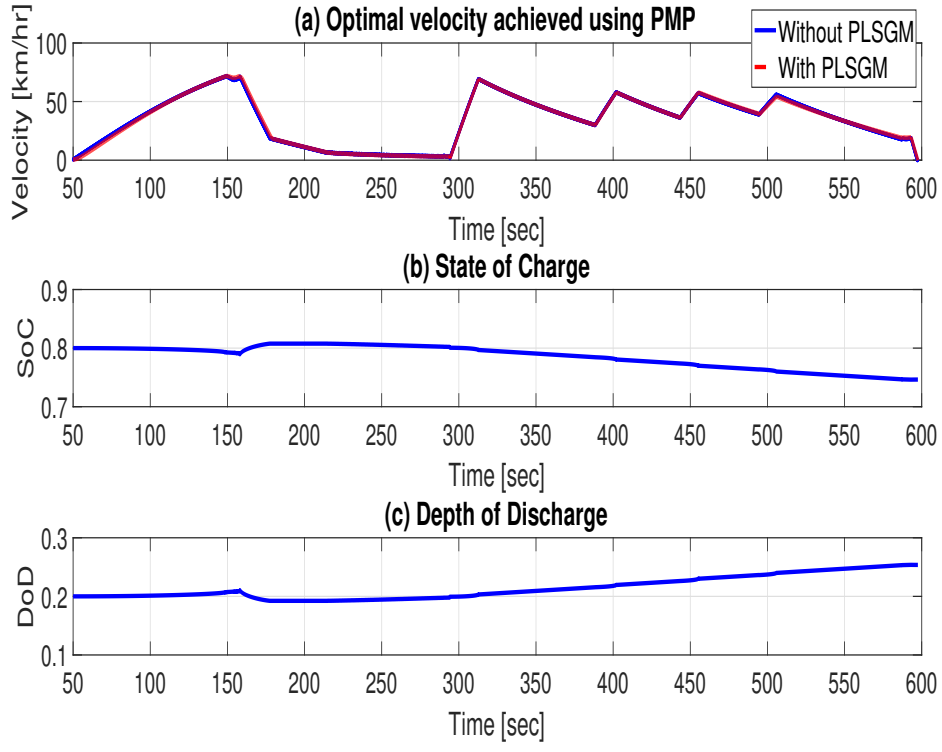

FIGURE 6.31: Optimal Velocity (Backward and PLSGM), SoC and DoD with multiple leading vehicles on the route

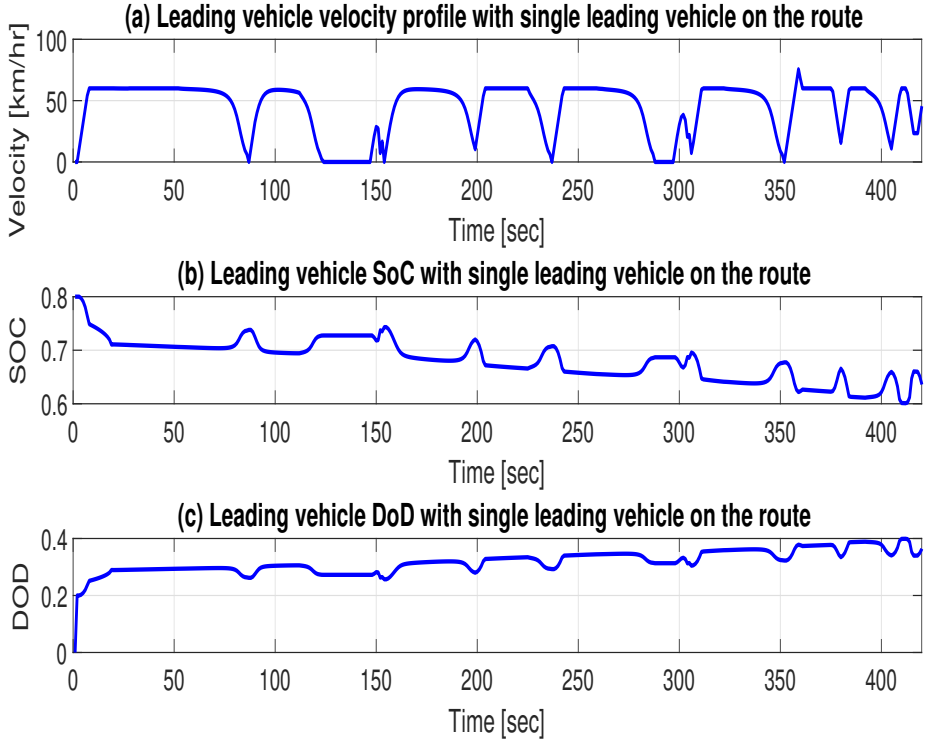

FIGURE 6.32: Velocity, SoC and DoD of leading vehicle without eco-driving assistance (single leading vehicle)

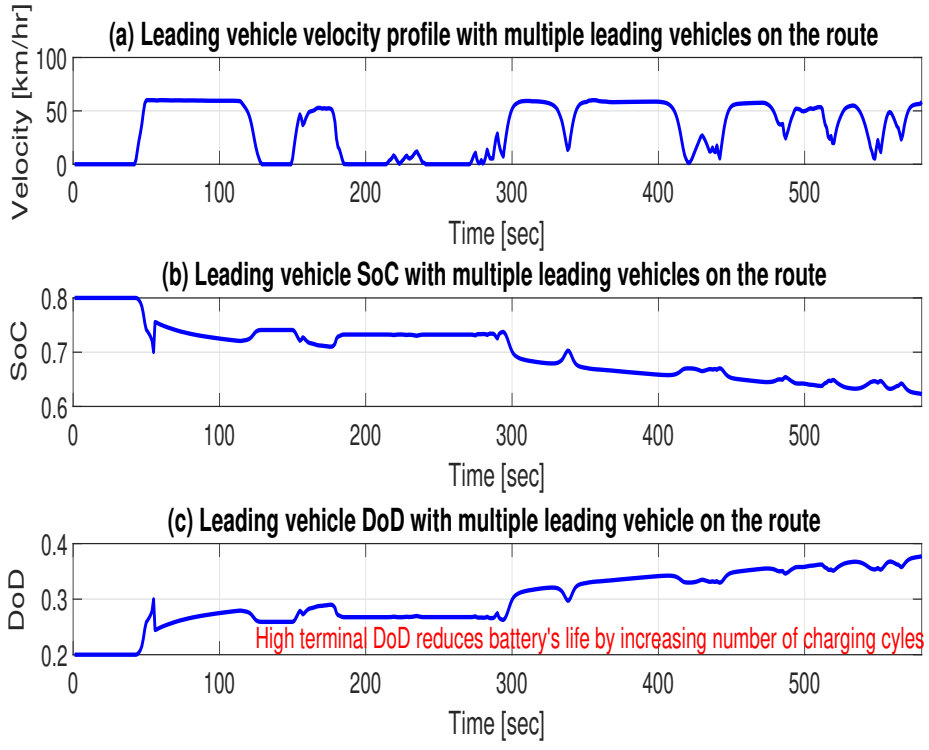

FIGURE 6.33: Velocity, SoC and DoD of leading vehicle without eco-driving assistance (multiple leading vehicles)

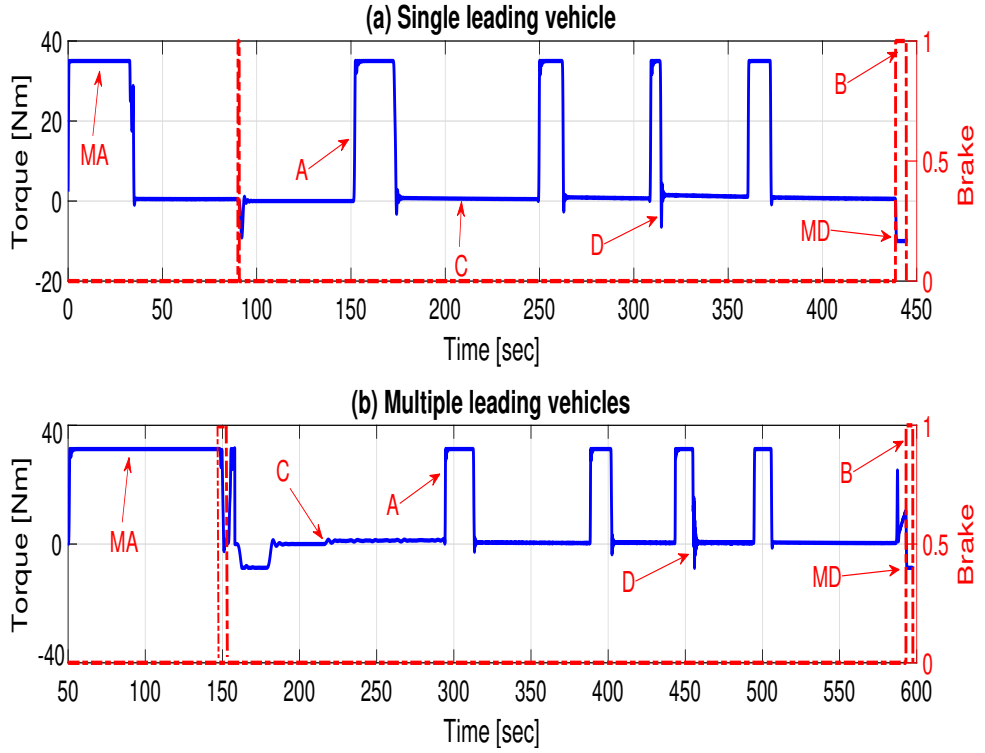

FIGURE 6.34: Comparison between optimal torque profiles with single and multiple leading vehicles on the route

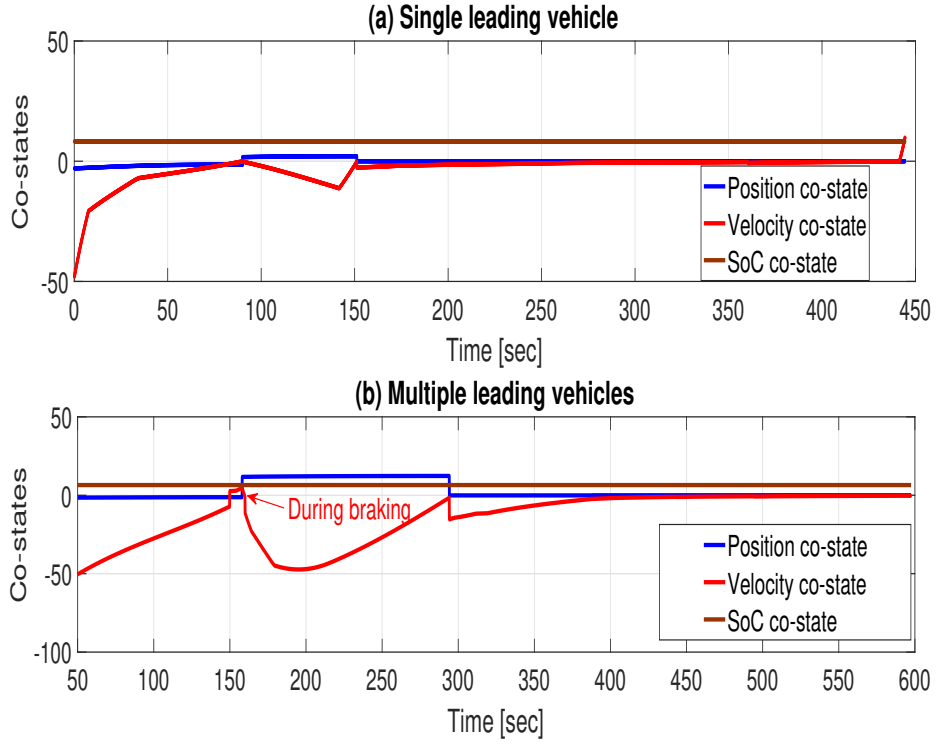

FIGURE 6.35: Co-states of EV and battery with single and multiple leading vehicles on the route

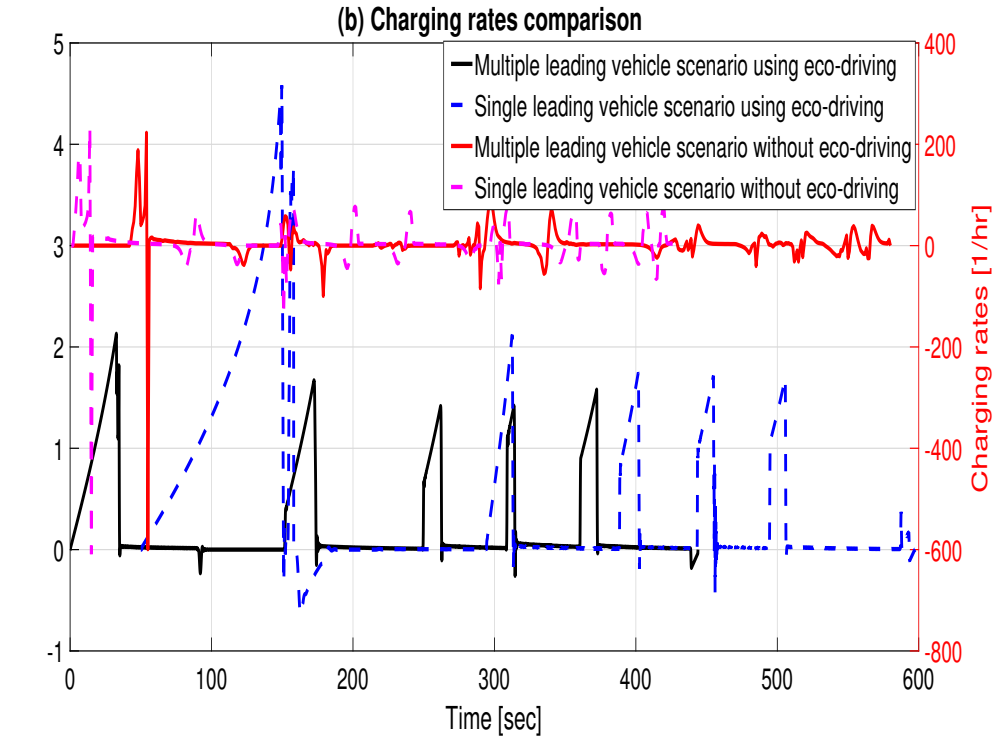

FIGURE 6.36: Charging rate comparison between with and without eco-driving assistance

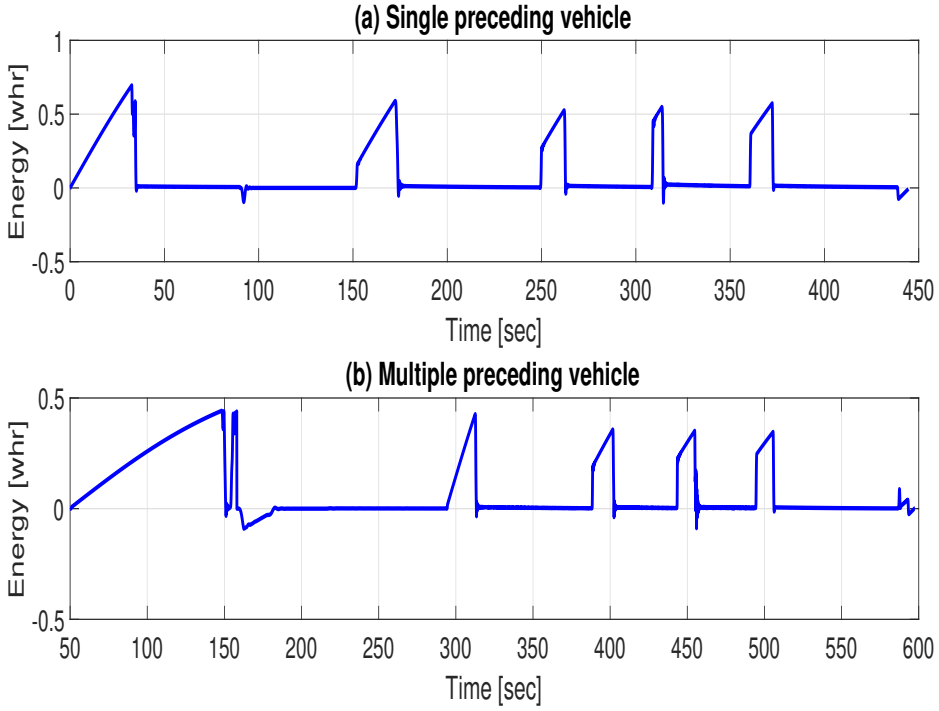

FIGURE 6.37: Energy consumption using eco-driving with single and multiple preceding vehicle

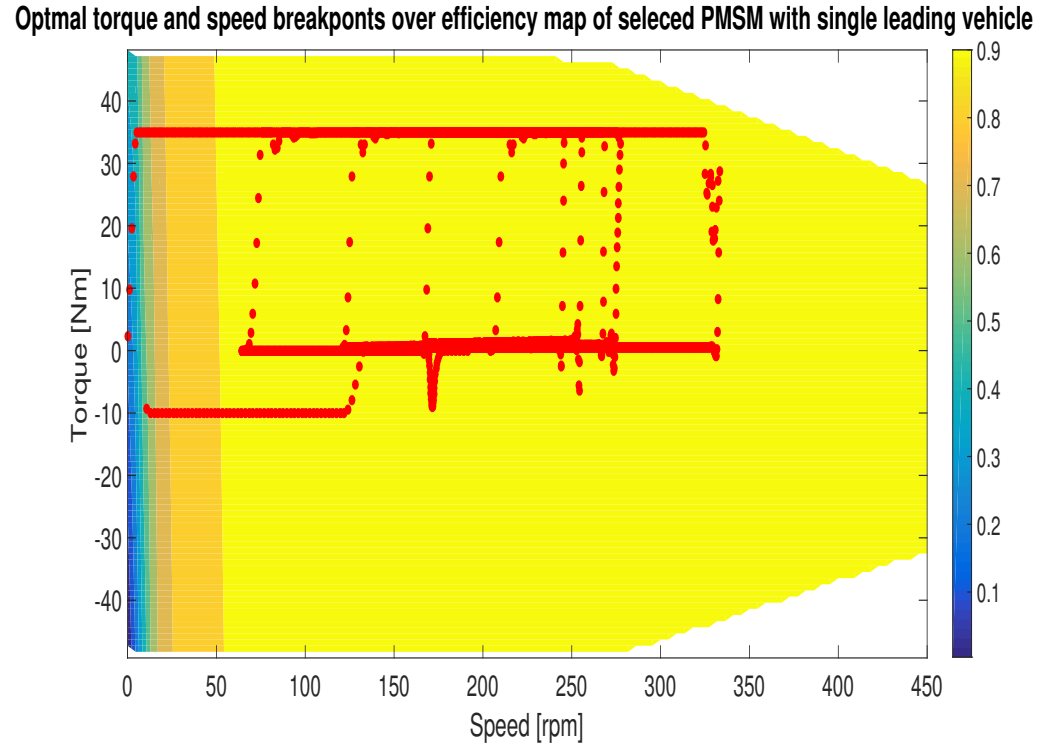

FIGURE 6.38: Efficiency map with optimal torque and speed breakpoints with single leading vehicle on the route

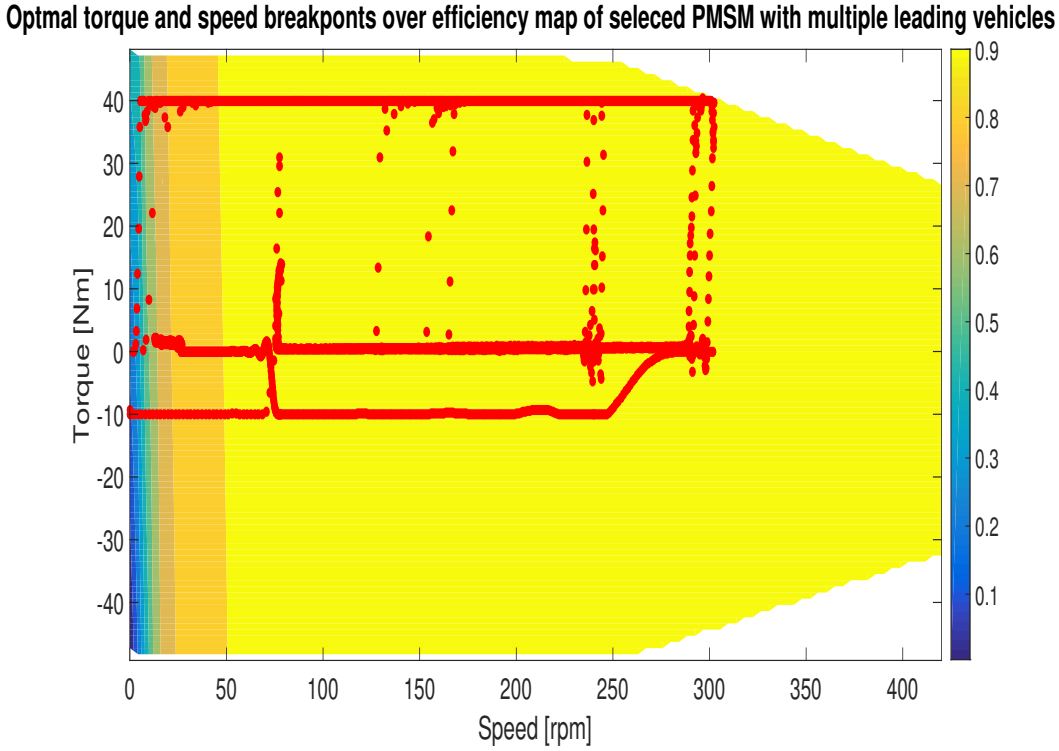

FIGURE 6.39: Efficiency map with optimal torque and speed breakpoints with multiple leading vehicles on the route

TABLE 6.15: Reaching time comparison between single and multiple leading vehicles (backward and PLSGM)

Scenario	**Signal 1**	**Signal 2**	**Signal 3**	**Signal 4**	**Signal 5**
Single leading (backward simulator)	91sec	151sec	250sec	308sec	361.2sec
Single leading (PLSGM)	92.3sec	156.9sec	249.5sec	305.7sec	368.4sec
Multiple leading (backward simulator)	158sec	294sec	388sec	443sec	494sec
Multiple leading (PLSGM)	157.1sec	295.1sec	386.1sec	442.3sec	490.8sec

TABLE 6.16: Energy consumption, average charging rates and DoD comparison between non-eco driving and eco-driving strategies with single and multiple leading vehicles

Scenario	**Energy consumption**	**Charging rates**	**DoD**
Single leading vehicle without eco-driving	460.32wh	3.165	.3265
EV using eco-driving single leading vehicle	364.94wh	.2725	.2282
Multiple leading vehicles without eco-driving	745.14wh	.4205	.3776
EV using eco-driving multiple leading vehicles	460.36wh	.3316	.2689

6.8 Convergence Time for all the Scenarios

Convergence time for all the scenarios are as mentioned in Table. 6.17. Machine used in simulating all the scenarios is Dell Core i7, 10th GEN, 1.50GHZ. First

TABLE 6.17: Convergence time for all the scenarios

Scenario	**Convergence time(sec)**	α
First	3.527	.048
Second	3.555sec	.048
Third	1.848sec	.065
Fourth	18.968sec	.075
Fifth	19.61sec	.075
Sixth	20.10sec	.055
Seventh	17.567sec	.055

scenario is unconstrained case, second scenario is with the inclusion of zero order battery model with free final velocity and third scenario is with the inclusion of zero order battery model with fixed final velocity. Similarly, fourth scenario is with the inclusion of traffic signals and fifth scenario is with the inclusion of traffic signals and speed limits. Sixth scenario is SoC dependent v_{oc} and r_0. Finally 7th scenario is with the inclusion of urban traffic.

6.9 Chapter Summary

Main focus of Chapter 6 revolves around the achieved results through simulation using Matlab. Seven different scenarios are considered i.e., from unconstrained to complex constrained scenario. Optimal control with different modes, states, co-states with continuity condition, where required, achieved efficiency over calculated torque and speed breakpoints are simulated. Energy consumption comparison, charging rates, terminal DoD are compared with vehicles which are not based on eco-driving assistance in some scenarios.

Chapter 7

Conclusion and Future Work

7.1 Conclusion on Achieved Results

In this thesis, energy minimization strategy for EV has been proposed. Energy consumption during the route is improved by optimizing velocity profile known as eco-driving which is calculated using PMP. It is concluded that minimizing energy consumption during a trip is equivalent to solving the necessary conditions of optimality. Moreover, PLSGM is used to counter both the issues faced in backward and forward vehicle modeling approaches to exactly follow the advised optimal velocity profile with consideration of powertrain limitations.

Battery dynamics are added to the system to extend the range of EV through optimizing battery's capacity. However, range extension is a very specific problem that requires same components as used in the literature to compare the range. In this thesis, range is improved through energy consumption comparison. Different models of battery are used i.e., zero order ideal model and first order Thevenin model. Longitudinal dynamics of EV is used with velocity as the decisive component. Dynamic efficiency model of PMSM is used to provide the mechanical power to the powertrain.

Seven different scenarios are simulated in this thesis, which is formulated and simulated in chapter 5 & 6 respectively. Proposed strategy of eco-driving has shown that PMP has the ability to handle scenarios from simple to complex i.e., close

to real traffic environment. Problem is well handled in the presence of different boundary and inequality constraints using TPBVP with either shooting or gradient method. However, with intermediate constraints, MPBVP with multiple shooting method showed that multi-phase problem can be converted to single phase problem. Conclusions with advantage are highlighted as:

1. Problem with battery dynamics and charging/discharging constraints with either fixed or free final velocities have successfully maintained the defined limits to contribute in improving battery's life, which gets affected using complete charging/discharged. v_{oc} and r_0 characteristics with SoC in chapter 3 clearly highlight the advantage of this bounded charging and discharging.

2. Problem with traffic signals using the applied approach has successfully followed the continuity of co-states thereby reaching the signals during their green duration and following speed limits. Moreover, energy consumption comparison has shown 4% improvement as compared to the problem using TPBVP. Chapter 4 explains how this point helps in achieving the necessary conditions.

3. EV with traffic i.e., either single or multiple leading vehicles have successfully crossed the signals without braking with keeping safe gap with leading vehicles. Moreover, driver using PLSGM has successfully followed the advised optimal speed that is calculated using PMP. Energy consumption comparison has shown $5 - 20\%$ improvement.

4. Battery life improvement analysis is performed through the comparison of charging rates, terminal DoD. Charging rate comparison has shown improvement that also relates to number of charging and discharging cycles. Less charging rate and terminal DoD mean less charging and discharging cycles thereby improving battery life and efficiency [89, 90]. Chapter 6 has shown that advantage achieved using the proposed approach that host EV has followed the constraints and has also provided the advantage in terms of energy consumption. Moreover, battery saving analysis has shown that proposed

strategy is helpful in reducing battery's degradation process, which otherwise would increase the cost of the system by early replacing the battery.

7.2 Future Directions

There can be number of future directions. However looking at the scope of the thesis, problem can be extended with the inclusion of separate or combination of various directions, as:

1. Lane changing feature using lateral dynamics
2. Inclusion of comfort and time factor
3. Routing problem using optimal route selection

7.2.1 Lane Changing using Lateral Dynamics

It has been observed that problem with traffic has faced an issue i.e., with dense traffic, extra time is taken by EV to reach the destination. This extra time taken by EV is due to the slowness of traffic which is not in control and depends upon leading vehicle and system has no ability to cross the leading vehicle. Lane changing feature gives another option i.e., to change the lane [91, 92], instead of following the leading vehicle as shown in Fig. 7.1. Optimal lane changing can add another advantage both in terms of energy saving but also reducing the trip time of EV. This switching between the lanes requires the development of lateral dynamics along with longitudinal dynamics, which further enhances the complexity.

7.2.2 Inclusion of Comfort and Time Factor

It has been observed that comfort factor to the driver and other people in EV adds another advantage during the trip. Comfort factor can be included using constraint on maximum and minimum values of acceleration. Furthermore, trip

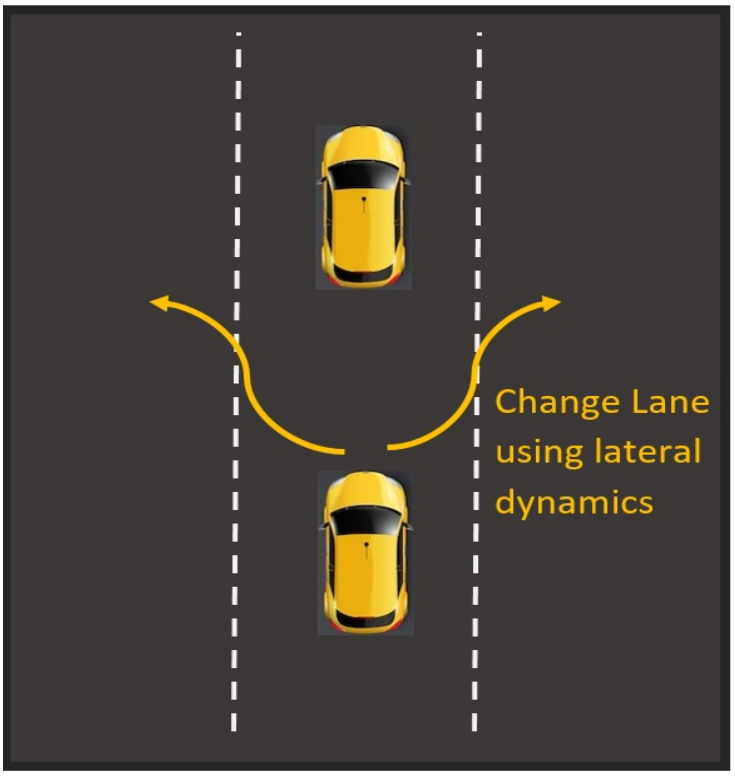

FIGURE 7.1: Lane changing feature

time plays a critical role hence it is recommended as future direction to include time in the objective function along with energy consumption.

7.2.3 Optimal Routing Problem

Nature of trip has a very significant impact on the energy consumption. With the advance development of latest Global Positioning System (GPS), selection of optimal route before the start of trip has become a key factor to further improve the energy consumption [93–96]. Optimal route selection can be based upon minimum time, shortest distance and minimum energy consumption. Hence, one of the key future directions that can be used as the extension of the problem simulated in this thesis, is the co-optimization of velocity and route to optimize both the route and speed of EVs. This optimal route selection along with the velocity profile can become very useful solution for the minimization of energy consumption for more than one vehicle especially to serve in logistics and supply chain.

Bibliography

[1] E. M. Bibra, E. Connelly, S. Dhir, M. Drtil, P. Henriot, I. Hwang, J.-B. Le Marois, S. McBain, L. Paoli, and J. Teter, "Global ev outlook 2022: Securing supplies for an electric future," 2022.

[2] R. E. Kopp and H. G. Moyer, "Trajectory optimization techniques," *Advances in control systems*, vol. 4, pp. 103–155, 1966.

[3] D. Morante, M. Sanjurjo Rivo, and M. Soler, "A survey on low-thrust trajectory optimization approaches," *Aerospace*, vol. 8, no. 3, p. 88, 2021.

[4] M. Pontani and B. Conway, "Optimal low-thrust orbital maneuvers via indirect swarming method," *Journal of Optimization Theory and Applications*, vol. 162, no. 1, pp. 272–292, 2014.

[5] S. Onori, L. Serrao, and G. Rizzoni, "Hybrid electric vehicles: Energy management strategies," 2016.

[6] D. E. Kirk, *Optimal control theory: an introduction*. Courier Corporation, 2004.

[7] S. C. Trümper, "Commercial fleets as early markets for electric vehicles," in *16th International IEEE Conference on Intelligent Transportation Systems (ITSC 2013)*. IEEE, 2013, pp. 1941–1946.

[8] E. Silvas, T. Hofman, N. Murgovski, L. P. Etman, and M. Steinbuch, "Review of optimization strategies for system-level design in hybrid electric vehicles," *IEEE Transactions on Vehicular Technology*, vol. 66, no. 1, pp. 57–70, 2016.

[9] N. Murgovski, L. Johannesson, J. Sjöberg, and B. Egardt, "Component sizing of a plug-in hybrid electric powertrain via convex optimization," *Mechatronics*, vol. 22, no. 1, pp. 106–120, 2012.

[10] E. Vinot, R. Trigui, B. Jeanneret, J. Scordia, and F. Badin, "Hevs comparison and components sizing using dynamic programming," in *2007 IEEE Vehicle Power and Propulsion Conference*. IEEE, 2007, pp. 314–321.

[11] J. N. Barkenbus, "Eco-driving: An overlooked climate change initiative," *Energy policy*, vol. 38, no. 2, pp. 762–769, 2010.

[12] D. J. Chang and E. K. Morlok, "Vehicle speed profiles to minimize work and fuel consumption," *Journal of transportation engineering*, vol. 131, no. 3, pp. 173–182, 2005.

[13] L. Tang, G. Rizzoni, and S. Onori, "Energy management strategy for hevs including battery life optimization," *IEEE Transactions on Transportation Electrification*, vol. 1, no. 3, pp. 211–222, 2015.

[14] H. Banvait, S. Anwar, and Y. Chen, "A rule-based energy management strategy for plug-in hybrid electric vehicle (phev)," in *2009 American control conference*. IEEE, 2009, pp. 3938–3943.

[15] R. M. Bagwe, A. Byerly, E. C. dos Santos, and Z. Ben-Miled, "Adaptive rule-based energy management strategy for a parallel hev," *Energies*, vol. 12, no. 23, p. 4472, 2019.

[16] G.-E. Katsargyri, I. V. Kolmanovsky, J. Michelini, M. L. Kuang, A. M. Phillips, M. Rinehart, and M. A. Dahleh, "Optimally controlling hybrid electric vehicles using path forecasting," in *2009 American Control Conference*. IEEE, 2009, pp. 4613–4617.

[17] B. Asadi, C. Zhang, and A. Vahidi, "The role of traffic flow preview for planning fuel optimal vehicle velocity," in *Dynamic systems and control conference*, vol. 44182, 2010, pp. 813–819.

[18] R. Bellman, "Dynamic programming," *Science*, vol. 153, no. 3731, pp. 34–37, 1966.

[19] F. Zhang, L. Wang, S. Coskun, H. Pang, Y. Cui, and J. Xi, "Energy management strategies for hybrid electric vehicles: Review, classification, comparison, and outlook," *Energies*, vol. 13, no. 13, p. 3352, 2020.

[20] J. Wollaeger, S. A. Kumar, S. Onori, D. Filev, Ü. Özgüner, G. Rizzoni, and S. Di Cairano, "Cloud-computing based velocity profile generation for minimum fuel consumption: A dynamic programming based solution," in *2012 American Control Conference (ACC)*. IEEE, 2012, pp. 2108–2113.

[21] E. Ozatay, S. Onori, J. Wollaeger, U. Ozguner, G. Rizzoni, D. Filev, J. Michelini, and S. Di Cairano, "Cloud-based velocity profile optimization for everyday driving: A dynamic-programming-based solution," *IEEE Transactions on Intelligent Transportation Systems*, vol. 15, no. 6, pp. 2491–2505, 2014.

[22] E. Ozatay, U. Ozguner, J. Michelini, and D. Filev, "Analytical solution to the minimum energy consumption based velocity profile optimization problem with variable road grade," *IFAC Proceedings Volumes*, vol. 47, no. 3, pp. 7541–7546, 2014.

[23] E. Ozatay, U. Ozguner, and D. Filev, "Velocity profile optimization of on road vehicles: Pontryagin's maximum principle based approach," *Control Engineering Practice*, vol. 61, pp. 244–254, 2017.

[24] N. Petit and A. Sciarretta, "Optimal drive of electric vehicles using an inversion-based trajectory generation approach," *IFAC Proceedings Volumes*, vol. 44, no. 1, pp. 14 519–14 526, 2011.

[25] D. Wissam, A. Chasse, A. Sciarretta, and P. Moulin, "Optimal energy management compliant with online requirements for an electric vehicle in eco-driving applications," *IFAC Proceedings Volumes*, vol. 45, no. 30, pp. 334–340, 2012.

[26] W. Dib, A. Chasse, P. Moulin, A. Sciarretta, and G. Corde, "Optimal energy management for an electric vehicle in eco-driving applications," *Control Engineering Practice*, vol. 29, pp. 299–307, 2014.

[27] H. He, D. Liu, X. Lu, and J. Xu, "Eco driving control for intelligent electric vehicle with real-time energy," *Electronics*, vol. 10, no. 21, p. 2613, 2021.

[28] P. Liao, T.-Q. Tang, R. Liu, and H.-J. Huang, "An eco-driving strategy for electric vehicle based on the powertrain," *Applied Energy*, vol. 302, p. 117583, 2021.

[29] E. Ozatay, U. Ozguner, S. Onori, and G. Rizzoni, "Analytical solution to the minimum fuel consumption optimization problem with the existence of a traffic light," in *Dynamic Systems and Control Conference*, vol. 45295. American Society of Mechanical Engineers, 2012, pp. 837–846.

[30] E. Ozatay, U. Ozguner, D. Filev, and J. Michelini, "Analytical and numerical solutions for energy minimization of road vehicles with the existence of multiple traffic lights," in *52nd IEEE Conference on Decision and Control*. IEEE, 2013, pp. 7137–7142.

[31] N. Wan, A. Vahidi, and A. Luckow, "Optimal speed advisory for connected vehicles in arterial roads and the impact on mixed traffic," *Transportation Research Part C: Emerging Technologies*, vol. 69, pp. 548–563, 2016.

[32] A. Vahidi and A. Sciarretta, "Energy saving potentials of connected and automated vehicles," *Transportation Research Part C: Emerging Technologies*, vol. 95, pp. 822–843, 2018.

[33] B. Asadi and A. Vahidi, "Predictive use of traffic signal state for fuel saving," *IFAC Proceedings Volumes*, vol. 42, no. 15, pp. 484–489, 2009.

[34] Asadi and Ardalan, "Predictive cruise control: Utilizing upcoming traffic signal information for improving fuel economy and reducing trip time," *IEEE transactions on control systems technology*, vol. 19, no. 3, pp. 707–714, 2010.

[35] G. De Nunzio, C. C. De Wit, P. Moulin, and D. Di Domenico, "Eco-driving in urban traffic networks using traffic signals information," *International Journal of Robust and Nonlinear Control*, vol. 26, no. 6, pp. 1307–1324, 2016.

[36] X. Wu, X. He, G. Yu, A. Harmandayan, and Y. Wang, "Energy-optimal speed control for electric vehicles on signalized arterials," *IEEE Transactions on Intelligent Transportation Systems*, vol. 16, no. 5, pp. 2786–2796, 2015.

[37] S. Zhang, Y. Luo, K. Li, and V. Li, "Real-time energy-efficient control for fully electric vehicles based on an explicit model predictive control method," *IEEE Transactions on Vehicular Technology*, vol. 67, no. 6, pp. 4693–4701, 2018.

[38] J. Han, A. Vahidi, and A. Sciarretta, "Fundamentals of energy efficient driving for combustion engine and electric vehicles: An optimal control perspective," *Automatica*, vol. 103, pp. 558–572, 2019.

[39] M. U. Ali, M. A. Kamran, P. S. Kumar, S. H. Nengroo, M. A. Khan, A. Hussain, H.-J. Kim *et al.*, "An online data-driven model identification and adaptive state of charge estimation approach for lithium-ion-batteries using the lagrange multiplier method," *Energies*, vol. 11, no. 11, p. 2940, 2018.

[40] G. Mohan, F. Assadian, and S. Longo, "Comparative analysis of forward-facing models vs backwardfacing models in powertrain component sizing," in *IET hybrid and electric vehicles conference 2013 (HEVC 2013)*. IET, 2013, pp. 1–6.

[41] M. Delavaux, W. Lhomme, and A. McGordon, "Comparison between forward and backward approaches for the simulation of an electric vehicle," in *Proceedings of the IEEE Vehicle Power and Propulsion Conference (VPPC2010), Lille, France*, 2010, pp. 3–5.

[42] L. Horrein, A. Bouscayrol, P. Delarue, J. Verhille, and C. Mayet, "Forward and backward simulations of a power propulsion system," *IFAC Proceedings Volumes*, vol. 45, no. 21, pp. 441–446, 2012.

[43] S. Lekshmi and L. P. PS, "Mathematical modeling of electric vehicles-a survey," *Control Engineering Practice*, vol. 92, p. 104138, 2019.

[44] G. Lino and S. Antonio, "Vehicle propulsion systems, introduction to modeling and optimization," *Berlin: Springer*, 2013.

[45] H. M. Y. Naeem, A. I. Bhatti, Y. A. Butt, and Q. Ahmed, "Velocity profile optimization of an electric vehicle with battery dynamic model," in *2019 12th Asian Control Conference (ASCC)*. IEEE, 2019, pp. 609–614.

[46] C. D. Rahn and C.-Y. Wang, *Battery systems engineering*. John Wiley & Sons, 2013.

[47] S. Drouilhet, B. Johnson, S. Drouilhet, and B. Johnson, "A battery life prediction method for hybrid power applications," in *35th Aerospace Sciences Meeting and Exhibit*, 1997, p. 948.

[48] L. Serrao, Z. Chehab, Y. Guezennee, and G. Rizzoni, "An aging model of nimh batteries for hybrid electric vehicles," in *2005 IEEE Vehicle Power and Propulsion Conference*. IEEE, 2005, pp. 8–pp.

[49] Z. Chehab, L. Serrao, Y. G. Guezennec, and G. Rizzoni, "Aging characterization of nickel: Metal hydride batteries using electrochemical impedance spectroscopy," in *ASME International Mechanical Engineering Congress and Exposition*, vol. 47683, 2006, pp. 343–349.

[50] M. Dubarry, V. Svoboda, R. Hwu, and B. Y. Liaw, "Capacity and power fading mechanism identification from a commercial cell evaluation," *Journal of Power Sources*, vol. 165, no. 2, pp. 566–572, 2007.

[51] Dubarry, Vojtech, Ruey, and B. Yann, "Capacity loss in rechargeable lithium cells during cycle life testing: The importance of determining state-of-charge," *Journal of Power Sources*, vol. 174, no. 2, pp. 1121–1125, 2007.

[52] L. Tribioli, "Energy-based design of powertrain for a re-engineered post-transmission hybrid electric vehicle," *Energies*, vol. 10, no. 7, p. 918, 2017.

[53] F. Dettù, G. Pozzato, D. M. Rizzo, and S. Onori, "Exergy-based modeling framework for hybrid and electric ground vehicles," *Applied Energy*, vol. 300, p. 117320, 2021.

[54] R. R. Thakkar, "Electrical equivalent circuit models of lithium-ion battery," *Management and Applications of Energy Storage Devices*, 2021.

[55] H. M. Y. Naeem, A. I. Bhatti, Y. A. Butt, and Q. Ahmed, "Velocity profile optimization of an electric vehicle (ev) with battery constraint using pontryagin's minimum principle (pmp)," in *2019 IEEE Conference on Control Technology and Applications (CCTA)*. IEEE, 2019, pp. 750–755.

[56] R. Zhang, B. Xia, B. Li, L. Cao, Y. Lai, W. Zheng, H. Wang, W. Wang, and M. Wang, "A study on the open circuit voltage and state of charge characterization of high capacity lithium-ion battery under different temperature," *Energies*, vol. 11, no. 9, p. 2408, 2018.

[57] H. Lei and Y. Y. Han, "The measurement and analysis for open circuit voltage of lithium-ion battery," in *Journal of Physics: Conference Series*, vol. 1325, no. 1. IOP Publishing, 2019, p. 012173.

[58] M. Li, "Li-ion dynamics and state of charge estimation," *Renewable Energy*, vol. 100, pp. 44–52, 2017.

[59] W.-Y. Chang, "The state of charge estimating methods for battery: A review," *International Scholarly Research Notices*, vol. 2013, 2013.

[60] N. Zhang, X. Ma, and L. Jin, "Energy management for parallel hev based on pmp algorithm," in *2017 2nd International Conference on Robotics and Automation Engineering (ICRAE)*. IEEE, 2017, pp. 177–182.

[61] H. He, R. Xiong, and J. Fan, "Evaluation of lithium-ion battery equivalent circuit models for state of charge estimation by an experimental approach," *energies*, vol. 4, no. 4, pp. 582–598, 2011.

[62] K. Ogata, *Discrete-time control systems*. Prentice-Hall, Inc., 1995.

[63] A. V. Oppenheim, A. S. Willsky, S. H. Nawab, G. M. Hernández *et al.*, *Signals & systems*. Pearson Educación, 1997.

[64] A. V. Oppenheim, J. R. Buck, and R. W. Schafer, *Discrete-time signal processing. Vol. 2*. Upper Saddle River, NJ: Prentice Hall, 2001.

[65] D. Linden, "Handbook of batteries and fuel cells," *New York*, 1984.

[66] N. B. Hadj, R. Abdelmoula, M. Chaieb, and R. Neji, "Permanent magnet motor efficiency map calculation and small electric vehicle consumption optimization." *Journal of Electrical Systems*, vol. 14, no. 2, 2018.

[67] K. N. D. Ranaweera *et al.*, "Development and experimental testing of a speed controlled pmsm drive using psim visual programming environment," *Development and Experimental Testing of a Speed Controlled PMSM Drive Using PSIM Visual Programming Environment*, 2019.

[68] O. Von Stryk and R. Bulirsch, "Direct and indirect methods for trajectory optimization," *Annals of operations research*, vol. 37, no. 1, pp. 357–373, 1992.

[69] S. Campbell, "Practical methods for optimal control and estimation using nonlinear programming. vol. 19," 2011.

[70] D. Bertsekas, "Dynamic programming and optimal control, i and ii, athena scientific, belmont, massachusetts," *New York-San Francisco-London*, 1995.

[71] L. C. Evans, "An introduction to mathematical optimal control theory version 0.2," *Lecture notes available at http://math. berkeley. edu/˜ evans/control. course. pdf*, 1983.

[72] H. P. Geering, *Optimal control with engineering applications*. Springer, 2007.

[73] L. S. Pontryagin, *Mathematical theory of optimal processes*. CRC press, 1987.

[74] H. J. Sussmann and J. C. Willems, "300 years of optimal control: from the brachystochrone to the maximum principle," *IEEE Control Systems Magazine*, vol. 17, no. 3, pp. 32–44, 1997.

[75] H. B. Keller, *Numerical methods for two-point boundary-value problems*. Courier Dover Publications, 2018.

[76] D. B. Meade, B. S. Haran, and R. E. White, "The shooting technique for the solution of two-point boundary value problems," *Maple Technical Newsletter*, vol. 3, no. 1, pp. 1–8, 1996.

[77] S. N. Ha, "A nonlinear shooting method for two-point boundary value problems," *Computers & Mathematics with Applications*, vol. 42, no. 10-11, pp. 1411–1420, 2001.

[78] M. Wang, S. P. Hoogendoorn, W. Daamen, R. Hoogendoorn, and B. van Arem, "Driver support and cooperative systems control design: Framework and preliminary results," in *2012 American Control Conference (ACC)*. IEEE, 2012, pp. 5751–5756.

[79] L. Mikulski, "Control structure in optimization problems of bar systems," *International Journal of Applied Mathematics and Computer Science*, vol. 14, no. 4, pp. 515–529, 2004.

[80] G. H. Meyer, *Initial value methods for boundary value problems: theory and application of invariant imbedding*. Academic Press, 1973.

[81] D. D. Morrison, J. D. Riley, and J. F. Zancanaro, "Multiple shooting method for two-point boundary value problems," *Communications of the ACM*, vol. 5, no. 12, pp. 613–614, 1962.

[82] N. Kim, A. Rousseau, and D. Lee, "A jump condition of pmp-based control for phevs," *Journal of Power Sources*, vol. 196, no. 23, pp. 10 380–10 386, 2011.

[83] J. S. Arora, "Numerical methods for unconstrained optimum design," *Introduction to optimum design*, pp. 411–441, 2004.

[84] S. Lian, S. Meng, and Y. Wang, "An objective penalty function-based method for inequality constrained minimization problem," *Mathematical Problems in Engineering*, vol. 2018, 2018.

[85] C. Yu, K. L. Teo, L. Zhang, and Y. Bai, "A new exact penalty function method for continuous inequality constrained optimization problems," *Journal of Industrial and Management Optimization*, vol. 6, pp. 895–910, 2010.

[86] S. A. Kalogirou, "Preface to the third edition." Elsevier Inc., 2017.

[87] H. M. Y. Naeem, A. I. Bhatti, Y. A. Butt, and Q. Ahmed, "Eco-driving control of electric vehicle with battery dynamic model and multiple traffic signals," *Proceedings of the Institution of Mechanical Engineers, Part D: Journal of Automobile Engineering*, vol. 236, no. 6, pp. 1133–1143, 2022.

[88] K. M. Gaikwad and M. S. Chavan, "Removal of high frequency noise from ecg signal using digital iir butterworth filter," in *2014 IEEE Global Conference on Wireless Computing & Networking (GCWCN)*. IEEE, 2014, pp. 121–124.

[89] A. McEvoy, T. Markvart, L. Castañer, T. Markvart, and L. Castaner, *Practical handbook of photovoltaics: fundamentals and applications*. Elsevier, 2003.

[90] J. Garche, C. Dyer, P. T. Moseley, Z. Ogumi, D. A. Rand, and B. Scrosati, *Encyclopedia of electrochemical power sources*. Newnes, 2013.

[91] J. A. Laval and C. F. Daganzo, "Lane-changing in traffic streams," *Transportation Research Part B: Methodological*, vol. 40, no. 3, pp. 251–264, 2006.

[92] W.-L. Jin, "A multi-commodity lighthill–whitham–richards model of lane-changing traffic flow," *Transportation Research Part B: Methodological*, vol. 57, pp. 361–377, 2013.

[93] R. Jaballah, M. Veenstra, L. C. Coelho, and J. Renaud, "The time-dependent shortest path and vehicle routing problem," *INFOR: Information Systems and Operational Research*, vol. 59, no. 4, pp. 592–622, 2021.

[94] C. Prins, P. Lacomme, and C. Prodhon, "Order-first split-second methods for vehicle routing problems: A review," *Transportation Research Part C: Emerging Technologies*, vol. 40, pp. 179–200, 2014.

[95] A. Chabrier, "Vehicle routing problem with elementary shortest path based column generation," *Computers & Operations Research*, vol. 33, no. 10, pp. 2972–2990, 2006.

[96] K. Ahn and H. Rakha, "The effects of route choice decisions on vehicle energy consumption and emissions," *Transportation Research Part D: Transport and Environment*, vol. 13, no. 3, pp. 151–167, 2008.

Appendix A

$$\dot{v_a} = -\frac{v_a}{R_a C_a} + \frac{I(t)}{C_a} \tag{A.1}$$

where

$$f(t) = v_a \tag{A.2}$$

Using the first derivative property of Laplace transform:

$$\dot{v_a}(t) \xleftrightarrow{\mathscr{L}} \mathrm{S}V_a(\mathrm{s}) - v_a(0^-) \tag{A.3}$$

On applying integration by parts

$$\mathscr{L}[\dot{v_a}(t)] = \int_{0^-}^{inf} \dot{v_a}(t) e^{-\mathrm{st}} dt) \tag{A.4}$$

It becomes;

$$\mathrm{s}V_a(\mathrm{s}) - V_a(0) = -\frac{V_a(\mathrm{s})}{C_a R_a} + \frac{I(\mathrm{s})}{C_a} \tag{A.5}$$

Appendix B

Approximate relation between continuous frequency i.e., s and discrete frequency i.e., z is expressed as:

$$z = e^{\mathrm{s}T} \tag{B.1}$$

where T is the sampling time.

ZoH transfer function in continuous frequency domain is expressed as:

$$H(\mathrm{s}) = \frac{Y(\mathrm{s})}{X(\mathrm{s})} = \frac{(1 - e^{\mathrm{s}T})}{\mathrm{s}T} \tag{B.2}$$

using the relation B.1, ZoH transfer function relation between continuous and discrete frequency domain as:

$$H(\mathrm{z}) = \frac{Y(\mathrm{z})}{X(\mathrm{z})} = (1 - \mathrm{z}^{-1})\mathcal{Z}\left[\mathcal{L}^{-1}\left(\frac{H(\mathrm{s})}{\mathrm{s}}\right)\right] \tag{B.3}$$